The Philosophical Magazine

FIRST PUBLISHED IN 1798

A Journal of Theoretical Experimental and Applied Physics

Vol. 4 August 1959 No. 44
Eighth Series

£1 5s. 0d., plus postage
Annual Subscription £13 10s. 0d., payable in advance

Printed and Published by
TAYLOR & FRANCIS LTD
RED LION COURT, FLEET STREET, LONDON, E.C.4

THE PHILOSOPHICAL MAGAZINE

Authors wishing to submit papers for publication in the Journal should send manuscripts directly to the Publishers.

Manuscripts should be typed in *double* spacing on one side of quarto (8 × 10 in.) paper, and authors are urged to aim at absolute clarity of meaning and an attractive presentation of their texts.

References should be listed at the end in alphabetical order of authors and should be cited in the text in terms of author's name and date. Diagrams should normally be in Indian ink on white card, with lettering in soft pencil, the captions being typed on a separate sheet.

A leaflet giving detailed instructions to authors on the preparation of papers is available on request from the Publishers.

Authors are entitled to receive 25 offprints of a paper in the Journal free of charge, and additional offprints can be obtained from the Publishers.

The *Philosophical Magazine* and its companion journal, *Advances in Physics*, will accept papers for publication in experimental and theoretical physics. The *Philosophical Magazine* publishes contributions describing new results, letters to the editor and book reviews. *Advances in Physics* publishes articles surveying the present state of knowledge in any branch of the science in which recent progress has been made. The editors welcome contributions from overseas as well as from the United Kingdom, and papers may be published in English, French and German.

Contents of May, 1959

Price £1 5s. 0d. per part plus postage
Subscription price per volume £4 15s. 0d. post free, payable in advance

Printed and Published by
TAYLOR & FRANCIS LTD
RED LION COURT, FLEET STREET, LONDON, E.C.4

Orders originating in U.S.A. and Canada should be sent to the Academic Press Inc., 111 Fifth Avenue, New York, 3, N.Y., U.S.A.

INTERNATIONAL JOURNAL OF
RADIATION BIOLOGY
and related studies in Physics, Chemistry and Medicine

Contents of April, 1959

Price per part £1 0s. 0d. plus postage

Subscription per volume (4 issues) £3 15s. 0d. post free, payable in advance

Printed and Published by

TAYLOR & FRANCIS LTD

RED LION COURT, FLEET STREET, LONDON, E.C.4

Orders originating in U.S.A. and Canada should be sent to the Academic Press Inc., 111 Fifth Avenue, New York 3, N.Y., U.S.A.

Journal of Electronics and Control

A Philosophical Magazine Associated Journal

Editor:
J. THOMSON, M.A., D.Sc., M.I.E.E., F.Inst.P.

Consultant Editor:
Professor N. F. MOTT, F.R.S.

Editorial Board:
Professor P. AIGRAIN (France)
Professor H. B. G. CASIMIR (Holland)
J. F. COALES (U.K.)
Professor K. G. EMELEUS (U.K.)
D. W. FRY (U.K.)
Dr. W. KLEIN (Germany)
Dr. R. KOMPFNER (U.S.A.)

Contents of April, 1959

Price per part £1 5s. plus postage
Price per volume £7 post free, payable in advance
6 monthly issues per volume

Printed and Published by

TAYLOR & FRANCIS LTD
RED LION COURT, FLEET STREET, LONDON, E.C.4

Orders originating in U.S.A. and Canada should be sent to the Academic Press Inc., 111 Fifth Avenue, New York, 3, N.Y., U.S.A.

Advances in Physics

A Quarterly Supplement of the Philosophical Magazine

Contents of April, 1959

Price per part £1 plus postage

Price per annum £3 15s. post free

Printed and Published by

TAYLOR & FRANCIS LTD

RED LION COURT, FLEET STREET, LONDON, E.C.4

Contents of April, 1959

Price per part £1 5s. 0d. plus postage
Subscription per volume (4 issues) £4 15s. 0d. post free, payable in advance

Printed and Published by

TAYLOR & FRANCIS LTD

RED LION COURT, FLEET STREET, LONDON, E.C.4

Orders originating in U.S.A. and Canada should be sent to the Academic Press Inc., 111 Fifth Avenue, New York, 3, N.Y., U.S.A.

Physics in Medicine and Biology

A Taylor & Francis Journal published in association with The Hospital Physicists' Association

Contents of April, 1959

Subscription price per volume £3 10s. post free, payable in advance

4 parts per volume—£1 per part plus postage

Printed and Published by

TAYLOR & FRANCIS, LTD

RED LION COURT, FLEET STREET, LONDON, E.C.4

Orders originating in U.S.A. and Canada should be sent to the Academic Press Inc., 111 Fifth Avenue, New York, 3, N.Y., U.S.A.

INTERNATIONAL JOURNAL

OPTICA ACTA

European Journal of Optics | **Journal Européen d'Optique** | **Europäische Zeitschrift für Optik**

Contents of April, 1959

Price per part £1 (1375 fr.), (DM 11.75), ($2.80), plus postage

Subscription price per volume (4 parts) £3 15s. (5155 fr.), (DM 44), ($10.50), post free, payable in advance

Printed and Published by

TAYLOR & FRANCIS LTD

RED LION COURT, FLEET STREET, LONDON, E.C.4

The Effect of Surface Films on the Slip of Substrates†

By T. Evans‡ and D. R. Schwarzenberger
Tube Investments Research Laboratories, Hinxton Hall,
Nr. Saffron Walden, Essex

[Received October 30, 1958; and in revised form February 13, 1959]

Abstract

The influence which surface polycrystalline films of carbon, platinum, iron and chromium have on the slip distribution of deformed single crystal specimens of silver has been examined by electron microscopy using a new technique. A thin oriented film of gold has been evaporated on the surface of silver specimens and the polycrystalline film deposited on the gold film. After deformation of the specimens and subsequent stripping of the composite films, the gold film has given information about the slip distribution in the substrate which has been found to be influenced by the presence of the surface polycrystalline film. It is proposed that this influence depends upon the adhesion between the surface film and the substrate and also the mechanical properties of the film itself.

§ 1. Introduction

Since the discovery by Roscoe in 1934 that oxide films on cadmium single crystals increased their critical shear strength and also strengthened the crystals even at high strains, much work has been done on the effects of surface films on the mechanical properties of crystals. It has been demonstrated (see for instance Pickus and Parker 1951) that surface films decrease the creep rate of single crystals whilst Gilman (1952) showed that the critical shear stress for twinning in zinc single crystals can be raised by 50% when they are copper plated. A comparison by many workers (e.g. Andrade and Henderson 1951, Gilman and Read 1952) of the stress-strain curves of many types of single crystals with and without surface films on them has confirmed the Roscoe effect. The influence of the surface films cannot be explained in terms of load sharing as this would make the strengths of the films impossibly large, so it appears that the mechanical deformation of the crystals themselves is being influenced.

Shapiro and Read (1951) have compared the rate of increase of internal friction with vibration amplitude for cadmium single crystals with and without oxide coatings during deformation. The rate was much more rapid for the coated crystals. This implies that the primary effect of the oxide film was to hinder the exit of dislocations from the surface thus causing them to pile up under the film. Further evidence for this has

† Communicated by the Authors.
‡ Now at the Physics Department, University of Reading, Berkshire.

been obtained by Gilman (1955) from a study of the reflection of monochromatic x-rays from the surfaces of zinc crystals. He found that the presence of a 1000 Å copper film resulted in greater surface distortion which again indicates that the primary effect of the films is a hindrance to the exit of dislocations; the greater surface distortion being due to possible piled up groups of dislocations under the surface films. Metzger and Read (1958) confirm that the main effect is probably the hindrance to the exit of dislocations from the surface.

The experiments reported in the present paper were done to obtain information about the mechanism by which these surface films modify the mechanical properties of the crystals by examining the influence upon the slip in the underlying crystal and attempting to correlate it with the way in which the surface films have deformed. The experiments were performed with single crystals of silver coated on one surface with an oriented single crystal film of gold. Brame and Evans (1958) showed that when such a specimen is deformed, the mobile dislocations pass from the silver through the gold film, producing slip in the silver and gold. This type of specimen can therefore be considered as one which exhibits fine slip which can be investigated by detaching the gold film after deformation and examining it by transmission in the electron microscope. The effect of a polycrystalline film on the slip pattern has now been investigated by evaporating such a film on to the specimen, deforming, and examining both films together and in isolation. Polycrystalline films of different materials have been used, and the observations made with these suggest that the magnitude of the effect which a film has in influencing the deformation of the substrate depends upon the adhesion between the two and upon the mechanical properties of the film itself.

§ 2. Experimental Procedure

Silver single crystals in the shape of tensile specimens were produced by a soft mould technique (Brame and Evans 1958). The surfaces were prepared by chemical polish and ionic bombardment followed immediately by evaporation of a gold film, 300 Å in thickness with a substrate temperature of 270°C. Polycrystalline films of carbon, platinum, iron or chromium with a nominal thickness of 300 Å were then evaporated on the oriented gold films with the substrate maintained at room temperature or at slightly elevated temperatures (up to 120°C). In all cases, the grain size of the polycrystalline films was less than 200 Å. Figure 1 represents this composite specimen. The specimens were deformed in tension to approximately 15% elongation and the films detached for examination in the Siemens electron microscope (Elmiskop I) operating at 80 kv. In the cases of carbon, platinum and chromium polycrystalline films, the single crystal gold and the polycrystalline films were detached together by attacking the silver substrate with dilute nitric acid. The slip distribution in the substrates was examined by dissolving away the polycrystalline

film and examining the gold film in isolation. The double layer examination thus gave information on how the polycrystalline film accommodated the applied strain, and also on the relation between this and the deformation in the gold film, whilst examination of the gold films alone indicated the type of deformation undergone by the substrate. However, for iron polycrystalline films it was not possible to carry out this procedure fully as the iron was dissolved extremely rapidly in the nitric acid and only the gold film was available for examination. Information on the structure of all these films could be obtained by transmission electron diffraction. The results presented represent behaviour which appears typical for the various polycrystalline films investigated with a large number of specimens.

Fig. 1

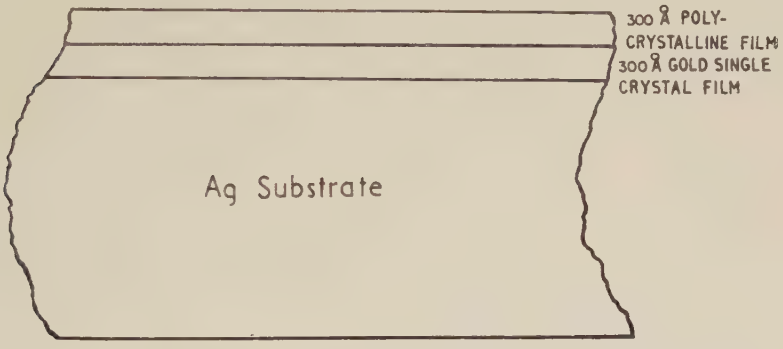

§ 3. Results

3.1. *Oriented Gold Films on Silver Substrates*

Before considering the effects of polycrystalline films on the slip in the substrate, it is necessary to examine the deformation of the silver single crystals in the presence of an oriented gold film alone. It has been shown (Brame and Evans 1958) that the gold film deforms by fine slip from dislocation sources in the silver. In an effort to determine the amount of slip which takes place on an individual slip plane, a single crystal gold film, 50 Å in thickness, was oriented on a silver substrate. The substrate orientation was such that the primary slip plane made an angle of 45° with the surface and the slip direction was 55° to the slip trace. Occasionally the gold film slipped off as shown diagrammatically in fig. 2; but usually only slip traces appeared. Figure 3 (Pl. 93) shows a slipped off part of the gold film with a definite slip line extending from both ends of the crack. This result implies that with a gold film present on the surface, the elementary slip distance is markedly less than about 100 Å. with a step height of less than about 70 Å. It has not been possible to show experimentally whether or not this is the normal slip distance for a similar clean silver specimen. Intuitively it would be expected that the gold

would have some influence in reducing the step height and causing more dislocation sources to become operative in the silver. Nevertheless, as slip lines are formed through the gold film, the mode of deformation of the composite specimen can be considered as representative of the silver alone.

Fig. 2

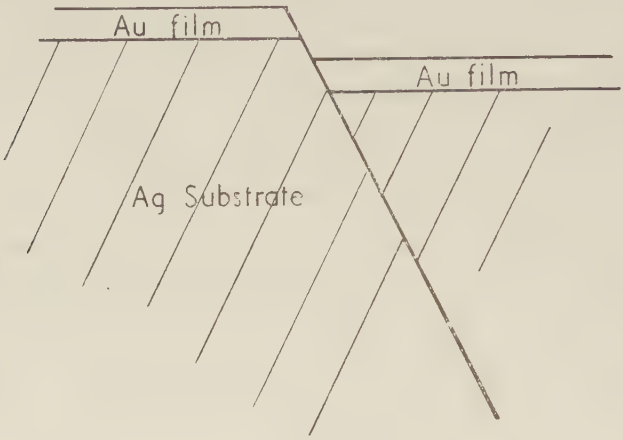

3.2. *Polycrystalline Films on the Oriented Gold Film*

3.2.1. *Carbon polycrystalline films*

In the first series of experiments, a carbon film, 300 A in thickness, was deposited onto the oriented gold film with the substrate at room temperature. The specimen was then deformed in tension and the gold/carbon double-layer examined. Transmission diffraction showed that in all cases the carbon film was substantially amorphous. The carbon film accommodated the applied strain entirely by cracking perpendicular to the tensile direction with the crack direction bearing no relation to the slip traces in the underlying gold film. This implies that the carbon film was sufficiently adherent to the gold for the stress to be transmitted but not sufficiently adherent for the detailed deformation of the gold surface (i.e. formation of slip steps) to influence the nature of the cracking. The slip in the gold film was not obviously changed by the presence of the carbon film. Figure 4 (*a*) (Pl. 94) shows a transmission micrograph of a gold–carbon double-layer in which the parallel carbon cracks are perpendicular to the tensile direction, AB. The slip traces visible due to purely thickness contrast in the gold appear along directions CD and EF. These bear no relation to the carbon cracking direction. The definition of the slip lines is unfortunately reduced owing to the presence of the carbon film. Figure 4 (*b*) shows a micrograph at higher magnification in which the slip traces can be seen more clearly. It is also evident that the carbon film between the cracks has relaxed as the cracks have opened which indicates that a large amount of detachment from the gold film has occurred.

3.2.2. *Platinum polycrystalline films*

A polycrystalline film of platinum was deposited onto the gold, again with the substrate at room temperature. Subsequent deformation and examination of the double layer showed that, unlike the previous case,the cracks in the platinum film were in the same direction as the slip in the substrate. Figure 5 (Pl. 95), for example, is a transmission micrograph of a gold platinum double-layer. It is possible to detect the slip in the underlying gold film along direction AB, parallel to the cracks in the platinum. It is also interesting to note that there does not appear to be heavy deformation in the gold film where the platinum cracks. The change in the crack direction from carbon to platinum shows that, in the latter case, the platinum film adheres sufficiently for the detailed deformation of the substrate to influence the mode of deformation of the platinum film. Examination of the gold film after removal of the platinum shows that the presence of the polycrystalline film does not noticeably influence the distribution of slip in the substrate. As with carbon, relaxation of the platinum film occurs which opens the cracks.

3.2.3. *Iron polycrystalline films*

Polycrystalline films of iron deposited with the substrate at room temperature showed varying effects on the underlying gold films with different specimens: these possibly arise from variations in the initial substrate orientation. In some cases the slip appeared to be unchanged by the presence of the overlying iron film, whilst in others there was a distinct clustering of the slip into coarse bands with some fine slip in between. Figure 6 (Pl. 95) shows this kind of deformation in the gold film. When the substrate temperature was raised to between 70°C and 120°C for the evaporation of the iron the clustering of the slip was accentuated with a consequent diminution of the fine slip in between. Figure 7 (Pl. 96) shows a gold film which had been extracted after deformation from a specimen on which the iron film had been deposited at 100°C. Examination of the iron films themselves showed that they had cracked in well-defined directions, found by optical examination to be along the slip traces.

3.2.4. *Chromium polycrystalline films*

When polycrystalline chromium films were deposited with the substrate at room temperature the effects on the slip in the gold film were most marked. Examination of the gold/chromium double-layer showed that the chromium had cracked in preferred directions, with the underlying gold also cracking within the chromium cracks. Between the main cracks in the chromium were subsidiary smaller cracks within which the gold film had not cracked. Figure 8 (Pl. 97) shows the cracking of the chromium with the associated cracking of the underlying gold film. Examination of the gold film in isolation made it definite that the deformation of the substrate had taken place in extremely localized bands with

no fine slip whatsoever between these coarse bands. Figure 9 (Pl. 97) shows such a region and emphasizes the strong influence which the chromium film had in modifying the mode of deformation of the substrate. It is concluded from this evidence that the slip in the substrate is now effectively confined to the cracked regions of the overlying chromium and the fine slip which is associated with clean crystals has now been completely inhibited. Although the cracks in the chromium have opened out it is considered that this is not due to extensive detachment but to the exceptional elongation of the substrate surface arising from the localization of the slip.

§ 4. Further Experiment

The effect of removing an overlying polycrystalline film has been investigated in the following manner. An oriented gold film was evaporated on a single crystal silver specimen and a polycrystalline iron specimen deposited on this, using a substrate temperature of 120°c. The specimen was deformed in tension and then cut in half, care being taken to keep the deformation due to cutting in an extremely localized region. The gold film recovered from one half showed that the deformation had been localized into bands with very little fine slip in between (fig. 10, Pl. 98). From the other half the iron was removed by exposure to nitric acid fumes, and the specimen then given a second deformation in tension. In this case the gold film showed the course bands associated with the first deformation, but, also between them and parallel to them abundant fine slip due to the second deformation, as shown in fig. 11 (Pl. 98). These results are consistent with the hypothesis that the main function of surface films in strengthening single crystals is to inhibit the passage of dislocations out of the surface.

§ 5. Discussion

The results of previous workers favour the hypothesis that when a plated crystal is deformed, the dislocations pile up below the film. For significant plastic deformation to occur it is necessary to consider how these dislocations move out of the surface despite the presence of the surface film. It is not conceivable that the dislocations from the substrate pass through the film as this is usually finely polycrystalline, and thus unfavourable for transfer. When they move out of the crystal surface there is a relative shift in the surfaces on either side of the slip plane, which forms a step if the dislocations have an edge component and no step if they are pure screws. The thin polycrystalline film could accommodate the resulting stress in a number of ways.

(1) The film could adhere perfectly and crack along the slip traces as shown in fig. 12. In such a case it is probable that the surface film cracks along the slip trace due to the stress concentration produced by the surface distortion resulting from the piled-up dislocations. This type of cracking would result for all types of dislocation if no detachment occurred.

(2) There is a detachment of the film which would tend to reduce the stress concentration set up by the relative shift in the surfaces on either side of a slip trace. The case of edge dislocations moving out of the surface in a slip plane making an angle α will first be considered. Figure 13 illustrates the step formed on the surface with the film partially detached

Fig. 12

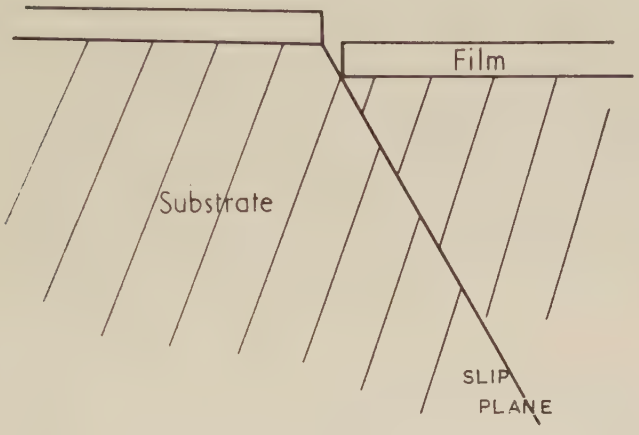

Fig. 13

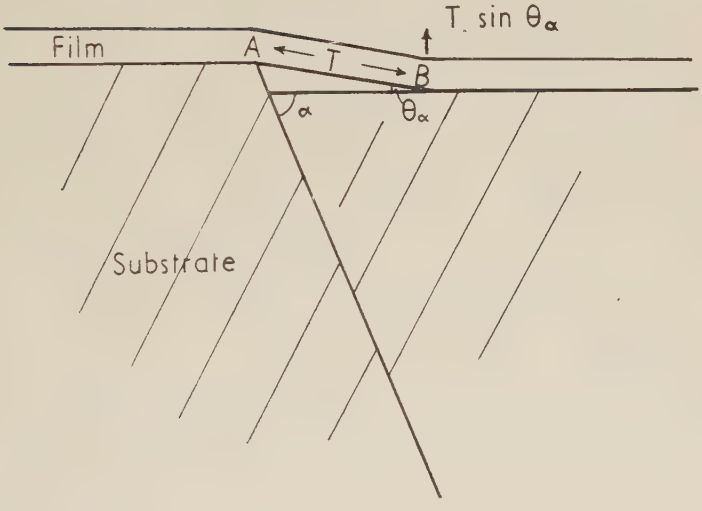

on one side and making an angle θ_α with the crystal surface. If the stress in portion AB of the film is T and the adhesion term ($T \sin \theta_\alpha$) is constant it can be shown that the strain along AB is then independent of the step height. This implies that if the film cracks above a slip trace with the emergence of edge dislocations it would crack immediately a step begins to form without detachment. Lipsett and King (1957) found that for

such dislocations passing out of the surface of their cadmium single crystals there was no optical evidence for detachment of the gold surface film from the substrate. However, in the experiments with the platinum polycrystalline films extensive detachment occurred together with cracking above the slip traces. For this to occur in the case of the emergence of edge dislocations it would be necessary for the stripping of the film to be restricted so that a stress concentration sufficient to crack the film could be formed above the slip trace.

With the emergence of screw dislocations any detachment of the film would be accompanied by a movement of the film in a symmetrical way on either side of the slip trace. The movement of the film is not a detachment by lifting perpendicular to the surface as in the case of edge dislocations but is a sliding of the film over the substrate surface as indicated in fig. 14. On either side of the slip trace there is a relative shift of the substrate by an amount $n\bar{b}$ where n = number of dislocations of the Burgers

Fig. 14

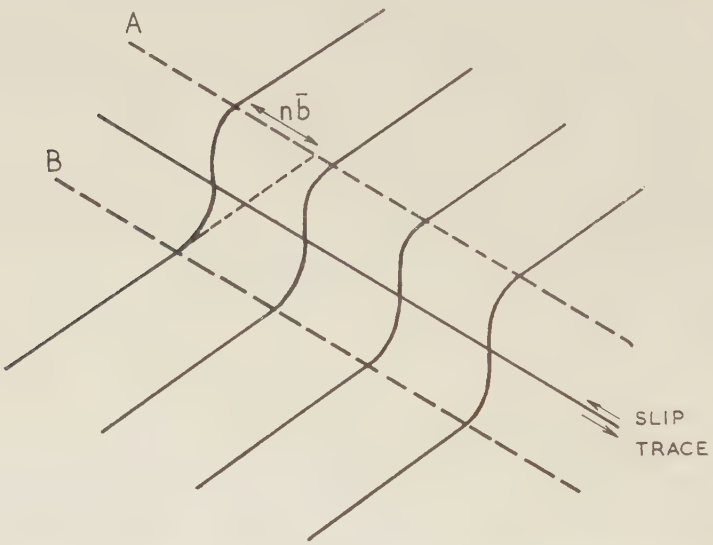

vector $\bar{b}$ which have passed out of the surface, and the film must slide by this amount to accommodate the strain without cracking. The amount of detachment which the film undergoes, i.e. the distance AB, determines whether or not a sufficient strain can be set up in the film above the slip trace to crack the film. Lipsett and King's observations showed that a large amount of loosening and flaking of the film occurred where screw dislocations emerge from the surface and they infer that more detachment of the film occurs in this case than when edge dislocations emerge. The film prefers to detach rather than crack owing to the shearing nature of the strains in the film when screw dislocations emerge as opposed to the tensile strains for edge dislocations.

With the emergence of general dislocations with edge and screw components, it appears from the above considerations that the mode of cracking is determined by the adherence of the film to the substrate. The edge component requires a restriction of the stripping to set up a stress concentration sufficient to crack the film in tension whilst the screw component favours sliding over the surface which must again be limited to set up an appreciable stress concentration above the slip traces. Both these cases are related to the adhesion between the film and substrate, the higher the adhesion, the more favourable is the possibility of cracking above the slip traces. With a carbon film, the underlying slip traces in the substrate did not set up sufficient stress concentrations to cause the film to crack along them; cracking in this case occurred perpendicular to the tensile direction as would be expected with a loosely adhering film. The cracks opened on the gold substrate which also supports the hypothesis of a loosely adhering film being allowed to relax after cracking. Platinum, iron and chromium films however possessed sufficient adhesion to allow the slip traces to concentrate stresses sufficient to cause the localized cracking directed along their length.

The mechanical properties of the polycrystalline film itself are also important in determining the process of cracking. It has been assumed in the analysis that the film is perfectly elastic up to the breaking strain. This is supported by the fact that no thinned regions have been observed on either side of the cracks. It is probable that with these fine-grained films any plastic deformation would be confined to grain boundary movement leading to cracking at the grain boundaries. Although attention has been confined to the relative adhesion between film and substrate, the various films have different elastic ranges, elastic moduli and breaking strains, depending upon the strengths of the grain boundaries.

The mode of deformation of the substrate after the overlying film has cracked will now be considered. In the case of platinum where the characteristic fine slip was still found in the gold the film had become sufficiently detached because of the comparatively low adhesion for it not to present a large enough barrier to the emergence of dislocations which form the fine slip traces. This is supported by the fact that the cracks in the platinum opened appreciably on the gold due to relaxation of the film on the substrate after deformation. In the case of the iron however, where bunching of the slip was observed, the limited detachment at the cracked regions now made these parts favourable for the emergence of dislocations as illustrated in fig. 15. Thus the deformation in the substrate was almost completely confined to slipping in regions where cracking had occurred in the overlying iron film. However, some fine slip could still be seen between the bunches. This was not the case in the observations made with chromium. Here the deformation of the substrate was exclusively confined to slip at the chromium cracks which implies that there was a limited amount of detachment at the cracked regions which became favoured positions for slip in preference to other parts where

the film was still strongly adhering and inhibiting slip. The experiments indicate that the chromium films were the most strongly adhering.

We may conclude that the experiments support the hypothesis that the adherence and the mechanical properties of an evaporated polycrystalline film determine the way in which the deformation of the substrate is modified. These determine the effectiveness of the film in inhibiting slip from the surface. Any slip which does occur after cracking tends to be confined to those regions of the substrate in the neighbourhood of cracks.

Fig. 15

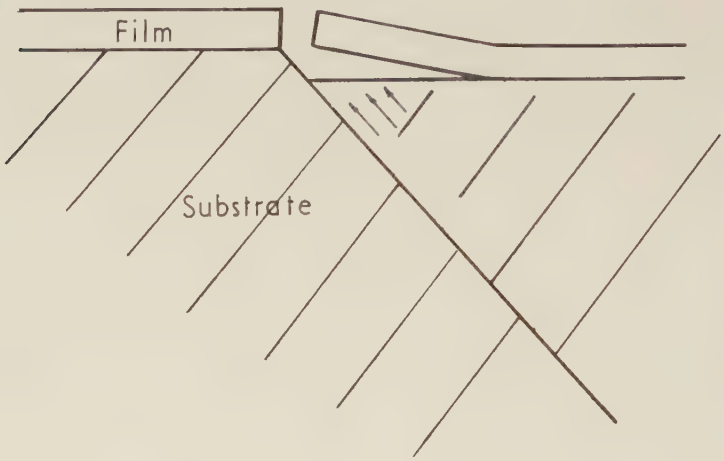

Acknowledgments

The authors wish to thank Dr. J. W. Menter for his interest throughout this work. This paper is published by permission of the Chairman of Tube Investments Limited.

References

Andrade, E. N. da C., and Henderson G., 1951, *Phil. Trans. roy. Soc.* A, **244,** 177.

Brame, D. R., and Evans, T., 1958, *Phil. Mag.*, **3,** 971.

Gilman, J. J., 1952, *Nature, Lond.*, **169,** 149; 1955, *A.S.T.M. Special Technical Publication*, No. 171, 3.

Gilman, J. J., and Read, T. A., 1952, *Trans. Amer. min. (metall.) Engrs*, **194** (*J. Metals*, **4**), 875.

Lipsett, F. R., and King, R., 1957, *Proc. phys. Soc. Lond.* B, **70,** 608.

Metzger, M., and Read, T. A., 1958, *Trans. Amer. Inst. Radio Engrs, N.Y.*, **212,** 236.

Pickus, M. R., and Parker, E. R., 1951, *Trans. Amer. Inst. min. (metall.) Engrs*, **191** (*J. Metals*, 3), 792.

Roscoe, R., *Nature, Lond.*, **133,** 912.

Shapiro, S., and Read, T. A., 1951, *Phys. Rev.*, **82,** 341.

Isotope Effect in Vacancy Diffusion†

By K. Tharmalingam and A. B. Lidiard
Department of Physics, University of Reading, Berkshire

[Received March 12, 1959]

Abstract

The experimental determination of correlation factors in diffusion in crystals is of great value in elucidating diffusion mechanisms. Schoen (1958) has recently proposed a method applicable to both metals and non-metals based on measurements of the relative diffusion rates of two different isotopes of the diffusing element. His analysis was based on an equation derived from an approximate expression for the correlation factor for vacancy diffusion. It is shown in the present paper that his basic equation is exact for all systems having at least two-fold rotational symmetry about the vacancy-solute jump directions.

§ 1. Introduction

It is a feature of many mechanisms of atomic diffusion in crystalline solids that the directions of successive jumps of an atom are correlated. The existence of these correlations introduces an additional factor into the expression for the diffusion coefficient. This correlation factor, as it is called, can in principle be calculated exactly when the diffusion mechanism is specified; and considerable importance is therefore attached to the experimental determination of correlation factors alone, since direct information about the diffusion mechanism can thereby be obtained. This approach has been successfully exploited in the cases of AgBr and AgCl to demonstrate the occurrence of migration by the interstitialcy mechanism (Compton and Maurer 1956, Friauf 1957, Miller and Maurer 1958; see also Compaan and Haven 1958). These materials are ionic conductors and the correlation factor for self-diffusion was obtained from the ratio of a radioactive tracer diffusion coefficient to ionic conductivity. An approach of comparable directness but applicable particularly to metals has been suggested by Schoen (1958) in a recent important letter. Schoen points out that correlation factors for both self- and impurity-diffusion may be obtained from accurate studies of the relative diffusion rates of two different isotopes of the diffusing species.

The principle behind Schoen's discussion is that in going from one isotope to another of differing mass we change one of the jump frequencies in a known way and hence change the correlation factor in a way which is calculable. The jump frequency which is changed is that for the isotope jump—in proportion to the inverse square root of the mass, as follows

† Communicated by the Authors.

from general statistical mechanical arguments (conclusion to § 3). In calculating the influence of this change upon the correlation factor for vacancy mechanisms Schoen uses an approximate expression derived elsewhere in this journal (Lidiard 1955, LeClaire and Lidiard 1956). If the correlation factor for isotope α is ϕ_α then that for isotope β is

$$\phi_\beta = \left[1 + \frac{(1-\phi_\alpha)}{\phi_\alpha}\left(\frac{m_\alpha}{m_\beta}\right)^{1/2}\right]^{-1}. \quad . \quad . \quad . \quad . \quad . \quad (1.1)$$

In addition Schoen shows that the two diffusion coefficients D_α and D_β are then related by

$$\left(\frac{D_\beta}{D_\alpha} - 1\right) \Big/ \left(\left(\frac{m_\alpha}{m_\beta}\right)^{1/2} - 1\right) = \phi_\beta. \quad . \quad . \quad . \quad . \quad . \quad (1.2)$$

In the absence of correlation effects the left hand side would be unity. Equation (1.2) applies equally to self-diffusion and to impurity-diffusion. The possibility of determining correlation factors in metals is of great importance for the determination of the underlying physical factors. In the case of self-diffusion eqn. (1.2) permits a direct test of the vacancy mechanism, since values of ϕ have been calculated (Compaan and Haven 1958), whereas in impurity diffusion experimental values of ϕ will tell us which are the rate determining vacancy jumps —information very relevant to an electronic theory of diffusion parameters (e.g. Lazarus 1954).

In later work Schoen (1959) found that eqn. (1.1) could also be deduced from higher approximations to the correlation factor in cubic lattices. This suggested that (1.1) was true exactly and it is the purpose of the present paper to demonstrate its validity for systems having at least two-fold rotational symmetry about the atomic jump directions; e.g. self-diffusion and impurity diffusion in pure solutes having cubic lattices.

§ 2. Notation and Method

The diffusion coefficient can be calculated by using the method of random walks, by means of which the diffusion coefficient is related simply to the mean square displacement of an atom from its initial position. When the diffusing atoms are moved by the agency of vacancies present in low concentration the correlation factor can be calculated from the averaged movement of a single atom as caused by a single vacancy. In particular for systems having rotational symmetry about all jump directions of the diffusing atom (henceforth called the solute) the correlation factor is

$$\phi = \frac{1 + \overline{\cos\theta}}{1 - \overline{\cos\theta}}, \quad . \quad . \quad . \quad . \quad . \quad . \quad . \quad . \quad (2.1)$$

in which $\overline{\cos\theta}$ is the mean cosine of the angle between two successive jumps of the solute atom (Compaan and Haven 1956, LeClaire and Lidiard 1956). We shall here employ the matrix formulation as set out in the second of these two papers and shall relate $\overline{\cos\theta}$ for atom α to $\overline{\cos\theta}$ for atom β, assuming that the only jump frequency which is changed is that for solute-vacancy exchange.

In order to explain our basic equation clearly we show in the figure a small section of a f.c.e. lattice; but our formulation applies to all lattices having the necessary symmetry.

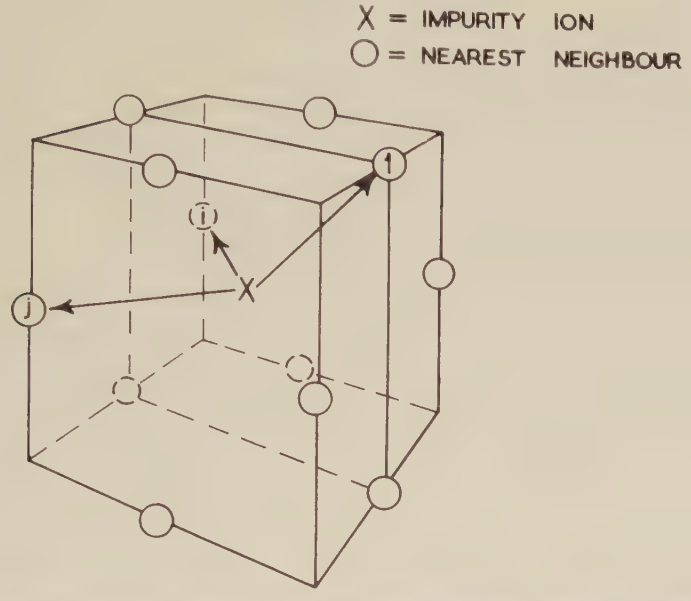

Solute atom X (origin) and its twelve nearest neighbour sites in a f.c.e. lattice. It is supposed that the atom has just jumped from position 1 so that a vacancy is initially present at this site. $\overline{\cos\theta}$ is then obtained from the probabilities that the vacancy will return to the origin from the various sites $i=1 \ldots 12$, by summing the product of each probability with the corresponding $\cos\theta$ value.

Let the impurity atom define the origin of sites and let all other sites be numbered 1, 2, ... i, etc.; i from 1 to z specifies the nearest neighbours to the origin and i from $z+1$ to z' specifies those more distant sites which can be reached by two successive nearest neighbour displacements from the origin ($z'=54$ for f.c.c.). We suppose that the vacancy is initially at site 1, the solute and the vacancy having just exchanged places. The vacancy is now allowed to undergo further jumps: at each stage we require the probability that the vacancy has returned to the origin (thereby moving the solute for the second time). It is convenient to introduce a column matrix $\mathbf{p}_n$ each of whose elements p_{ni} is the probability that after n jumps site i is occupied by a vacancy. The elements of $\mathbf{p}_n$ are related to those of $\mathbf{p}_{n-1}$ by a set of linear equations, each coefficient P_{ij} being the probability that a vacancy at site j goes to site i as it makes its nth jump. In matrix notation

$$\mathbf{p}_n = \mathbf{P}\mathbf{p}_{n-1}. \quad \ldots\ldots\ldots \quad (2.2)$$

The origin site is not included in the $\mathbf{p}_n$ or in $\mathbf{P}$ since we are only interested in the first occasion on which the vacancy arrives back at the origin. If the chance that a vacancy on site i ($i = 1, \ldots z$) goes back to the origin as it jumps is g, then we can write

$$\overline{\cos\theta} = -g \sum_{n=0}^{\infty} \boldsymbol{\tau}\mathbf{p}_n, \qquad (2.3)$$

in which the row matrix $\boldsymbol{\tau}$ has elements which are zero for $i > z$ and are $+\cos\theta_{1i}$ for $1 \leqslant i \leqslant z$, θ_{1i} being the angle between the $0 \to 1$ and the $0 \to i$ direction. By (2.2) and (2.3) we have

$$\overline{\cos\theta} = -g\boldsymbol{\tau} \sum_{n=0}^{\infty} \mathbf{P}^n\mathbf{p}_0,$$

in which $\mathbf{p}_0$, the initial probability density has elements $p_{0i} = \delta_{i1}$. On introducing the matrix $(\mathbf{I} - \mathbf{P})^{-1}$ we can write

$$\overline{\cos\theta} = -g\boldsymbol{\tau}(\mathbf{I} - \mathbf{P})^{-1}\mathbf{p}_0. \qquad (2.4)$$

We can write such an equation for both isotopes α and β of the diffusing element. The matrices $\boldsymbol{\tau}$ and $\mathbf{p}_0$ are the same in both cases. But the two solute-vacancy exchange frequencies differ, other jump frequencies remaining unaltered. Hence g is changed and some elements P_{ij} are changed. The method by which we shall relate $\overline{\cos\theta_\beta}$ to $\overline{\cos\theta_\alpha}$ is to express $\mathbf{P}_\beta$ in terms of $\mathbf{P}_\alpha$ and the matrix of changed elements. In this way we shall now demonstrate eqn. (1.1).

§ 3. Demonstration of Eqn. (1.1)

We shall need the following lemma.

Lemma: The row matrix $\boldsymbol{\tau}$ is an eigenvector of the matrix $\mathbf{S}$ where

$$S_{ij} = [(I - P)^{-1}]_{ij}, \quad 1 \leqslant j \leqslant z$$
$$= 0, \quad j > z.$$

Since τ_k is zero if $k > z$ it will be sufficient to show that $\boldsymbol{\tau}$ is an eigenvector of the matrix $\mathbf{S}'$

$$S_{ij}' = [(I - P)^{-1}]_{ij}, \quad 1 \leqslant i, j \leqslant z,$$
$$= 0 \text{ otherwise.}$$

We notice that $(P^n)_{ij}$ gives the probability that a vacancy initially at site j be at site i after n jumps. For i and j both in the first coordination shell (i.e. $i, j \leqslant z$) elements $(P^n)_{ij}$ are the same for those pairs i, j standing in equivalent relation to the origin. In systems having rotational symmetry about all z directions $0 \to i$, this means equal angles between $0 \to i$ and $0 \to j$. The same must be true of the elements S_{ij}'. Each column of $\mathbf{S}'$ thus contains the same z elements in a different order, and in column j equal elements appear for sites i for which $\cos\theta_{ij}$ is the same. Now we may erect spatial vectors from the origin to each site i having magnitude given by S_{ij}'; and these will form a symmetrical array about the axis $0 \to j$.

The process of multiplying $\boldsymbol{\tau}$ into the jth column of $\mathbf{S}'$ multiplies each element by $\cos\theta_{1i}$. This is equivalent to resolving the vectors which we erected on to the direction $0\rightarrow 1$ and adding the result. But equally well we could add the individual vectors and resolve the sum. The sum is in the direction $0\rightarrow j$, by rotational symmetry, and of magnitude independent of j. Hence the result of multiplying $\boldsymbol{\tau}$ into the jth column of $\mathbf{S}'$ is a constant times $\cos\theta_{1j}$, i.e. we may write

$$\boldsymbol{\tau}\mathbf{S}'=\lambda\boldsymbol{\tau}, \qquad . \; . \; . \; . \; . \; . \; . \; . \; . \qquad (3.1)$$

in which the constant λ is the product of $\boldsymbol{\tau}$ with the first column of S'. Equation (3.1) therefore establishes our lemma.

To proceed with the proof we need to examine the changes in $\mathbf{P}$ in going from α to β. Clearly no change in P_{ij} results for $j>z$. Changes are produced in those elements for which $1\leqslant j\leqslant z$ and $1\leqslant i\leqslant z'$ where z' is the total number of sites which can be reached by not more than two nearest neighbour displacements from the origin. It may be noted that none of the absolute jump *frequencies* corresponding to the vacancy displacements $j\rightarrow i$ is altered, but the *relative* probabilities which make up $\mathbf{P}$ are altered; vacancies in nearest neighbour positions exchange at different rates with the two isotopes and their *relative* probability of jumping to other sites is changed in consequence. All the elements altered in going from α to β are changed in the same proportion, r. Hence

$$(P_\beta)_{ij}=r(P_\alpha)_{ij}, \quad \begin{cases} 1\leqslant i\leqslant z' \\ 1\leqslant j\leqslant z \end{cases}.$$

We can therefore write

$$\mathbf{P}_\beta=\mathbf{P}_\alpha+(r-1)\mathbf{F}, \qquad . \; . \; . \; . \; . \; . \; . \; . \qquad (3.2)$$

in which

$$F_{ij}=(P_\alpha)_{ij}, \quad \begin{cases} 1\leqslant i\leqslant z' \\ 1\leqslant j\leqslant z \end{cases},$$

$$=0 \text{ otherwise.} \qquad . \; . \; . \; . \; . \; . \; . \qquad (3.3)$$

It follows that

$$(\mathbf{I}-\mathbf{P}_\beta)^{-1}=(\mathbf{I}-\mathbf{P}_\alpha-(r-1)\mathbf{F})^{-1}$$

$$=(\mathbf{I}-(r-1)(\mathbf{I}-\mathbf{P}_\alpha)^{-1}\mathbf{F})^{-1}(\mathbf{I}-\mathbf{P}_\alpha)^{-1}. \qquad . \; . \; . \; . \qquad (3.4)$$

If we put

$$(\mathbf{I}-\mathbf{P}_\alpha)^{-1}\mathbf{F}\equiv\mathbf{L}, \qquad . \; . \; . \; . \; . \; . \; . \; . \qquad (3.5)$$

then

$$(\mathbf{I}-\mathbf{P}_\beta)^{-1}=\sum_{n=0}^{\infty}(r-1)^n\mathbf{L}^n(\mathbf{I}-\mathbf{P}_\alpha)^{-1}. \qquad . \; . \; . \; . \; . \qquad (3.6)$$

Let us examine the form of $\mathbf{L}$. By (3.5)

$$L_{ik}=\sum_j(I-P_\alpha)_{ij}^{-1}F_{jk}.$$

From (3.3) it then is easy to see that

$$L_{ik}=0 \quad \text{if} \quad k>z$$
$$=\sum_{j=1}^{z'}(I-P_\alpha)_{ij}^{-1}P_{jk}, \quad 1\leqslant k\leqslant z.$$

This last term equals

$$\sum_{j=1}^{\infty}(I-P_\alpha)_{ij}^{-1}P_{jk},$$

since if $1\leqslant k\leqslant z$, P_{jk} is zero for $j>z'$. Hence

$$L_{ik}=-\delta_{ik}+(I-P_\alpha)_{ik}^{-1}, \quad 1\leqslant k\leqslant z$$
$$=0, \quad k>z.$$

By the lemma it follows that $\boldsymbol{\tau}$ is an eigenvector of $\mathbf{L}$

$$\boldsymbol{\tau}\mathbf{L}=(\lambda-1)\boldsymbol{\tau}, \qquad \ldots\ldots\ldots \quad (3.7)$$

in which λ is the product of $\boldsymbol{\tau}$ with the first column of $(\mathbf{I}-\mathbf{P}_\alpha)^{-1}$. Hence

$$\boldsymbol{\tau}\mathbf{L}^n=(\lambda-1)^n\boldsymbol{\tau}. \qquad \ldots\ldots\ldots \quad (3.8)$$

If we now substitute (3.8) and (3.6) into eqn. (2.4) for $\overline{\cos\theta_\beta}$, we get

$$\overline{\cos\theta_\beta}=-g_\beta\sum_{n=0}^{\infty}(r-1)^n(\lambda-1)^n\boldsymbol{\tau}(\mathbf{I}-\mathbf{P}_\alpha)^{-1}\mathbf{p}_0.$$

Now

$$\overline{\cos\theta_\alpha}=-g_\alpha\boldsymbol{\tau}(\mathbf{I}-\mathbf{P}_\alpha)^{-1}\mathbf{p}_0=-g_\alpha\lambda,$$

since the elements of $\mathbf{p}_0$ are zero except the first which is unity. Hence

$$\overline{\cos\theta_\beta}=\frac{g_\beta}{g_\alpha}\frac{\overline{\cos\theta_\alpha}}{(r+(r-1)\overline{\cos\theta_\alpha}/g_\alpha)}.$$

If we denote the ratio of the impurity–vacancy exchange frequencies for atoms β and α by ρ (e.g. $w_2(\beta)$, $w_2(\alpha)$ in notation of previous papers) then it follows that this result reduces to

$$\overline{\cos\theta_\beta}=\frac{\rho\,\overline{\cos\theta_\alpha}}{1+(1-\rho)\overline{\cos\theta_\alpha}}. \qquad \ldots\ldots\ldots \quad (3.9)$$

Combination of eqns. (3.9) and (2.1) gives the corresponding relation between correlation factors ϕ_β and ϕ_α, namely,

$$\phi_\beta=\left[1+\frac{(1-\phi_\alpha)}{\phi_\alpha}\rho\right]^{-1}. \qquad \ldots\ldots\ldots \quad (3.10)$$

It is possible in going from one impurity element to another that the only frequency which is changed is that for impurity–vacancy exchange; in which case eqn. (3.10) gives the relation between the correlation factors of different impurities. But at present this seems rather unrealistic and probably the best use of (3.10) is for two different isotopes of the same

chemical element; for then a general discussion based on statistical mechanics leads us to expect

$$\rho = (m_\alpha/m_\beta)^{1/2}; \quad . \quad . \quad . \quad . \quad . \quad . \quad . \quad . \quad (3.11)$$

whence eqn. (1.1) follows.

We may summarize the argument leading to (3.11) as follows. Firstly we can calculate the number of atoms of a given kind crossing any given plane in the lattice by using the methods of the canonical ensemble (Wert 1950). Since the problem is classical the distribution function $\exp(-E/kT)$ separates into a potential energy factor and a number of independent kinetic energy factors, one for each atom. Changing the mass of an atom without changing its chemical nature leaves the potential energy factor unchanged but changes the appropriate kinetic energy factor through $p^2/2m$. The relative numbers of different isotopes of the same element crossing a given plane are thus dependent only on their masses and are independent of the other masses or forces in the system. Detailed calculation shows the proportionality to be as $m^{-1/2}$. This is exact and is true for any plane. The essential physical aproximation is that if this plane is situated to contain the saddle points for a number of possible vacancy jumps, then none of the atoms crossing into vacancies is reflected back before completing its jump. In view of the height of most potential barriers it seems a very good approximation. The dependence of jump frequency on $m^{-1/2}$ then follows. If appreciable reflection of atoms after they had crossed the saddle point were to occur a slower dependence on mass would be found. Experiments on diffusion of interstitial solutes (e.g. H and D in metals for which there are no correlation effects) seem to rule out the possibility at the present time.

§ 4. Summary and Conclusion

By employing the matrix formulation of the problem of calculating correlation factors for vacancy diffusion we have related the correlation factors for two different isotopes α and β of the same diffusing element. The result applies to both self-diffusion and impurity diffusion and is valid for systems having at least two-fold rotational symmetry about the jump directions. As first shown by Schoen (1958) the relation proved here enables the direct experimental determination of correlation factors. This knowledge is important to any electronic theory of diffusion. This is demonstrated by Schoen's own experimental results on diffusion of ^{109}Cd and ^{115m}Cd tracers in pure silver and copper. Within experimental error no dependence on isotopic mass was disclosed. From this one may deduce that the rate determining step in the diffusion process is vacancy–solvent exchange and not vacancy–solute exchange as often assumed previously. For diffusion of Ni in Cu the converse seems to be true (Johnson 1946).

Acknowledgments

The authors are very much indebted to Dr. A. H. Schoen for discussions and correspondence which led them to the present investigation. One of us (K. T.) wishes to acknowledge a research grant from A.E.R.E., Harwell.

References

Compaan, K., and Haven, Y., 1956, *Trans. Faraday Soc.*, **52,** 786; 1958, *Ibid.*, **54,** 1498.
Compton, W. D., and Maurer, R. J., 1956, *J. Phys. Chem. Solids*, **1,** 191.
Friauf, R. J., 1957, *Phys. Rev.*, **105,** 843.
Johnson, W. A., 1946, *Trans. Amer. Inst. min. (metall.) Engrs*, **166,** 114.
Lazarus, D., 1954, *Phys. Rev.*, **93,** 973.
Le Claire, A. D., and Lidiard, A. B., 1956, *Phil. Mag.*, **1,** 518.
Lidiard, A. B., 1955, *Phil. Mag.*, **46,** 1218.
Miller, A. S., and Maurer, R. J., 1958, *J. Phys. Chem. Solids*, **4,** 196.
Schoen, A. H., 1958, *Phys. Rev. Letters*, **1,** 138; 1959, *Convair Research Note* No. 25.
Wert, C., 1950, *Phys. Rev.*, **79,** 601.

An Unusual Grain Boundary Diffusion Effect in Impure Nickel†

By H. Mykura
Department of Natural Philosophy, The University, Glasgow

[Received March 20, 1959]

Abstract

The formation of ridges at the grain boundaries of nickel during thermal etching has been observed. The effect is attributed to the diffusion of vacancies along the grain boundaries into the specimen, caused by the formation of internal gas bubbles.

§ 1. Introduction

While examining grain boundary grooves in thermally etched nickel, it was found that, while in pure Ni the usual groove profile develops (Mullins 1957), some impure Ni develops ridges at the grain boundaries. These ridges can be conveniently measured with an interference microscope, and typical examples are shown in fig. 1 (Pl. 99). The ridges have the usual grain boundary groove superimposed on them. The ridge height varies widely for different boundaries and changes abruptly when a twin boundary meets a grain boundary, i.e. when the orientation difference across the boundary changes.

Fig. 2

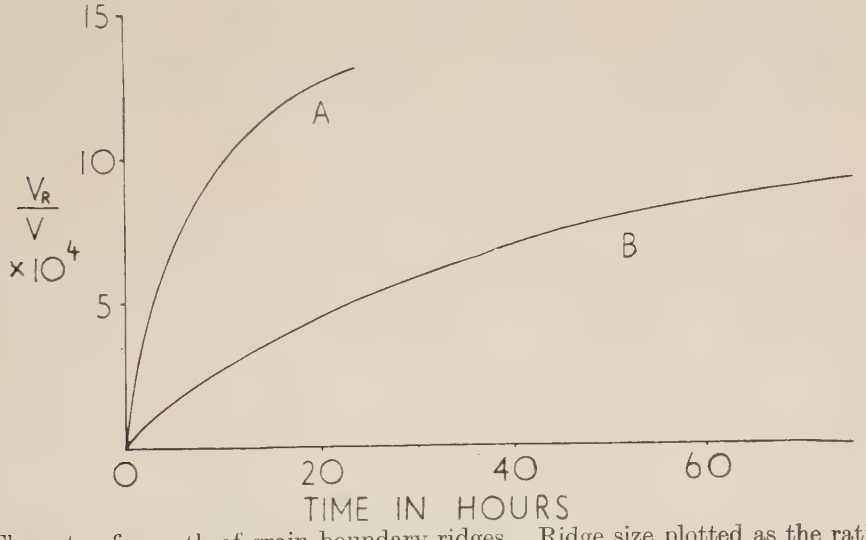

The rate of growth of grain boundary ridges. Ridge size plotted as the ratio ridge volume/specimen volume V_R/V.
A—specimen 0·015 cm thick heated at 1200°C.
B—specimen 0·020 cm thick heated at 1000°C.

† Communicated by the Author.

The ridges grew rapidly at first and then progressively more slowly, the time scale depending on specimen thickness and temperature. As the ridges grew, they became broader and the groove on top of the ridge became more pronounced. Figure 2 shows typical growth curves and fig. 3 the change of shape with time.

The specimens were heated in a vacuum furnace, cooled to room temperature for measurement and then reheated. The working pressure was about 10^{-5} mm of Hg, the residual gas being mainly hydrocarbon oil vapour, so that the residual atmosphere was reducing.

Fig. 3

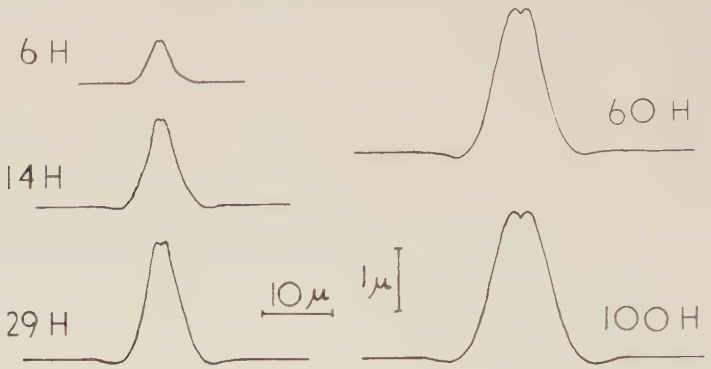

The change of ridge shape with time. Specimen 0·020 cm thick heated at 1000°c.

Ridge formation was always observed with 'Bright Annealed Nickel Foil' (from Johnson, Matthey & Co.) whose nominal maximum non-metallic impurities are: Si 0·10%, C 0·05%, S 0·005%, O—not given. With Johnson-Matthey 'Specpure' Ni and with powder-metallurgically produced Ni (nominally 99·99% pure) from Henry Wiggin & Co., only normal grain boundary grooves were observed.

§ 2. The Mechanism of Ridge Formation

As the ridges were not observed in the two purer nickels, the effect is almost certainly due to impurities. The ridges were similar on all parts of the specimen, irrespective of stresses due to specimen weight, so the effect is not due to extrusion by gross compression stresses.

The diffusion of vacancies into the material along the grain boundary would produce ridges as observed: each vacancy entering the specimen adding one atom to the ridge. The driving force of vacancy diffusion is most likely to be the formation of gas bubbles in the material, as in the experiments of Barnes *et al.* (1958). In those experiments the gas was Helium injected as fast α-particles. Here the bubbles are presumably produced by the formation of CO or H_2O from particles of Oxide and/or carbon present as impurity in the specimen.

A specimen was sectioned, polished and etched after heat treatment and searched for bubbles with an oil-immersion lens but nothing was seen. Any bubbles formed are therefore submicroscopic in size. This is not unexpected; in the experiments of Barnes *et al.* the bubbles were resolved only with an electron microscope and visible optically through their clustering and etching behaviour. In the present experiments bubbles might form at the sites of, say, oxide particles and have a size and spatial distribution less favourable for direct observation.

If one takes the surface free energy of Ni to be 1800 erg cm^{-2} (Hayward and Greenough, to be published) then a bubble of radius 10^{-5} cm would have an equilibrium gas pressure of 360 atm and contain about 80 vacancies per gas molecule. For a radius of 10^{-6} cm the values are 3600 atm and 8 vacancies per gas molecule. The average ridge volume per square centimetre of surface was measured for several specimens heated for a sufficient time to have reached nearly 'saturation' ridge size. The ratio ridge volume specimen volume was $1{\cdot}8 \pm 0{\cdot}6 \times 10^{-3}$, independent of specimen thickness or temperature. If we assume gas bubbles with 20 vacancies per gas molecule, then the observed ridge volume is equivalent to a gas content of about 30 p.p.m. by weight. An approximately equal number of vacancies has probably diffused from the surface direct to a bubble so that the total gas content may be twice this. The author has not had access to a vacuum fusion gas analysis apparatus, so no direct determination of the gas content has been attempted. However, such relatively small gas contents would be difficult to measure accurately on the thin foil specimens used.

§ 3. The Evidence for Vacancy Diffusion along Grain Boundaries

Grain boundary diffusion is known to depend on the orientation difference across the boundary, being least for small orientation differences. Though measurements have been reported only for pure tilt boundaries, the variation should be similar for general (tilt plus twist) boundaries (McLean 1957). The orientations of six pairs of grains were measured and in all cases a large orientation difference was associated with a large grain boundary ridge and small ridges with small orientation differences.

Neither coherent nor incoherent twin boundaries shows grain boundary diffusion effects and no ridges were formed on such boundaries. On the other hand second-order twin boundaries (i.e. boundaries between crystals which have a common twin) should behave like ordinary boundaries, and are in fact found to produce ridges (fig. 1). Barnes *et al.* (1958) distinguish between 'single ended' and 'double ended' incoherent twin boundaries: single ended boundaries joining an ordinary grain boundary at one end while double ended boundaries are between two twin boundaries. They state that single ended boundaries show grain boundary diffusion and double ended do not. In these experiments a large number of incoherent and second order twin boundaries were examined and in all cases second order twin boundaries formed ridges, whether single or double ended, and in no case did either type of incoherent twin boundary show the effect.

The ridge formation phenomenon has also been observed in reverse. On the hypothesis given above, vacancy diffusion should cease when the gas pressure in the bubble is in equilibrium with the pressure due to surface tension. As both vary with temperature, a bubble which is in equilibrium at one temperature will contain excess vacancies when the temperature is lowered. If we assume that no gas is lost from the bubble and apply the perfect gas laws, then the volume ratio

$$\frac{V_2}{V_1} = \left(\frac{\gamma_1 T_2}{\gamma_2 T_1}\right)^{3/2}$$

where T = absolute temperature, γ = surface tension. If $T_2 = 1273°\text{K}$, $T_1 = 1473°\text{K}$, $\gamma_2 = 1900\,\text{erg cm}^{-2}$ and $\gamma_1 = 1800\,\text{erg cm}^{-2}$ then $V_2/V_1 = 0{\cdot}74$. Figure 4 shows the experimental result for a specimen heated first at 1200°C and then at 1000°C. The specimen did not quite reach equilibrium at 1200°C, so the decrease in ridge size (measured value: 1·00 to 0·84) would be expected to be less than the theoretical maximum. While this is only just measurable, the effect is much more striking when a grain boundary has migrated away from its ridge. The vacancies liberated by the shrinking bubbles then produce a grain boundary groove much deeper than normal.

Fig. 4

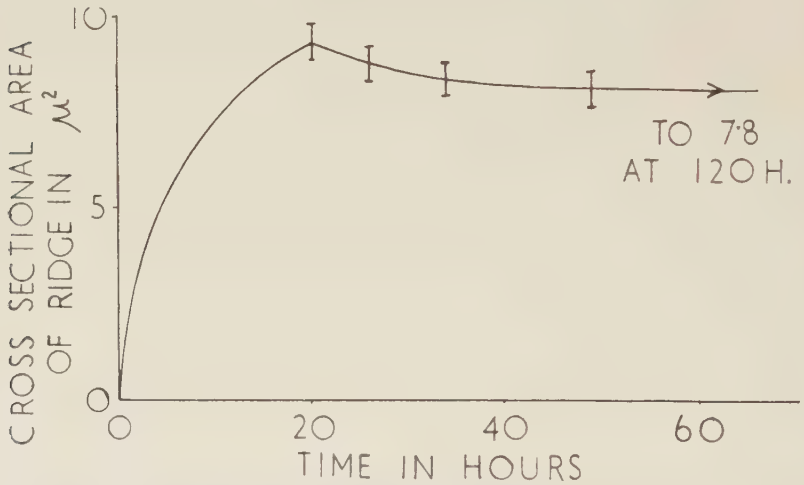

The reduction of ridge size on reheating a specimen at a lower temperature: specimen first heated 20 hours at 1200°C, then heated at 1000°C.

§ 4. Other Observations

The sideways spread of the ridge with time is in accord with surface diffusion theory (Mullins 1957, 1959). The predicted formation of a depression below the original surface on each side of the ridge is just visible (fig. 3).

The rate of ridge growths can be estimated theoretically. If one assumes that grain boundary diffusion is very much faster than volume diffusion, ridge growth will be limited by the diffusion of material out of the grain to the boundary. For all the specimens measured the mean grain diameter ($2r$) was nearly equal to the specimen thickness. One can therefore treat this approximately as the problem of material diffusing out of a sphere of diameter equal to specimen thickness. The solution of the analogous heat conduction equation is given by Carslaw and Jaeger (1947); the time for half the material to diffuse out is $0{\cdot}035r^2/D$. The values of the self diffusion constant D of Ni are extrapolated from Reynolds *et al.* (1957). The results were:

Specimen thickness $2r$	Temperature °C	Self diffusion const., D cm^2 sec^{-1}	Time for ridges to grow to half full size	
			Theory $t=0{\cdot}035r^2/D$	Measured
0·015 cm	1200°C	$1{\cdot}3\times10^{-10}$	$1{\cdot}5\times10^{4}$ sec	8 ± 3 hours
0·005 cm	1200°C	$1{\cdot}3\times10^{-10}$	$1{\cdot}7\times10^{3}$ sec	$1\pm\frac{1}{2}$ hour
0·020 cm	1000°C	$4{\cdot}2\times10^{-12}$	8×10^{5} sec	100 ± 40 hours

In view of the simplifying assumptions, one can say that there is reasonable agreement and that the observed rate of ridge formation is consistent with the diffusion of vacancies from the grain boundaries and surface and the complementary flow of Ni atoms in the opposite direction.

§ 5. Discussion

Prior to the work of Barnes *et al.* (1958) it was generally thought that dislocation lines were the chief source of vacancies in metal crystals. The observations on grain boundary ridges reported here give supporting evidence to the thesis that dislocations are inadequate sources when large numbers of vacancies are required and that vacancies will move from the surface along grain boundaries and into the grains.

Acknowledgment

The author is grateful to the Director, Mechanical Engineering Research Laboratories, East Kilbride, for permission to use an interference microscope.

References

Barnes, R. S., Redding, G. B., and Cottrell, A. H., 1958, *Phil. Mag.*, **3**, 97.
Carslaw, H. C., and Jaeger, J. C., 1947, *The Conduction of Heat in Solids* (Oxford: Clarendon Press).
McLean, D., 1957, *Grain Boundaries in Metals* (Oxford: Clarendon Press).
Mullins, W., 1957, *J. appl. Phys.*, **28**, 333; 1959, *Ibid.*, **30**, 77.
Reynolds, J. E., Averbach, B. L., Cohen, M., and Hilliard, J. E., 1957, *Acta Met.*, **5**, 29.

Dislocation Arrangements in Aluminium Deformed in Tension or by Fatigue†

By R. L. Segall and P. G. Partridge
Crystallographic Laboratory, Cavendish Laboratory, Cambridge

[Received March 6, 1959]

Abstract

A comparison has been made of transmission electron microscope observations on polycrystalline aluminium deformed in tension or by fatigue. The dislocation distribution in aluminium deformed in tension was studied as a function of stress. At stresses up to 3 kg mm^{-2} the distribution is extremely irregular; at higher stresses up to the fracture stress, polygon boundaries are formed which become increasingly well developed with increasing stress. Observations have been made on specimens fatigued at high stress, giving a life of 10^5 cycles, and low stress, giving a life greater than 10^6 cycles. The dislocation distribution in the former is similar to that in the unidirectionally deformed specimens. The low stress fatigue specimens show two new features. Firstly, polygonization does not occur despite a high dislocation density, and secondly a high density of dislocation loops similar to that found in quenched specimens is observed in some areas. The latter observation suggests the formation of large numbers of point defects during fatigue.

§ 1. Introduction

Studies of recovery and recrystallization, of the release of stored energy, of lattice distortion and of flow stress have revealed important differences between initially annealed metals deformed in tension and by fatigue. The behaviour in fatigue depends on the stress level, and, following Kemsley (1956), we arbitrarily define low stress tests as those in which the fatigue life is greater than 10^6 cycles and high stress tests as those in which failure occurs in fewer than 10^5 cycles. Copper failed by fatigue at low stress does not recrystallize; softening occurs by recovery which begins at a temperature below the normal recrystallization temperature and is not complete at 900°c (Wood 1955, Kemsley 1957). Clarebrough *et al.* (1957) showed by a calorimetric method that for copper specimens fatigued at high stress, energy is released by a combination of recovery and recrystallization but for the specimens fatigued at low stress only recovery occurs. Various workers (Gough and Wood 1936, Barrett 1937) have shown that for a number of fatigued metals the spreading of the x-ray diffraction spots along the Debye–Scherrer arcs on back reflection photographs is negligible compared to that on specimens extended unidirectionally to a similar strain.

† Communicated by the Authors.

Broom and his co-workers have studied another important difference between fatigued and unidirectionally deformed material. Experiments by Broom *et al.* (1956) suggested that diffusion rates were increased by cyclic stressing in a number of precipitation-hardening aluminium alloys. Broom and Ham (1957) have observed an increased temperature dependence of the flow stress on fatigued copper and aluminium. This result and the results of their annealing experiments in copper (Broom and Ham 1959) are consistent with the assumption that a considerable number of vacancies in the form of aggregates and possibly single vacancies are produced by fatigue.

In view of these differences it was decided to compare by the transmission electron microscope technique the distribution and density of dislocations in unidirectionally deformed and fatigued aluminium.

§ 2. Experimental Techniques

Both the tensile and fatigue specimens were made from super-pure aluminium (99·99%) supplied by the British Aluminium Co. The tensile specimens were produced from 1/16 in. thick sheet which was reduced 80% by rolling and then cut into strips $0{\cdot}012 \times 0{\cdot}50 \times 2{\cdot}0$ in. The specimens were subsequently annealed in air to produce a grain size of about 10μ. The deformation was performed in tension at a rate of $10^{-5}\,\mathrm{sec}^{-1}$. Under these conditions the specimens fractured at a true stress of about $7\,\mathrm{kg\,mm}^{-2}$ after 35% elongation. Since it was expected that the dislocation arrangement at any point on the curve would be related to the flow stress at that point, subsequent specimens were strained by different amounts corresponding to approximately equal stress increments up to the fracture stress.

In order to ensure in the fatigue studies that the dislocation arrangement was typical of fatigue it was essential to avoid any superimposed unidirectional stresses. While the requirement of zero mean stress is best satisfied by using a thick test piece, the preparation of thin electron microscope specimens from them becomes increasingly difficult. For pure annealed aluminium a satisfactory compromise was made with test pieces 1/16 in. thick, fatigued in plane bending. The fatigue specimens were prepared from 1/16 in. thick sheet annealed to give a similar grain size to that in the tensile specimens. Standard plane bending test pieces of this thickness were then fatigued in reverse plane bending on a commercial Avery testing machine. The stress was adjusted to give fatigue lives between 5×10^4 cycles and 3×10^6 cycles.

Electron transmission microscopy was carried out using a Siemens Elmiskop I operating at 100 kv. The tensile specimens were thinned in the normal way by electropolishing (Tomlinson 1958). It was found that thin foils could be obtained from the 1/16 in. thick specimens provided that these were large enough and that the polishing conditions were carefully controlled. To ensure that the area selected for examination in the fatigue specimens corresponded to the high stress region near the surface of the bend test-piece, initial thinning was carried out from one side only.

the other side being protected with lacquer (Hirsch *et al.* 1959). Final polishing was from both sides, the lacquer being stripped from the protected surface.

§ 3. Deformation in Tension

3.1. *Observations*

Figure 1† shows the positions on the stress/strain curve corresponding to the specimens selected for examination in the electron microscope.

Fig. 1

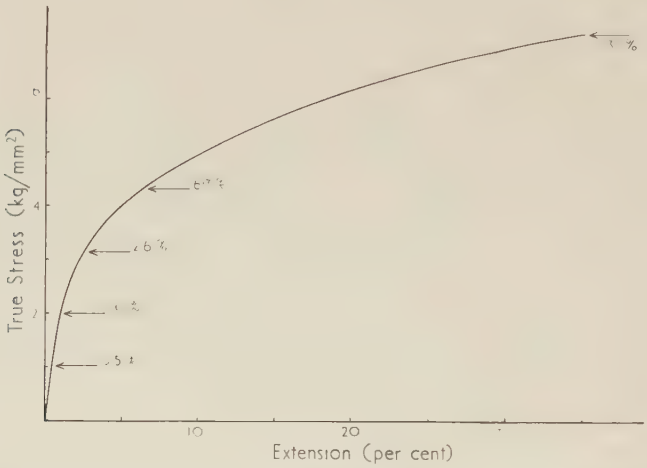

True stress elongation curve for polycrystalline aluminium, showing points at which specimens were selected for examination in the electron microscope.

The appearance of the metal prior to deformation is shown in fig. 2. Only isolated dislocations are present and regions of several hundred square microns completely free of dislocations are often found. The average density of dislocations in annealed specimens is about $5 \times 10^6\,\mathrm{cm}^{-2}$. Specimens stressed to $1\,\mathrm{kg\,mm}^{-2}$ contain many areas similar to those in the annealed material. However, in certain local regions the density in an area of 20 square microns is as high as $5 \times 10^8\,\mathrm{cm}^{-2}$. The individual dislocation lines in these regions tend to be long, often about $10\,\mu$. Typical irregular configurations of dislocations in a region of high dislocation density can be seen in fig. 3. Specimens stressed to $2\,\mathrm{kg\,mm}^{-2}$ still contain areas comparatively free of dislocations but the regions of high density are more frequent and the maximum local dislocation density in an area of 20 square microns is about $7 \times 10^8\,\mathrm{cm}^{-2}$. Many areas however are identical in appearance to those in specimens stressed to $1\,\mathrm{kg\,mm}^{-2}$; in particular the long dislocation lines are still observed (fig. 4).

† All figures except fig. 1 are as plates.

The appearance of the dislocation arrangement in specimens stressed to $3\,\mathrm{kg\,mm^{-2}}$ is however significantly different from that in specimens deformed at lower stresses. Thus there is a tendency for dislocations to occur in groups (fig. 5); furthermore the dislocations are shorter and most areas contain some dislocations. The arrangement suggests that in the densest regions local sub-boundaries are being formed. It should be noted however, that, whilst fig. 5 represents a typical region, there are still some areas of low dislocation density which resemble those found in the specimens stressed to $1\,\mathrm{kg\,mm^{-2}}$ and $2\,\mathrm{kg\,mm^{-2}}$. The density of dislocations in areas similar to that of fig. 5 is about $10^9\,\mathrm{cm^{-2}}$.

At a stress of $4\,\mathrm{kg\,mm^{-2}}$ there are already a few sub-boundaries (fig. 6) which are well developed compared with those found in specimens stressed to $3\,\mathrm{kg\,mm^{-2}}$ (fig. 5). Most of the dislocations in specimens stressed to $4\,\mathrm{kg\,mm^{-2}}$ lie in an irregular sub-boundary network, which separates regions comparatively free of dislocations (figs. 7 and 8). Again a considerable variation in dislocation density is apparent. Figure 7 shows an area very similar to that found in the specimens stressed to $3\,\mathrm{kg\,mm^{-2}}$. However, in the specimen stressed to $4\,\mathrm{kg\,mm^{-2}}$ the overall dislocation density is about $2\times10^9\,\mathrm{cm^{-2}}$.

Figure 9 shows a typical area in a specimen stressed to $7\,\mathrm{kg\,mm^{-2}}$. The cell structure is well developed in most parts of the specimen. The subgrain diameter is about $2\,\mu$ and the average change in orientation across a sub-boundary is about $1°$. In general the regions between the sub-boundaries are free of dislocations. The density of dislocations averaged over both the sub-boundary region and the enclosed low density region was found to be about $4\times10^9\,\mathrm{cm^{-2}}$.

3.2. *Summary*

When considering the dislocation density in relation to the flow stress, it is important to note the extreme irregularity of the dislocation distribution at stresses up to $3\,\mathrm{kg\,mm^{-2}}$. The resistance to deformation is provided not by a uniform internal stress field but by regions of high dislocation density.

At higher stresses the rate of work-hardening decreases and polygonization begins, while the rate of increase of dislocation density also decreases. In a polycrystal the constraints will produce local bending, i.e. dislocations in a local region will tend to be of one sign. The rearrangement of these dislocations to form sub-boundaries is favoured energetically and it is interesting to observe the extremely low dislocation density in the interior of the cells. This is even more marked in material reduced 80% by rolling; here the sub-boundaries are very sharp and the cells seldom contain any dislocations. With increasing stress all the dislocations in the interior of the subgrains appear to be swept into the sub-boundaries.

The results obtained by transmission electron microscopy can be compared with the x-ray microbeam work of Hirsch and Kellar (1952), Hirsch

(1952) and Kelly (1954). Kelly found that the sub-grain size in aluminium reaches a minimum of $2{\cdot}8\,\mu$ after 30% extension, which is in good agreement with the results of the present work. For specimens of initial grain size between $27\,\mu$ and $53\,\mu$ (compared with $10\,\mu$ in the present experiments) Kelly found a total angular misorientation across one original grain of 19° after 30% extension. Assuming uniform bending across the grain this gives an angle between adjacent sub-grains of about 2° for the smallest grain size. This agrees reasonably well with the estimate of 1° made in the present experiments.

It should be noted that dislocation loops are often observed in unidirectionally deformed specimens, see for example at A in figs. 5, 7 and 9.

§ 4. Deformation by Fatigue

4.1. *High Stress Fatigue Experiments*

As discussed in the introduction, high stress fatigue experiments are arbitrarily defined as those in which failure occurs in fewer than 10^5 cycles. The dislocation configuration in these specimens is similar to that observed in unidirectionally deformed specimens. Polygonization is observed, as shown in fig. 10. However, the sub-grain size is larger and the number of dislocations within the sub-grains is greater than that observed in unidirectionally deformed specimens with a similar dislocation density.

4.2. *Low Stress Fatigue Experiments*

The low stress fatigue specimens show two important features. Firstly no polygonization is observed although the total dislocation density in some regions is as great as $6 \times 10^9\,\mathrm{cm}^{-2}$; this is as shown in fig. 11 after failure in $1{\cdot}8 \times 10^6$ cycles. This figure shows a region of maximum density, but most areas contain a density of dislocation well in excess of that for which polygonization is well developed in unidirectionally deformed specimens. In the fatigue specimens none of these dense regions shows any tendency for polygonization.

The second feature is the appearance in some areas of an extremely high density of dislocation loops. This is shown in fig. 12 after $1{\cdot}4 \times 10^6$ cycles, an estimated 50% of the fatigue life. The similarity of these specimens to those of quenched aluminium (Hirsch *et al.* 1958) is striking. Figure 13 shows at higher magnification an area of a specimen after $2{\cdot}5 \times 10^6$ cycles, an estimated 90% of the fatigue life. A number of loops and a typically irregular dislocation similar to those observed by Hirsch *et al* (1958) can be seen. Close examination of fig. 12 reveals that some of the irregular dislocations form part of rather irregular helices, e.g. at A.

Since the loops are stable there is little doubt that they are prismatic in type, similar to those observed in quenched aluminium. There is however a difference between the quenched and fatigued specimens. In the former the loops are in the main uniformly distributed except that regions surrounding dislocations or near grain boundaries are generally devoid of

loops. In the fatigued specimens however a high density of loops often occurs in regions of high dislocation density. Similar observations have been made in specimens of quenched Al–4% Cu (Thomas and Whelan 1959) and occasionally in specimens of quenched Al (Silcox, unpublished).

The density of loops in these local regions of high density is about $5 \times 10^{14}\,\mathrm{cm}^{-3}$; the density of dislocations in the form of loops is about $3 \times 10^{9}\,\mathrm{cm}^{-2}$ and the average diameter of the loops is about 200 A. Assuming the loops to be collapsed discs of vacancies, the corresponding concentration of vacancies is found to be about 5×10^{-5}. The density of other dislocations in these areas is about $4 \times 10^{9}\,\mathrm{cm}^{-2}$. These figures are very similar to those obtained in the quenching experiments, where the density of loops is about $10^{15}\,\mathrm{cm}^{-3}$, the loop diameter is about 200–1000 A depending on the quenching rate, the density of dislocations in loops is about $10^{10}\,\mathrm{cm}^{-2}$ and the corresponding concentration of vacancies is about 10^{-4}. As was mentioned above, loops are also observed in unidirectionally deformed specimens. However the density of loops is much lower; the greatest density of loops observed in any area of a tensile specimen is about $2 \times 10^{13}\,\mathrm{cm}^{-3}$.

§ 5. Discussion

The results described in the preceding sections help to clarify some features of the behaviour of fatigued metals.

The circumferential spread of the X-ray spots around the Debye–Scherrer rings in a back-reflection photograph is due to plastic curvature. The sharpness of the X-ray diffraction spots from low stress fatigue specimens shows that there is no plastic curvature in these specimens and therefore no polygonization. This is in accord with the present results. The dislocations appear to be arranged in a rather irregular manner. While there is some tendency for the formation of a random network (as suggested previously by a number of workers, see for example Hirsch 1956), many of the dislocations are long and twisted, meandering from one slip to another (fig. 11). The absence of an excess density of dislocations of one sign in any given area is as expected, since in low stress fatigue the resultant macroscopic deformation is very small, unlike that in unidirectional tension.

The annealing behaviour of fatigue specimens (Wood 1955, Clarebrough *et al.* 1957, Kemsley 1957) also appears to be conditioned by the lack of plastic curvature. Recent transmission electron microscope observations on the mechanism of recrystallization of Ni (Bollman 1958) and Ag (Bailey, unpublished) suggest that recrystallization is due to the absorption of deformed areas by the growth of small sub-grains produced after large deformations. The mobility of the low angle boundaries appears to increase with increasing misorientations, and the driving force is the difference in dislocation density on the two sides of the boundary. Absence of sufficient plastic curvature appears to suppress recrystallization, and recovery takes place over a wide range of temperature by polygonization

in the grains and by the movement of the existing large angle grain boundaries (Bailey, unpublished). This is similar to the case of the low stress fatigue specimens, although it is not clear whether recovery takes place by grain boundary movement and by climb and annihilation of dislocations of opposite sign or by the climb and annihilation process alone. The experiments on high stress fatigue indicate that the degree of polygonization is intermediate between that in the low stress fatigue and that in the unidirectionally deformed material. This is in agreement with the recrystallization behaviour as measured on the stored energy experiments of Clarebrough *et al.*, in which the high stress fatigue specimens were found to recrystallize, but more often energy was released during recovery of the high stress fatigued specimens than in the case of the unidirectionally deformed specimens.

With regard to the observations on dislocation loops, although some of the irregularly shaped loops may be the result of certain dislocation interactions, there is little doubt that most of the more or less circular loops are produced by the collapse of discs of point defects. The nature of the very irregular and sometimes helical dislocations also indicates the occurrence of climb and the presence of large numbers of point defects. In fact, as already mentioned above, the distribution and nature of the loops and dislocations are similar to those found in quenched Al–4% Cu (Thomas and Whelan 1959). The point defects might be produced by a dislocation intersection mechanism (Seitz 1952) or other processes involving jogs on dislocations (Friedel 1956, Mott 1957, Cottrell 1957). It is not possible to decide from the present experiments the type of point defect produced by fatigue. During plastic deformation, vacancies, aggregates of vacancies, interstitials and aggregates of interstitials can be formed directly by the mechanism of Friedel (1956). Whatever the mechanism, the results show clearly the presence of large numbers of point defects, thus supporting the hypothesis of Broom and his co-workers and their explanations of the anomalous diffusion rates and anomalous hardening of fatigue specimens.

Acknowledgments

We wish to thank Professor N. F. Mott, F.R.S. and Dr. W. H. Taylor for their interest and encouragement. We are especially grateful to Dr. P. B. Hirsch for suggesting the experiment and for many stimulating discussions. Our thanks are also due to Mr. J. Bell for help with the photographic work. One of us (R. L. S.) is indebted to the Commonwealth Scientific and Industrial Research Organization, Australia and the other (P. G. P.) to the Admiralty for financial support.

References

Barrett, C. S., 1937, *Trans. Amer. Soc. Met.*, **25**, 1115.

Bollmann, W., 1958, *Fourth International Conference on Electron Microscopy* (in the press).

Broom, T., Molineux, J. H., and Whittaker, V. N., 1956, *J. Inst. Met.*, **84**, 356.

Broom, T., and Ham, R. K., 1957, *Proc. roy. Soc.* A, **242,** 166; 1959, *Ibid.*, A, **251,** 186.
Clarebrough, L. M., Hargreaves, M. E., West, G. W., and Head, A. K., 1957, *Proc. roy. Soc.* A, **242,** 160.
Cottrell, A. H., 1957, *Institute of Metals Monograph and Report Series* No. 23, p.1.
Friedel, J., 1956, *Les Dislocations* (Paris: Gauthier-Villars).
Gough, H. J., and Wood, W. A., 1936, *Proc. roy. Soc.* A, **154,** 510.
Hirsch, P. B., 1952, *Acta Cryst.*, **5,** 172; 1956, *Prog. Met. Phys.*, VI (London: Pergamon Press), p. 236.
Hirsch, P. B., and Kellar, J. N., 1952, *Acta Cryst.*, **5,** 162.
Hirsch, P. B., Partridge, P. G., and Segall, R. L., 1959, *Phil. Mag.*, **4,** 721.
Hirsch, P. B., Silcox, J., Smallman, R. E., and Westmacott, K. H., 1958, *Phil. Mag.*, **3,** 897.
Kelly, A., 1954, *Acta Cryst.*, **7,** 554.
Kemsley, D. S., 1956, *J. Inst. Met.*, **85,** 153; 1957, *Ibid.*, **85,** 417.
Mott, N. F., 1957, *Report of Lake Placid Conference on Dislocations and Mechanical Properties of Crystals* (New York: Wiley), p. 458.
Seitz, F., 1952, *Advanc. Phys.*, **1,** 43.
Thomas, G., and Whelan, M. J., 1959, *Phil. Mag.*, **4,** 511.
Tomlinson, H. M., 1958, *Phil. Mag.*, **3,** 867.
Wood, W. A., 1955, *Phil. Mag.*, **46,** 1028.

The Relationship between Plastic Flow and the Fracture Mechanism in Magnesium Oxide Single Crystals†

By R. J. Stokes, T. L. Johnston and C. H. Li
Honeywell Research Center, Hopkins, Minnesota

[Received February 2, 1959]

Abstract

Magnesium oxide crystals plastically deformed under a three-point load develop internal slits coplanar with the (110) slip plane and parallel to the [001] bending axis in the tension region. Using etch pit techniques it has been shown that the slits lie along the edge of a (110) slip band and are confined between two adjacent orthogonal ($1\bar{1}0$) slip bands.

It is proposed that under certain circumstances edge dislocations moving in one of the ($1\bar{1}0$) slip planes pile into the barrier provided by a wider (110) slip band and coalesce to form a slit nucleus along the lines of intersection. This nucleus lies parallel to the (110) plane and grows by cleavage over this plane until it meets another ($1\bar{1}0$) slip band where it becomes halted. Thus cracks can be nucleated where slip bands intersect but, more important, they can also be *stabilized* by slip bands.

If microcracks form in the early stages of plastic flow their growth is unrestricted and the material is brittle. If the crystal is first plastically deformed to introduce sufficient slip the growth of the microcracks is impeded in certain directions and they develop into narrow slits. The material is then able to deform even further. The correlation between crystal ductility and the appearance of the fracture surface is consistent with this interpretation. For brittle specimens fracture starts from a point, whereas for ductile specimens the fracture appears to start from one of the narrow slits.

§ 1. Introduction

In an earlier paper (Stokes *et al.* 1958) we have described the location and orientation of stable microcracks formed during the compression of magnesium oxide single crystals. These cracks were shown to be a direct consequence of slip over {110} planes and it was proposed that they were nucleated by the coalescence of edge dislocations under the influence of an applied shear stress. In this particular case, it was considered that the barrier, against which the dislocations piled up, consisted of a kink band created during deformation.

More recently, we have found cracks in the tension region of crystals undergoing three-point bending whose location and orientation (i.e. parallel to the (110) slip planes) were the same as for those developed in compression (Stokes *et al.* 1959a). These microcracks were stable, in the sense that the crystals could continue to deform plastically in their presence even though their dimensions exceeded the critical value ($\sim 10\,\mu$) estimated from Griffith's equation. In the present paper we discuss the origin,

† Communicated by the Authors.

growth and stabilization mechanism for these microcracks as well as the role that they play in the final fracture.

§ 2. Experimental Techniques

The testing methods were essentially the same as those described elsewhere (Stokes *et al.* 1959a, b); crystal beams of fixed dimensions, $\frac{1}{4}$ in. $\times \frac{1}{8}$ in. cross section and 1 in. in length, were centrally loaded at an estimated maximum strain rate of $1{\cdot}5 \times 10^{-5}$ per sec. There were, however, two important modifications used in these experiments.

First, for reasons which will become apparent, it was necessary to deform many of the crystals while they were continuously polished in hot, fresh, 85%-orthophosphoric acid. To facilitate this a supply of fresh acid was allowed to drip constantly from a reservoir into a glass or Teflon tray held in light contact with the lower (tension) surface of the crystal. The acid was heated by a small resistance heater wound around the outlet of the reservoir, maintaining a temperature of $\sim 100°$C at the specimen. Surface tension drew the hot acid up around the specimen so that it was almost completely immersed. The remainder of the apparatus was protected from the acid overflow by acid-resistant paint.

Second, it was necessary to reveal the distribution of slip after deformation by the use of a selective etching solution. Depending upon their surface condition, the crystals were either etched immediately or were first lightly polished for 15 sec in boiling acid to re-establish a microscopically smooth surface. In view of the high dislocation density an etching time of only 3 min, rather than the conventional 15 min (Stokes *et al.* 1958), proved most effective. While individual dislocation etch pits were difficult to resolve, this treatment provided a clear distinction between slipped and unslipped regions.

§ 3. The Mechanical Properties of Magnesium Oxide Crystals

3.1. *The Variation in Yield Strength and Ductility*

The mechanical properties of different batches of magnesium oxide crystals supplied by the Norton Company showed wide variation both in their strength and in the extent to which they deformed before fracture. We have measured resolved shear stresses for the onset of macroscopic plastic flow ranging from values of 6000 to 15 000 p.s.i. for different crystals†. This scatter in yield strength was reduced when specimens were cleaved from the same parent crystal, but the wide variation in plastic deflection to fracture remained. In some cases the crystals broke with no detectable macroscopic deformation whatsoever, while others underwent a deflection which corresponded to an estimated (i.e. assuming an elastic beam) surface strain of up to 15%.

† Shear stress (τ) here is determined by resolving the maximum tension stress (σ max) at the centre of the beam into the [110] slip direction, whereupon $\tau = \sigma \text{ max}/2$. σ max is calculated from the simple elastic beam formula.

It was thought that the reproducibility might be improved if the plastic damage introduced into the surface of the crystals by cleavage and subsequent handling was removed with a chemical polish (Stokes *et al.* 1959 b). Even with specimens standardized in this way the same unpredictable mechanical properties persisted. There were slight differences in the mechanical behaviour between polished and unpolished material however; polished specimens undergoing plastic deformation frequently exhibited yield drops, each of which was accompanied by an audible creak. These were associated with a sudden burst of slip.

Fig. 1

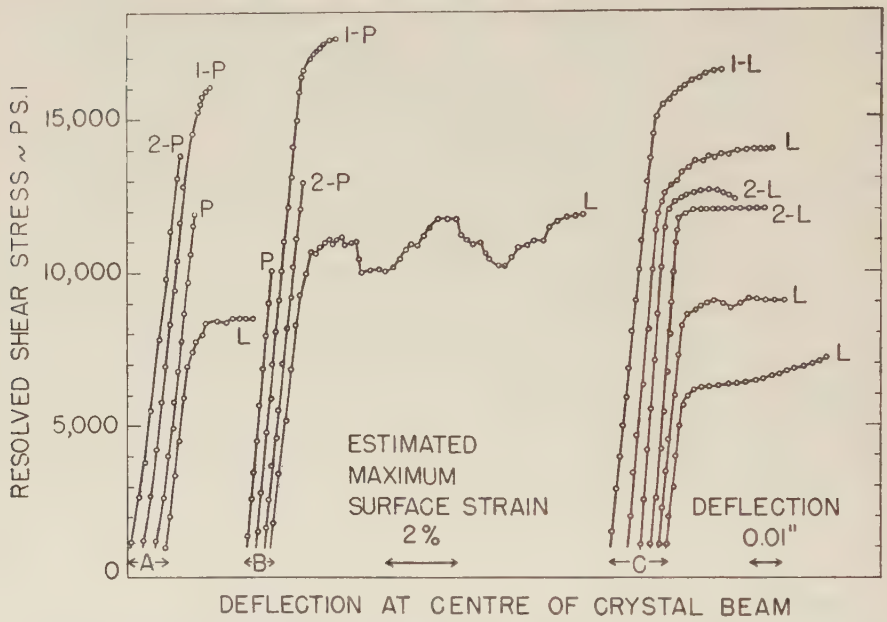

Representative stress–deflection curves for different magnesium oxide crystals. (A) Crystals tested in air; as-cleaved condition. (B) crystals tested in air; chemically polished condition. (C) Crystals tested in hot orthophosphoric acid.

Specimens numbered 1 or 2 were cleaved from the same parent crystal.

P—signifies cleavage lines originating at a point.

L—signifies cleavage lines originating along a line.

More consistent observations were obtained if a polished specimen was either removed from the testing machine and frequently repolished during the early stages of deformation or if it was continuously polished by immersing the tension surface in hot acid. (The dissolution rate was slow, an estimated 1 μ/min.) Under these conditions it was *always* possible to achieve some plasticity, although the exact amount was still subject to some scatter. The effect of the hot acid may be somewhat analogous to that of water in the familiar Joffe experiment on sodium

chloride, in that microcracks which would otherwise embrittle the material were removed during the early stages of plastic flow. A detailed understanding of the role of the acid awaits further experiments; for the purpose of the present work however, it allowed ductility to be obtained consistently.

Figure 1 includes representative stress–deflection curves obtained with a number of specimens having different surface treatments. Within the accuracy of our observations, both the intermittent and the continuous polish were equally effective in promoting ductility.

3.2. *Correlation Between the Appearance of the Fracture Surface and Crystal Ductility*

Examination of the fracture surface of each specimen revealed an interesting correlation. While the source of fracture was always located in the tension region, its position and form was related to the amount of preceding plastic deformation. For the most brittle specimens, i.e. those which showed little or no macroscopic deflection, the cleavage lines always appeared to radiate from a point which was generally located at the specimen corner. This type of fracture surface is characteristic of extremely brittle materials; in germanium under normal test conditions, for example, the tear lines can be traced back to a point (Johnston *et al.* 1958). The observation suggests catastrophic propagation of a crack from a tiny defect.

For the more ductile specimens on the other hand the cleavage lines were observed to originate from a line which was located either at the surface or inside the crystal in the tension region. In addition, the fracture surface contained other linear steps parallel to the originating line, along which new cleavage lines were generated. It would appear that the greater amount of preceding plastic deformation had influenced the crack propagation during fracture. These two characteristic fracture surfaces can be compared in fig. 2 (Pl. 105).

It must be made quite clear that this behaviour was dictated by the plasticity rather than the particular environment under which the crystals were tested. In other words, irrespective of the surface treatment, if a crystal was sufficiently ductile, fracture appeared to originate along a line, if it was brittle, fracture originated from a point. For the remainder of this paper we will be concerned primarily with the fracture of the more ductile material.

§ 4. The Formation and Stability of Slits

4.1. *The Orientation of the Fracture Source*

The orientation of the line from which cleavage appeared to start in the ductile specimens is illustrated diagrammatically in fig. 3. All future mention of crystallographic surfaces and directions will be made with reference to this diagram. Examination of the crystal fracture surface

(surface II in the diagram, henceforward to be referred to simply as II) showed that the length of the line lay parallel to the bending axis, [001], while its profile intersected the edge surface (I) of the specimen along a line parallel to the slip direction, either [110] or [$\bar{1}$10]. This is shown clearly in fig. 4 (Pl. 106) where photomicrographs taken on adjacent surfaces of a fractured crystal are mounted side by side†. In other words, the line was actually a narrow step in the fracture surface lying coplanar with one of the two slip planes whose zone axis was parallel to the bending axis. Originally this step constituted one surface of an internal slit as has previously been described (Stokes *et al.* 1958, 1959a). Thus in order to understand the fracture process we need first to be able to specify the mechanism whereby these slits are generated.

Fig. 3

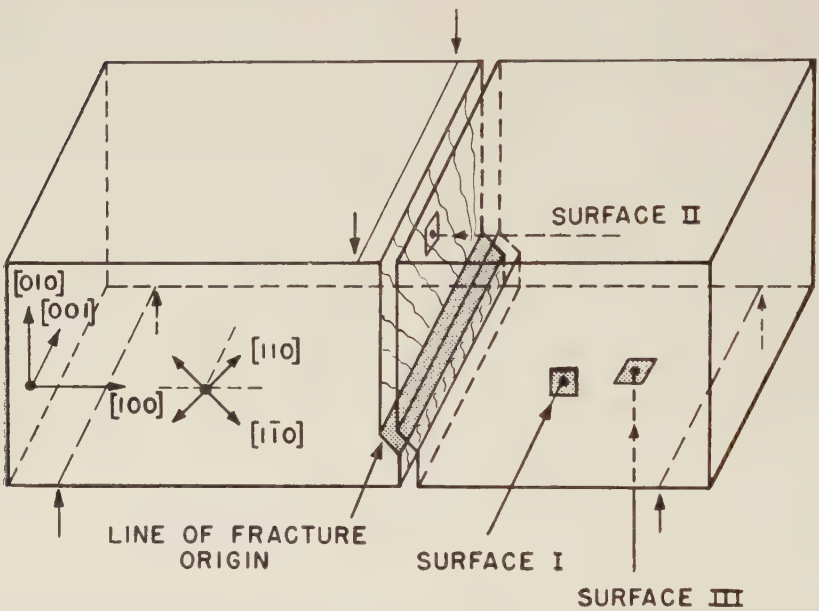

Diagrammatic reconstruction of a crystal fractured under three point bending, showing the orientation of the step along which fracture starts.

A microscopic survey of the tension surface (III) of specimens which had been deformed with both an intermittent and a continuous polish frequently revealed the existence of slits actually intersecting the tension

† The photomicrograph of the line profile was taken on a parallel internal surface obtained by cleaving the crystal. Continuously polishing a crystal in the hot acid tends to round off any sharp corners making illumination and focusing in these regions difficult for a good photomicrograph.

surface itself†. Figure 5 (*a*) (Pl. 106) and fig. 6 (Pl. 107) illustrate examples of surface slits in crystals which had not yet fractured. The sequence in fig. 5 shows how the final fracture originated from one such surface slit. Furthermore, fig. 5 (*b*) reveals that the slit had switched out of the usual (110) slip plane into the (100) cleavage plane at the tension surface. (The slip plane component appears as a thin dark line because of its orientation and is located just inside the tension surface.) Thus, even though the stable surface slit of fig. 5 (*a*) contained a component in the cubic cleavage plane, the crystal still underwent a further estimated 1% plastic elongation in air before fracture. It is extremely interesting to note that a magnesium oxide crystal can support a cleavage notch under a tension stress of approximately 20 000 p.s.i. without immediate catastrophic failure.

4.2. *Slits and Glide Bands*

From the photomicrographs it can be appreciated that a ductile specimen generally contained many more slits than the particular one responsible for eventual failure. In some cases more than 50 such slits were counted within a single crystal. While the larger ones were readily visible under the microscope (or even to the naked eye), the finer ones could best be seen under transmitted polarized illumination. It was possible therefore on a single specimen to witness slits at different stages of their development. In order to define the situation of the slit profile more precisely with respect to the bands of slip, crystals were first given a light etch and then surveyed. The specimen edge (I and parallel surfaces produced by cleavage) provided the most useful source of information.

Figures 6, 7 (Pl. 108) and 8 (Pl. 109) are photomicrographs taken in the tension region of crystals which have been treated in this way. It can be seen that there were certain features common to all of the slits included in these photomicrographs; these features can be listed as follows:

(i) The slits were always to be associated with regions where orthogonal slip bands completely *intersected* one another. They were never found where a slip band terminated on intersection.

(ii) They were always orientated in a plane parallel to the 'wider' of the intersecting bands.

(iii) They were always located at the *edge* of the 'wider' slip band. In some cases slits were situated within the 'wider' band, but we believe this to be a secondary effect in that the slits were initially formed along the edge and subsequently became absorbed by the growing slip band.

(iv) More than one slit could be formed along the edge of a given 'wider' band (fig. 8), in which case they were generally confined to one edge

† It is interesting to note that a similar observation has been made on germanium at room temperature when tested in a chemical polish. Even though this material remains extremely brittle and the stress it supports is increased by a factor of $\sim 10^2$ the tension surface becomes covered by a network of linear parallel cracks immediately before fracture (Johnston *et al.* 1958).

although they have been observed simultaneously on both the acute and the obtuse edge (see fig. 9).

(v) Most of the slits spanned the gap left between two of the 'narrower' bands which intersected the 'wider' band at 90°. Thus the large slit in fig. 7 (*b*) spans the gap between the two 'narrower' slip bands A and B.

Not every slip band intersection gave rise to a slit, neither could any particular feature be identified for those bands which did form slits. However, that some special condition must exist was demonstrated by the following experiment. The crystal in fig. 7 was first deformed to the stage represented in fig. 7 (*a*). It was then cleaved along its length parallel to the edge surface (I) and the two halves further strained independently of one another. Both halves developed new slits in *exactly* the same location. These new slits can be seen for one half of the crystal in fig. 7 (*b*). Close microscopic investigation of the other half before straining gave no indication of a slit in the region where it was to be expected. The specific submicroscopic event to be associated with the nucleation of these slits will be discussed in § 4.3.

Fig. 9

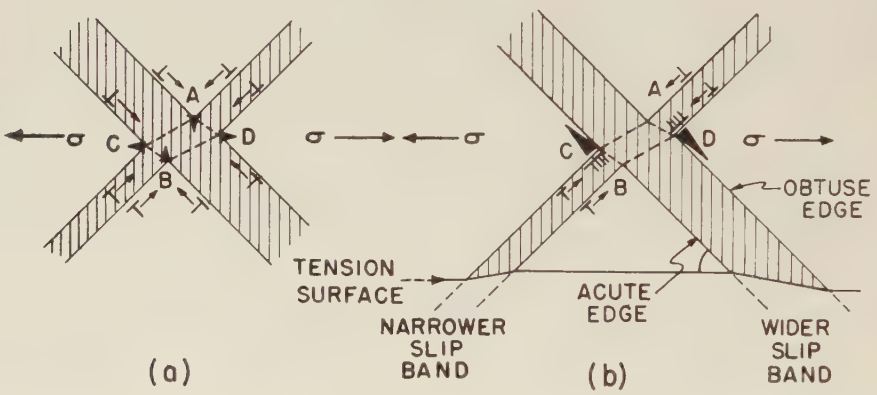

The nucleation of cracks by intersecting slip bands.
(*a*) The location and orientation of cleavage cracks formed by the interaction of individual slip dislocations (after Cottrell 1958). (*b*) The location and orientation of cracks formed by the pile-up and coalescence of edge dislocations on one slip band against the other.

The way in which the slit-nucleus grew to microscopic dimensions could be inferred by looking through the tension surface (III) of a deformed specimen. Slits then appeared under polarized illumination as dark lines parallel to the [001] direction. (It should be noted that this direction is parallel to the *edge* dislocation lines in the slip bands.) While most of the slits extended only part of the way across the crystal width with one end at the edge surface (I), some were observed to extend over the whole width, others were short and completely internal. Figure 10 (Pl. 109)

includes photomicrographs of an internal slit taken at different strains by focusing beneath the tension surface. Using the small gas bubbles as markers it can be seen that the slit has increased its length in both directions while its width remains unchanged.

Direct observation of the slit surface itself was possible with certain specimens; fig. 11 (Pl. 109) for example was taken on the surface (surface II rotated through 45°) of the large slit responsible for the failure of the specimen in fig. 7 (*c*). The figure shows that growth took place by cleavage and that the direction of propagation was predominantly (in the later stages at least) perpendicular to the length of the slit in a direction from top to bottom in the photomicrograph. Etch pits developed on the slit surface were due to dislocations on the {110} planes intersecting the slit surface along ⟨111⟩ directions. Presumably they were introduced by stresses at the tip of the slowly moving (110) plane cleavage crack (Gilman 1957). It was significant that the etch pit density was highest in the vicinity of the cleavage lines.

From the cleavage lines in fig. 11 it may be concluded that the slit nucleated along the line AB. This line corresponded with that tip of the slit profile in fig. 7 closest to the tension surface. In this particular case therefore it was possible to specify the particular pair of slip bands to be associated with the slit nucleation. Furthermore, the exact line of intersection along which nucleation took place could also be identified. A similar analysis has been performed on a number of slits and it has been found that only two of the four possible lines along which two bands intersect, develop cracks. These were located diametrically opposite one another as illustrated in fig. 9 (*b*). On the acute edge of the 'wider' slip band the site of nucleation was on that side of the 'narrower' band farthest from the tension surface, and vice versa.

A similar conclusion followed from observations of a few slits which appeared not to span the gap between two narrow bands completely, as described in feature (v) above. An example is included in fig. 7 (*a*) where only one tip of the slit profile was located at a slip band intersection. It was presumed that the other tip was located along a second 'narrower' slip band which did not emerge at the surface under observation.

Before discussing the mechanism of slit formation it is first necessary to describe briefly how slip bands are developed in magnesium oxide. We have reported elsewhere (Stokes *et al.* 1959 b) that slip first appears in polished crystals at a stress of approximately two thirds the macroscopic yield stress. At this stress the segments are short and appear to consist of a single line of dislocations. As the strain is further increased each of the individual slip lines become wider to form a slip band. The shear within the slip band is fairly uniform so that should it cut a pre-existing band the latter becomes sheared in the manner which can be seen in fig. 6. Each slip band expands like a Luders band by the nucleation and multiplication of dislocation loops *at its edge*. This process can also be seen to be taking place in fig. 6. In other words slip at any instant is confined to the edge

of a slip band. (A similar observation has also been reported by Washburn (private communication).)

4.3. *Proposed Mechanism of Slit Formation*

On the basis of evidence presented in the preceding section we conclude that the formation of slits involves a two-stage process. In the first, or nucleation, stage sub-microscopic slits form along a line where slip bands intersect. In the second stage this slit nucleus grows from some point along its length to a size and form which can readily be recognized under the microscope.

With respect to the first stage; our information concerning the nature of the slit nucleus is necessarily indirect. Let us consider the manner in which two orthogonal expanding slip bands can interact. The sign, position and direction of motion of the edge dislocations at any instant are illustrated in fig. 9. Different configurations develop depending upon whether one considers (*a*) the interaction of individual dislocations in the two slip bands or (*b*) the piling up of dislocations in one slip band against a barrier provided by the other. In the first configuration dislocation reactions of the kind

$$\tfrac{1}{2}a[110]+\tfrac{1}{2}a[1\bar{1}0]\rightarrow a[100]$$

take place along all four lines of intersection. Such a mechanism has been described by Cottrell (1958) and Orowan (1954) as a possible means of generating crack nuclei. However, as Cottrell has pointed out, the dislocation reaction for this particular slip system does not involve a reduction in elastic energy so the resulting cleavage dislocations are unlikely to be stable. Assuming for the moment that they are stable, then their situation and orientation would be as given in fig. 9 (*a*) with the slit nuclei lying in the cleavage plane rather than the slip plane. Micro-cracks formed at A or B in fig. 9 (*a*) would be situated within the slip band intersection and, for reasons to be discussed later, probably would not grow, while those formed at C or D would be orientated parallel to the tensions direction.

In our opinion the present observations are more consistent with the mechanism assumed by Stroh (1955) in which edge dislocations forced against a barrier coalesce to form the crack nucleus. It is proposed here that under certain circumstances an avalanche of dislocations released at the edge of the 'narrower' slip band are unable to intersect the orthogonal 'wider' slip band. These dislocations pile up, coalesce and nucleate a sub-microscopic slit, defined as the Stroh-crack. The Stroh-crack lies parallel to the edge dislocation lines which form it and thus to the [001] bending axis. The plane of the Stroh-crack is perpendicular to the 'narrower' slip band and therefore parallel to the 'wider' slip band. Again the Stroh-crack mechanism can function at all four lines of the slip band intersection, but for only two of these, C and D in fig. 9 (*b*) can the Stroh-crack grow. The reason for this will become clear later. C and D correspond with the two locations observed in the tension region.

The following questions then remain: how does the 'wider' band provide an effective barrier to edge dislocations and why are certain intersections preferred? At the moment the answer to these questions must remain conjectural. There is already evidence, in fig. 7 for example, that intersecting slip bands can provide a temporary barrier to one another. Many of the narrow slip bands in these photomicrographs terminate at a 'wider' slip band. When the strain is further increased they cut through and move on to the next 'wider' slip band. It will be noticed that no slip bands terminate in the region between two wide slip bands. As

Fig. 12

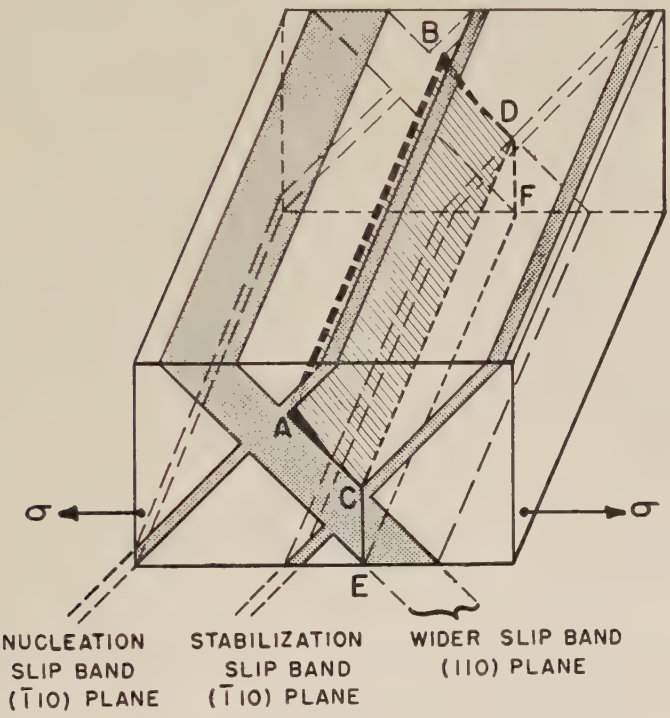

Proposed mechanism of slit formation. Slit nucleates along AB by pile-up and coalescence of edge dislocations in nucleation slip band. Slit grows by cleavage over (110) plane propagating in direction [$\bar{1}$10] perpendicular to AB. Slit is stabilized by slip band along line CD.

already suggested the specific event to be associated with crack nucleation may depend upon the *dynamic* growth of an existing narrow slip band, in that a burst of slip occurring along its edge cannot cut through the 'wider' slip band. Obviously further details of the growth and interaction of slip bands are essential to an understanding of the fracture process in this material.

The second stage of slit formation, the growth of the Stroh-crack, occurs by cleavage. The most satisfactory explanation for the combined observations of figs. 10 and 11 assumes that the Stroh-crack eventually attains the critical dimensions for cleavage propagation over the (110) plane under the applied stress σ. Propagation in the slip direction [110] starts from some point along its length AB in fig. 12, and continues over the edge of the 'wider' band until the crack front meets another slip band along the line CD where it becomes halted. It still remains free to extend lengthwise however, thereby developing into a narrow slit. In keeping with the previous notation (Stokes *et al.* 1958) the slit produced by the growth of the Stroh-crack is defined as the 'secondary crack'. It should be noted that for the crystal deformed under compression, as described in the earlier paper, the secondary crack was orthogonal to the Stroh-crack. This was due to the local stress field in the vicinity of the 'wider' slip band. In the present case where the crystal is under tension the secondary crack has the same orientation as the Stroh-crack.

4.4. *Slit Stabilization*

As described in the previous sections (4.2 and 4.3) the secondary crack was bound at both edges by slip bands, one of which provided the dislocations responsible for nucleating the crack while the other stopped its growth over the whole length. The manner in which slip bands can impede propagating cleavage cracks has been investigated by other authors (Gilman 1958, Melankholin and Regel 1955). In particular Gilman has shown that when a running {100} plane cleavage crack intersects a band of screw dislocations the density of cleavage lines increases for crystals of the rock-salt system. A similar behaviour is to be expected for a cleavage crack on the (110) plane especially since it intersects the band of screw dislocations orthogonally rather than at 45°, leading to a greater cleavage step height. Presumably the sudden increase in the total surface area and the extra amount of plastic work required to force the crack through the slip band becomes prohibitive with respect to the decrease in elastic strain energy associated with its growth and the crack is halted. By the same argument it seems unlikely that a Stroh-crack will grow when formed within a slip band, as is required along the lines A and B in fig. 9 (*b*).

4.5. *The Final Stage of Fracture*

The last stage in the breakdown of the crystal commences when the secondary cracks, which were bound at both edges by slip bands, switch their orientation into the (100) cleavage plane (EF in fig. 12). These cleavage plane components have still to cut their way through a region densely populated with screw dislocations (either the 'wider' or the 'narrower' slip band) so that the rate of propagation is restricted and the crack stable. The switch in orientation results in the edge profile of the cracks assuming an S-shape, which can just be distinguished for some of

the slits illustrated in fig. 8. A better example of a slit profile containing a cleavage component has been included in fig. 2 of a previous publication (Stokes *et al.* 1959a). When the cleavage component finally severs the slip bands it runs into an unslipped region where it can accelerate to a velocity high enough to overcome any further impedance which may be offered by slip bands, and catastrophic failure ensues†.

§ 5. Summary of the Fracture Mechanism

To summarize the mechanism of fracture for the particular conditions of our experiments, viz. fairly ductile crystals tested under three point loading at a low strain rate, we have the following stages:

(1) It seems reasonable to assume that a burst of edge dislocations moving along the edge of a certain narrow slip band piles up against the barrier provided by a 'wider' slip band. The pile-up coalesces to form a Stroh-crack nucleus lying in the plane of the 'wider' slip band.

(2) The Stroh-crack nucleus grows by cleavage over the (110) slip plane to form the secondary crack.

(3) The secondary crack becomes stabilized by a slip band which it intersects along its whole length, resulting in the formation of a slit, the dimensions of which are dictated by the slip band spacing.

(4) The secondary crack switches its orientation into the cubic cleavage plane where its rate of propagation is still restrained by the slip bands.

(5) The cubic cleavage plane component breaks through the slip band into an unslipped region where it accelerates for catastropic failure.

It remains to be determined whether or not this same mechanism applies under more general conditions, i.e. for brittle specimens (where, it will be remembered, cleavage lines originate from a point) or for different strain rates and loading conditions.

It should be pointed out that the majority of the ductile crystals used for the present observations preferred to slip almost exclusively over the two {110} slip planes whose zone axis was parallel to the bending axis (see figs. 6, 7 and 8 for example). This was the case even though the resolved shear stress was the same for the pair of {110} planes whose zone axis was perpendicular to the tension surface (III). The reason for the suppression of slip on the one system is not understood and its significance with respect to the generality of the above mechanism remains to be determined. There is other evidence in the literature to indicate that this mechanism of fracture may apply for other ductile crystals of the rock-salt system where slip is confined to a pair of planes having a common zone axis. Bobrikov (1957) has related the occurrence of microcracks on the surface of sodium and potassium chloride crystals deformed under tension to the

† It should be noted that the ragged profile apparent in fig. 7 (*c*) is entirely an illumination effect produced by rounding and slight chipping at this edge of the crystal. The true profile is more typically like that shown in fig. 4 (*a*), although even here there is an illumination problem at the lower edge of the crystal.

preferred activation of a slip on a given pair of {110} planes. Microcracks were observed only on that cube face which contained the zone axis of the two intersecting slip planes.

§ 6. Conclusions

In the first place we may conclude that microcracks can be nucleated where slip bands intersect. Second, and more important, this work lends further support to the contention that it is the growth rather than the nucleation of the microcrack which is the critical stage in the fracture process. Thus in the early stages of plastic flow where the slip bands are narrow and widely spaced, a microcrack, once formed, can grow and accelerate to a velocity high enough to overcome any impedance offered by other narrow slip bands. It is able to achieve the terminal velocity for fracture and the material is brittle. If, on the other hand, a crystal has been first plastically deformed to introduce a sufficient number of slip bands, microcracks can grow only in the controlled manner described here to form slits. Catastrophic failure does not then immediately occur and the material can deform further. We conclude that the distribution and density of slip is a most important factor in determining the fracture behaviour of magnesium oxide single crystals.

Acknowledgments

Acknowledgment is due to Mr. K. H. Olsen for his continued capable assistance. The authors are grateful to Dr. J. J. Harwood of the O.N.R. and Dr. F. J. Larsen, Director of Research, for their interest and permission to publish. This work was supported by the Office of Naval Research.

References

Bobrikov, V. P., 1957, *J. tech. Phys., Moscow*, **27,** 830.
Cottrell, A. H., 1958, *Trans. Amer. Inst. min. (metall.) Engrs*, **212,** 192.
Gilman, J. J., 1957, *Trans. Amer. Inst. min. (metall.) Engrs*, **209,** 449; 1958, *Ibid.*, **212,** 310.
Johnston, T. L., Stokes, R. J., and Li, C. H., 1958, *Acta Met.*, **6,** 713.
Melankholin, N. M., and Regel, V. R., 1955, *J. exp. theor. Phys.*, **29,** 817.
Orowan, E., 1954, *Dislocations in Metals* (A.I.M.E.), p. 69.
Stokes, R. J., Johnston, T. L., and Li, C. H., 1958, *Phil. Mag.*, **3,** 718; 1959 a, *Ibid.*, **4,** 137; 1959 b, *Trans. Amer. Inst. min. (metall.) Engrs*, **215,** 437.
Stroh, A. N., 1955, *Proc. roy. Soc.* A, **232,** 548.

Nuclear Disintegrations Produced by 900 MeV Neutrons†

By W. T. Morton
Department of Natural Philosophy, University of Glasgow

and B. A. Munir‡
Physics Department, University of Birmingham

[Received March 6, 1959]

Abstract

Ilford G5 nuclear research emulsions were irradiated with neutrons with an energy of the order of 900 Mev. The characteristics of the disintegrations observed in the heavy nuclei of the emulsion are given and compared with the corresponding results for 950 Mev protons.

§ 1. Introduction

The characteristics of the disintegration of the nuclei of a nuclear research emulsion produced by high energy protons have been studied by a number of workers. Lock and March (1955) and Lock *et al.* (1955) used protons with an energy of 600 Mev and 950 Mev respectively. Philbert (1956) used 900 Mev protons and Lannutti *et al.* (1955) used 2300 Mev protons. Many more studies have been made at lower energies, but in these meson production would not play an important part.

No similar studies have been made with neutrons with an energy of above 350 Mev (Bernardini *et al.* 1952).

§ 2. Experimental Procedure

The circulating proton beam of the Birmingham synchrotron working at an energy of 960 Mev was allowed to strike a 3 in. thick Be target placed within the vacuum chamber. Nuclear emulsions were placed in a collimated neutron beam at a distance of 10 metres from the Be target with their surfaces horizontal and one edge parallel to the neutron beam direction. Protons were bent away from the emulsions by the fringing field of the machine.

A Watson binocular microscope with a $\times 20$ oil immersion objective and $\times 10$ eyepieces was used to search the emulsions for two or more tracks appearing to originate at the same point. All events were examined using a $\times 90$ oil immersion objective and $\times 10$ eyepieces to confirm that the tracks did originate at the same point.

---

† Communicated by the Authors.
‡ Now at Physics Department, Florida State University, U.S.A.

The events were classified using the notation employed by Lock *et al.* (1955), in which an event with n secondary branches, of length greater than 10 microns, was denoted as an n prong event. Two-prong events in which the grain density of both prongs were equal, and in which it was not possible to ascertain the direction of motion of the particles responsible, were assumed to be due to elastic scattering and eliminated from the analysis.

Using the alpha particle method (Heidmann and Leprince-Ringuet 1948) 15% of the remaining events were assigned to reactions occurring in the light nuclei of the emulsion. Counter experiments, such as those of Booth *et al.* (1958) on the absorption cross section of neutrons with an energy of 765 Mev, indicate a value of the order of 25% for events occurring in light nuclei. This discrepancy is not surprising in view of the uncertainties in the alpha particle method. However, in the past this method has provided a means of eliminating a number of the interactions with light nuclei.

A total of 477 events were assigned to heavy nuclei reactions and for these the energy and angle of each prong was found. Range–energy tables were consulted to obtain the energy of prongs stopping within the emulsion and grain density measurements made for prongs leaving the emulsion employing relativistic electrons from π-μ-e decays for normalization.

§ 3. Prong Distribution

In fig. 1 the dotted line shows the prong distribution for heavy nuclei according to the alpha particle method in the present investigation; the solid line the distribution obtained by Lock and March for a proton bombarding energy of 600 Mev; and the broken line the results at a proton energy of 950 Mev of Lock *et al.* The three sets of results have been normalized to the same number of events with three or more prongs. An uncertainty in the two-prong results in the present experiment due to scattering of charged particles and scanning efficiency might be expected.

The present results tend to lie between the two proton results. The number of events with more than eight prongs in the present experiment shows that the neutron beam probably contains many neutrons with an energy greater than 600 Mev.

Because of the difference in charge of the bombarding particle, prong distributions of neutron induced reactions should not be strictly compared with prong distributions of proton induced reactions. By considering the measured cross-section for $p+p$ elastic scattering and $p+p$ collisions leading to π^+ and π^0 production, and also the cross section for $n+p$ elastic scattering and $n+p$ collisions leading to π^+, π^- and π^0 production, it is found that the total number of charged secondaries in a proton–nucleon reaction divided by the total number of charged secondaries in a neutron–nucleon reaction is about 1·6. This difference in prong distribution between neutron and proton induced reactions might be observed in

reactions in which only a few of the nucleons of the complex nucleus took a major part in the initial cascade. Hence when comparing stars induced by neutrons with proton induced stars it is perhaps valid to add 0·6 prongs to neutron induced stars with a small number of prongs. This modification would give a flatter prong distribution in closer agreement with the 950 MeV proton results.

Fig. 1

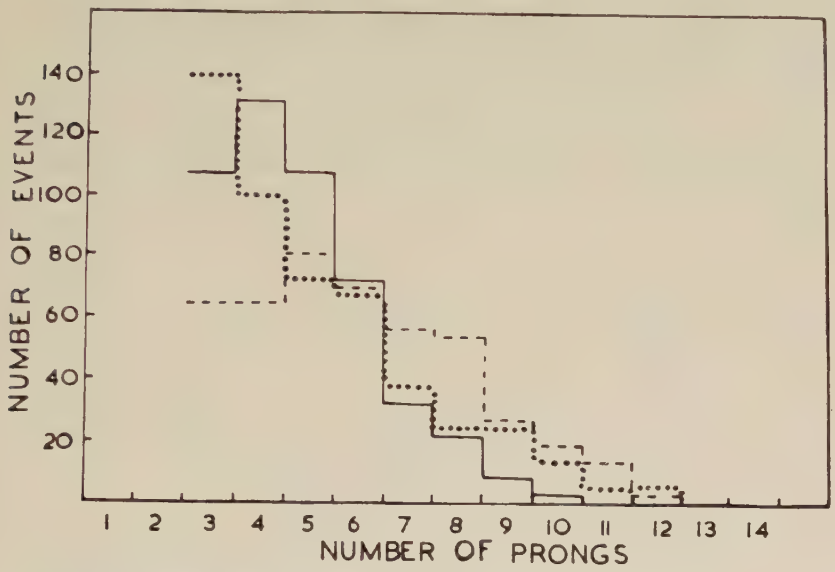

Prong distribution for various energies of bombarding particle.

The total mean prong number of the present experiment and that obtained for protons with an energy of 950 MeV are $4{\cdot}6 \pm 0{\cdot}2$ and $5{\cdot}0 \pm 0{\cdot}2$ respectively. Hence the evidence of a lower prong number for neutron induced stars is not conclusive.

§ 4. Energy and Angular Distribution of Prongs

Using the nomenclature of Brown *et al.* (1949), the tracks were divided into three classes according to their grain density. Tracks with a grain density corresponding to a proton of energy less than 30 MeV are referred to as black tracks. Those corresponding to a proton energy of between 30 MeV and 450 MeV are referred to as grey, and the remainder as shower tracks.

The average number of shower, grey and black tracks in the present investigation is 0·2, 1·4 and 2·8, while the results reported for 950 MeV protons were 0·54, 1·11 and 2·61. The proton data contained one-prong events and are not directly comparable with the present results. If it is assumed that the secondary of all one-prong events is a shower or a grey track the average number of shower plus grey tracks per star becomes 1·8

and this has to be compared with the value 1·6 obtained here. The average number of black tracks observed in the proton and neutron experiment are also equal within statistics.

The mean number of shower plus grey tracks for events with 2–4, 5–7 and 8–11 prongs for neutron induced stars is 1·3, 2·0 and 2·5 and for proton induced stars is 1·7, 2·3 and 2·3, respectively.

Figure 2 shows the angular distribution of shower, grey and black tracks observed in the present experiment. These results indicate, as expected, that the angular distribution of the emitted particles tend to isotropy as the energy of the emitted particle decreases.

Fig. 2

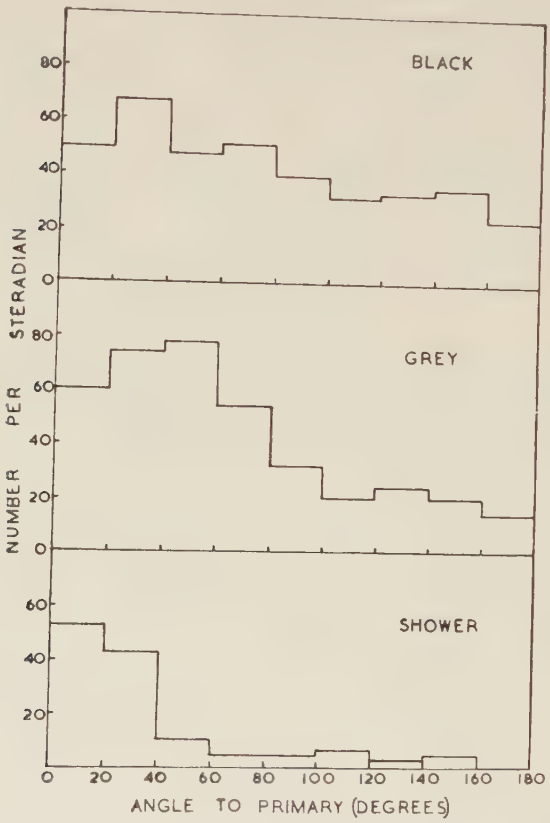

Angular distributions of black, grey and shower tracks.

The forward to backward ratio of shower, grey and black tracks in the present investigation is $7{\cdot}5 \pm 3{\cdot}0$, $3{\cdot}2 \pm 1{\cdot}5$ and $1{\cdot}9 \pm 0{\cdot}3$ and the results obtained for 950 Mev protons was 22 ± 7, $5 \pm 1{\cdot}5$ and $1{\cdot}4 \pm 0{\cdot}1$. The proton results contain one prong events and if these are assumed to be all shower tracks at forward angles then the forward to backward ratio in that study becomes 16 ± 5.

§ 5. Conclusions

The neutron beam obtained by charge exchange scattering of protons with an energy of 960 MeV on Be contains a considerable fraction of high energy neutrons. The nuclear disintegrations produced by these neutrons in the complex nuclei of a nuclear research emulsion are similar to the disintegrations produced by protons with an energy of the order of 950 MeV.

Acknowledgments

The authors would like to thank Dr. W. O. Lock, of Birmingham University, and Dr. P. V. March, of Glasgow University, for many useful discussions, and Miss J. Stewart for help with the microscope work. They are indebted to the Birmingham synchrotron counter group who obtained the neutron beam. One of us (W. T. M.) wishes to thank Professor P. B. Moon for allowing him to take part in work using the Birmingham synchrotron.

References

Bernardini, G., Booth, E. T., and Lindenbaum, S. J., 1952, *Phys. Rev.*, **85**, 826.

Booth, N. E., Hutchinson, G. W., and Ledley, B., 1958, *Proc. phys. Soc. Lond.*, **71**, 293.

Brown, R. H., Camerini, U., Fowler, P. H., Heitler, H., King, D. T., and Powell, C. F., 1949, *Phil. Mag.*, **40**, 862.

Heidmann, J., and Leprince-Ringuet, L., 1948, *C.R. Acad. Sci., Paris*, **226**, 1716.

Lannutti, J., Goldhaber, G., Goldsack, S. H., 1955, *Bull. Amer. phys. Soc.*, **30**, 3, E.1.

Lock, W. O., and March, P. V., 1955, *Proc. roy. Soc.* A, **230**, 222.

Lock, W. O., March, P. V., and McKeague, R., 1955, *Proc. roy. Soc.* A, **231**, 368.

Philbert, G., 1956, *C.R. Acad. Sci., Paris*, **234**, 141.

The Influence of Solute Atoms on the Damping due to Dislocations in Iron Alloys†

By P. M. Robinson and R. Rawlings
Department of Metallurgy and Fuel Technology, University College, Cardiff

[Received March 20, 1959]

Abstract

The effect of silicon and oxygen in solid solution on the damping of iron (vibrating at 1·03 c.p.s.) has been studied. The damping is independent of vibrational amplitude up to a critical amplitude. The variation of this critical amplitude with temperatures and solute concentration has been studied. From the temperature variation of the critical amplitude a binding energy of 0·004 ev between a silicon atom and a dislocation has been obtained. Above the critical amplitude, the damping varies with amplitude of vibration. This variation has been compared with that deduced by Granato and Lücke's (1956) model for mechanical damping due to dislocations.

§ 1. Introduction

There are many sources of damping in metals (Nowick 1954 b). The present work is confined to that due to static hysteresis. It was carried out using alloys of iron and silicon partly because of their commercial importance in the electrical industries and partly because of the sparsity of results on simple iron alloys in the field. The object of the research was to obtain information regarding the interaction of silicon and oxygen with dislocations in iron.

The diminishing of the damping due to static hysteresis by the addition of alloying elements has been studied by Weertman and Salkovitz (1955) and by Weinig and Machlin (1956). The former tested dilute solutions of lead at a frequency of 30 Kc.p.s. and found that the damping was amplitude independent up to a certain critical amplitude of vibration above which it became dependent upon the amplitude. The latter tested copper solutions at 1 c.p.s. and found that the damping varied with the amplitude for all amplitudes used.

§ 2. Materials and Experimental Procedure

The iron was kindly supplied by the British Iron and Steel Research Association and their analyses are given in table 1. Two samples of iron were used, one melted in air and the other the same iron melted in air and then melted in hydrogen to remove oxygen to a low concentration. From this batch of iron, iron–silicon alloys were melted and cast in a resistance-heated vacuum furnace. The silicon has a minimum purity of 99·9% Si,

† Communicated by the Authors.

the chief impurity being iron. The half pound ingots were hot rolled to 0·25 in. diameter pickled and cold drawn to 0·027 in. diameter. The making and working of the iron–silicon alloys were carried out in this Department.

Internal friction tests were carried out on specimens 2 in. × 0·027 in. by measuring the free decay of a torsion pendulum with a lamp and scale at 3 m distant and a frequency of 1·03 c.p.s. The tensile stress from the inertia bar on the specimen was 346 lb/sq. in. A small furnace surrounded the specimen, the temperature being determined by a chromel–alumel thermocouple (0·0148 in. thick) with its tip within 0·25 in. of the specimen centre. All tests were carried out in air.

Before testing, specimens were treated in dry hydrogen for three hours at 900° C. For the latter, the hydrogen was first passed over a commercial room temperature catalyst (to convert any oxygen to water vapour) and the water vapour adsorbed by activated alumina. This treatment was sufficient to completely decarburize the specimens.

Table 1. Analyses of Samples Used

Sample	C	Si	Mn	S	P	O	N
AHL†	0·0034	0·0025	0·005	0·005	0·001	0·0017	0·0035
AGB†	0·004	0·002	—	0·004	—	0·28	0·01
V2	—	1·1	—	—	—	—	—
V3	—	1·9	—	—	—	—	—
B15†	—	2·83	—	—	—	—	—

† Samples and analyses supplied by B.I.S.R.A.

The mean grain diameter of all specimens was the same, namely, 0·042 cm.

§ 3. Results

The effect of the amplitude of vibration on the damping at room temperature is shown in fig. 1. Here log amplitude is plotted against the number of vibrations. The damping, i.e. log decrement, is given by the slope of the graph. In each case there is an amplitude below which the log decrement is constant and above which it increases with amplitude. The surface strain corresponding to this amplitude will be referred to as the critical shear strain. The critical shear strains are listed in table 2 and increase with silicon concentration and oxygen concentration. The large effect of oxygen as compared with that of silicon is quite remarkable. The damping in the amplitude independent region also varies with solute concentration, being lowest for the highest concentration (see fig. 1 and table 2).

The effect of temperature on the damping in the amplitude independent range is shown in fig. 2 and the effect on the critical shear strain in fig. 3.

Fig. 1

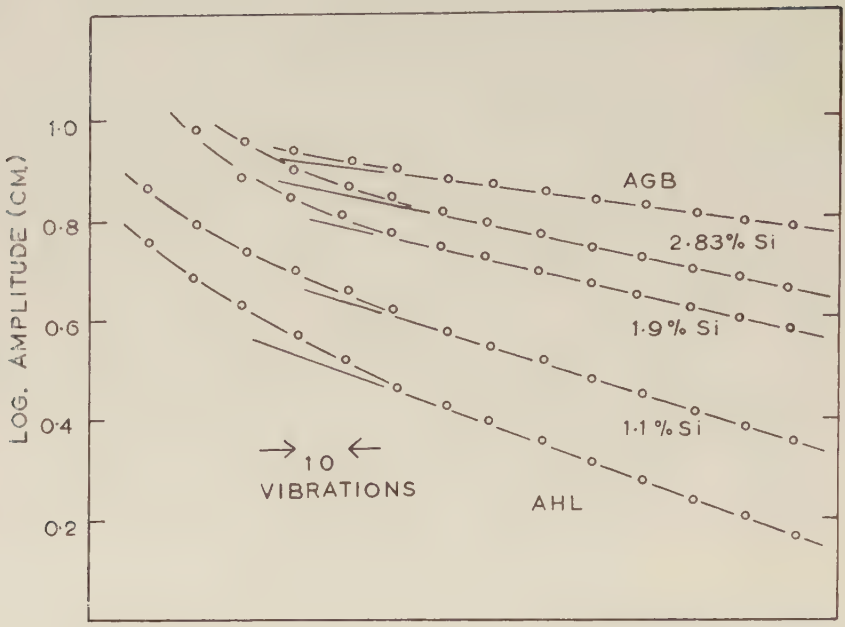

Variation of damping at 20°c with amplitude of vibration and solute concentration.

Fig. 2

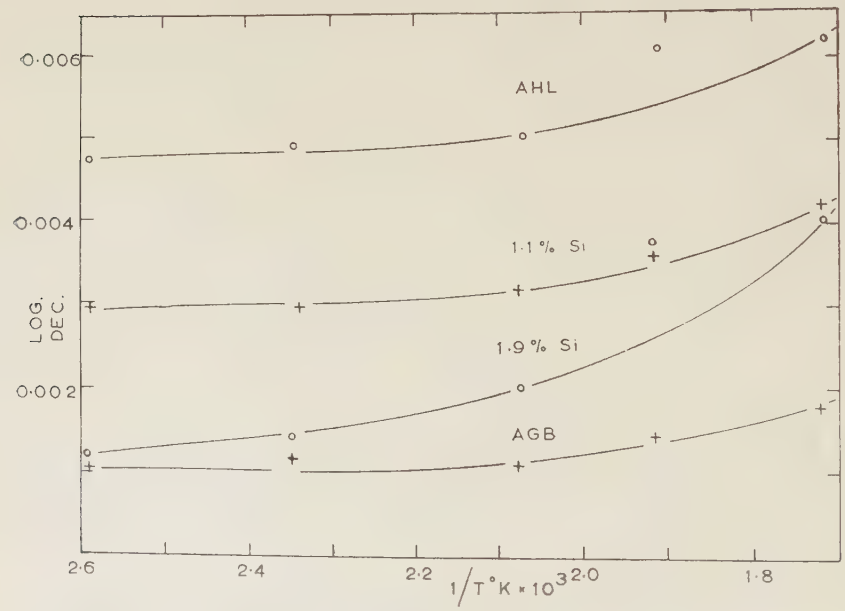

The effect of temperature on the damping in the amplitude independent range.

As might be expected, the damping increases and the critical shear strain decreases with increase in temperature. However, no variation of critical shear strain with temperature was detected for the high purity iron (AHL).

Fig. 3

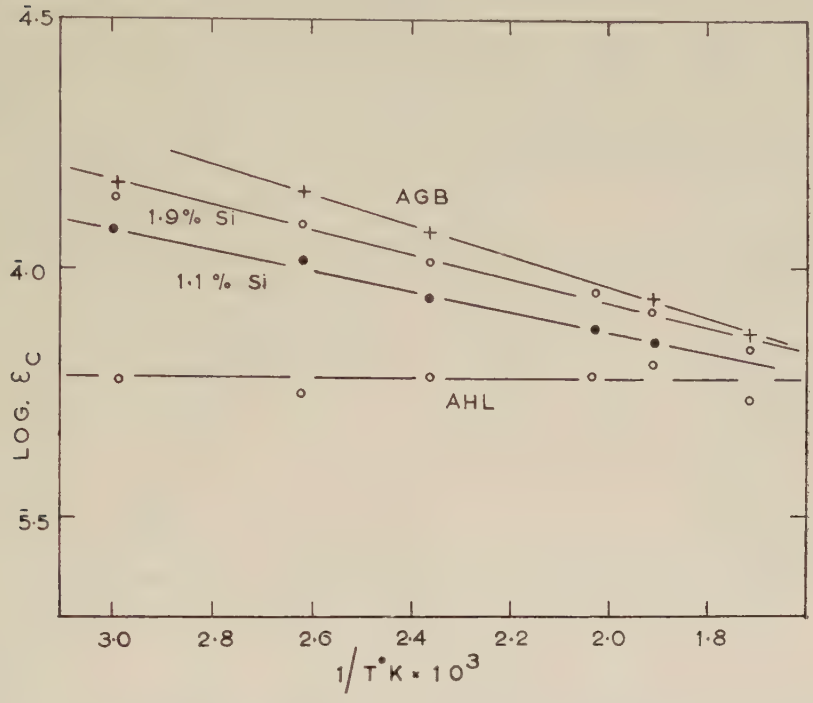

Variation of critical shear strain ϵ_c with temperature.

Table 2. Variation of Critical Shear Strain and Damping with Solute Concentration

Specimen	Critical strain amplitude	Critical shear strain	Amplitude independent damping	Amplitude dependent damping
AHL	2·7 cm	$6{\cdot}08 \times 10^{-5}$	0·0038	0·0057
AGB	7·95 cm	$1{\cdot}79 \times 10^{-4}$	0·0014	0·0015
1·1% Si	4·07 cm	$9{\cdot}21 \times 10^{-5}$	0·0029	0·0044
1·9% Si	6·03 cm	$1{\cdot}36 \times 10^{-4}$	0·0023	0·0033
2·83% Si	6·92 cm	$1{\cdot}56 \times 10^{-4}$	0·0021	0·0044

In the amplitude dependent range the damping values quoted in table 2 are the average values of the damping for amplitudes up to 2 cm above the critical value. In this range an increase in solute concentration decreases the damping; a decrease in temperature also decreases the damping as

may be seen in fig. 4 in which are plotted some results for the 1·9% Si iron alloy. Similar results were found for the 1·1% and the 2·83% Si iron alloy. There appeared to be no variation with temperature of the amplitude dependent damping in the case of the high purity iron (AHL).

Fig. 4

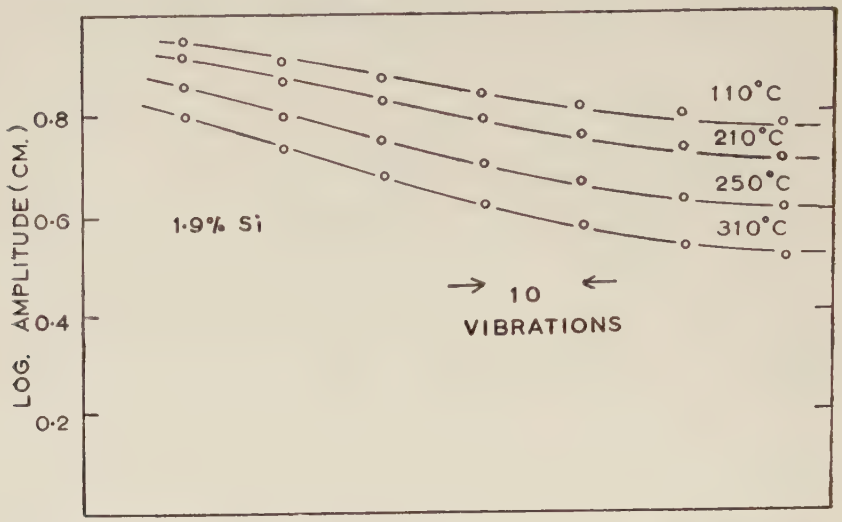

The effect of temperature on the damping in the amplitude dependent range.

§ 4. Discussion

Figure 1 shows that there is a sharp break in the plot of log amplitude/number of vibrations above which the damping is amplitude dependent. Weertman and Salkovitz (1955) have observed a similar sharp 'break-point' on testing lead containing small amounts of either bismuth, tin or cadmium. These measurements were carried out at a frequency of 30 Kc.p.s. Caswell (1957) has made similar observations on copper containing gold. However, Weinig and Machlin (1956) found that for copper alloyed with small amounts of either aluminium, silver, nickel or silicon the damping is amplitude dependent even for low amplitudes. These measurements were carried out at a frequency of 1 c.p.s.

The room temperature damping of pure metals and alloys is taken as being due to the movement of dislocations. Granato and Lücke (1956) have postulated a theory of the mechanical damping due to dislocations which they developed from the earlier theories of Koehler (1952) and Nowick (1950, 1954 a, b). Koehler suggested that the damping under a small applied stress was due to the bowing out of dislocation lines pinned by impurity atoms. The model which Granato and Lücke propose consists of a network of dislocations which are pinned by two different types of pinning points. If it is assumed that a well annealed crystal

contains a network of dislocations, the length of the dislocation loop, L_N, will be determined by the intersection of the dislocation network. On introducing impurity atoms, however, weaker pinning points will be formed due to the attraction of the solute atoms to the dislocation lines and the length of the dislocation loop will be shortened to L_C (see fig. 5). The model has to be modified in the mathematical treatment to take into account the distribution of lengths L_C which will occur.

Fig. 5

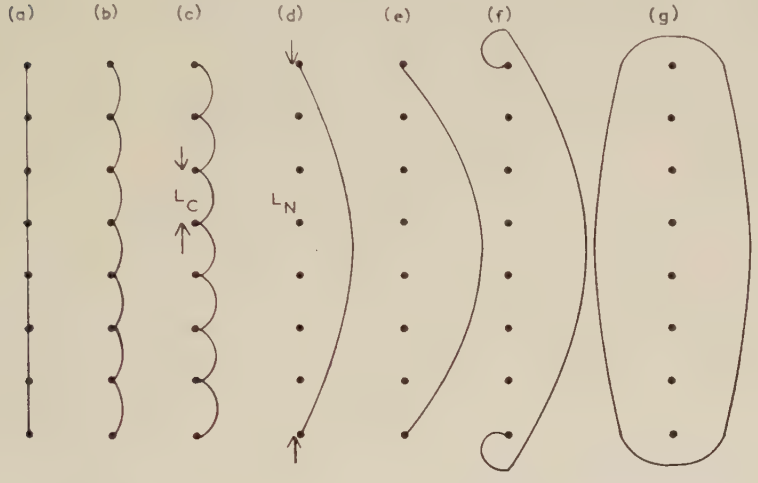

Dislocation damping model proposed by Granato and Lücke.

Granato and Lücke showed that this mechanism will lead to two types of damping, one a dynamic loss and the other a static loss. Under a small applied stress the dislocations vibrate between the impurity pinning points ((*a*) to (*c*)) and a dynamic loss will result due to the phase lag between the motion of the dislocation and the oscillating stress. This will contribute an amplitude independent, frequency dependent component to the damping. At low frequencies the damping will be small but it will reach a maximum near the resonant frequency, which is determined by the loop length.

As the stress is increased the dislocations are pulled from their impurity pinning points and expand to a new loop determined by the distance between the stronger pinning points (fig. 5 (*d*), (*e*)). This stress is believed to correspond to the critical shear strain determined in this work. On reversing the stress field the long loop will collapse along a path determined by the long loop length, thus giving a static hysteresis effect. When the loops have completely collapsed they are again pinned by the impurity atoms and the same type of path is followed in the other half cycle of stress. This will contribute to the damping a component which, at low frequencies, is amplitude dependent and frequency independent.

The damping is therefore composed of two components, i.e.

$$\Delta = \Delta_I + \Delta_H \quad . \quad . \quad . \quad . \quad . \quad . \quad . \quad . \quad (1)$$

where Δ is the total damping, Δ_I is the amplitude independent damping, Δ_H is the amplitude dependent damping. As the stress is increased further the dislocations will bow out and multiply according to the Frank–Read mechanism (fig. 5 (*d*) to (*g*)).

4.1. *Amplitude Dependent Loss*

According to the theory of Granato and Lücke all the amplitude dependent data are describable in terms of a single function of the form

$$\Delta_H = C_1/\epsilon_0 \exp(-C_2/\epsilon_0) \quad . \quad . \quad . \quad . \quad . \quad . \quad . \quad (2)$$

where ϵ_0 is the shear strain, and C_1 and C_2 are constants for a given metal.

Therefore, if the experimental data are plotted in the form

$$\log \epsilon_0 \Delta_H \quad \text{against} \quad 1/\epsilon_0$$

a straight line plot should be obtained. The slope of the line is given by

$$C_2 = K\epsilon' a/L_C \quad . \quad . \quad . \quad . \quad . \quad . \quad . \quad . \quad (3)$$

where ϵ' is the fractional difference in size of the solvent and solvent atoms, a is the lattice constant, K is a factor depending on the orientation and anisotropy of the specimen, L_C is the characteristic impurity pinned dislocation length. Granato and Lücke showed this to be true for the measurements of Weertman and Salkovitz (1955) on lead containing small amounts of either bismuth, tin or cadmium.

In the present investigation the amplitude independent background has been taken for Δ_I. This follows a convention introduced by Caswell (1957). although Kamentsky (1957) has pointed out that this background is not fully explained by the Granato and Lücke theory for Δ_I.

Figures 6 and 7 show that the experimental data for AHL, 1·1% Si and 1·9% Si irons are in good agreement with eqn. (2). The slope of the line C_2 increases with increasing silicon content (the difference between C_2 for the 0% Si and the 1·1%Si is very small but significant). This is in agreement with eqn. (3), which predicts that as the impurity pinning points become closer and more effective (i.e. as L_C decreases) C_2 will increase. However, the theory predicts that C_2 should be proportional to the concentration of impurity on the dislocation line, which would be expected in turn to be proportional to the average concentration in the metal. It is obvious from fig. 6 that this is not so. The rate of decrease of C_2 with silicon concentration is less than that required for proportionality.

Figure 7 shows that C_2 (the slope of the lines plotted) decreases with increase in temperature. This is attributed to an increase in L_C (see eqn. (3)) brought about by the fewer number of solute atoms at the dislocations at the higher temperatures. If solute atoms are attracted to the dislocations by a Cottrell mechanism, one would expect the concentration C to be equal to $C_0 \exp(Q/kT)$ where Q is the interaction energy. A plot

of $\log C_2$ against $1/T$ should thus be in a straight line of slope Q/k. This has been tried in fig. 8 using the results in fig. 7.

The points lie on a curve but appear to be asymptotic to a straight line at the lower temperatures. The deviation from a straight line at the higher temperatures may be attributed to shearing taking place at the crystal

Fig. 6

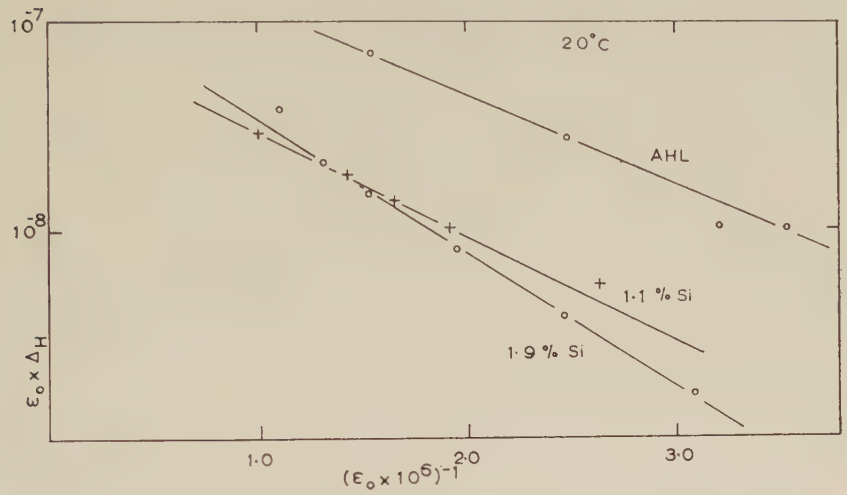

Relationship between the shear strain and the damping in the amplitude dependent range (20°C).

Fig. 7

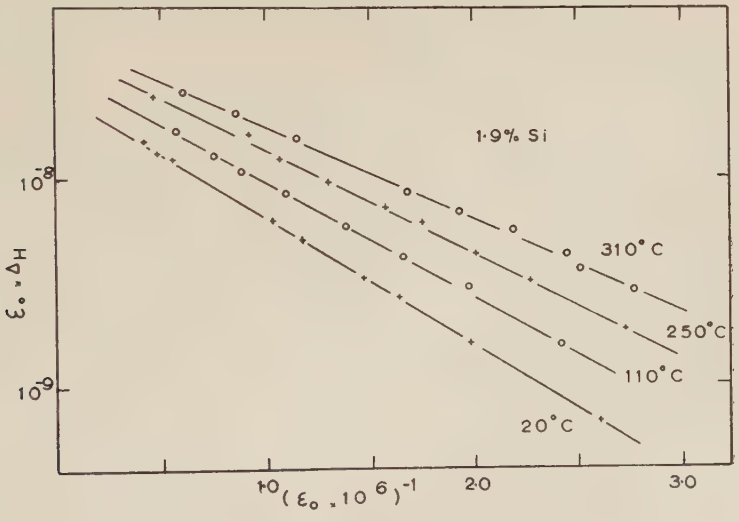

Variation of the shear strain with the damping in the amplitude dependent range at various temperatures.

boundaries. This is known to occur as the temperature is increased: e.g. (Gibbons 1953) an internal friction peak due to crystal boundary shearing has been observed at 570°c. The straight line portion of the graph corresponds to an interaction energy of approximately 0·012 ev. This value may not be very accurate since it involved taking the differences of differences in its calculation.

A second method of estimating Q is to consider the variation of the critical shear strain with temperature. According to Cottrell (1953) the yield strength of an alloy is proportional to C, the concentration on the dislocation lines, provided C is small (as it is in this case). The temperature variation of C is given by

$$C = C_0 \exp(Q/kt),$$

Fig. 8

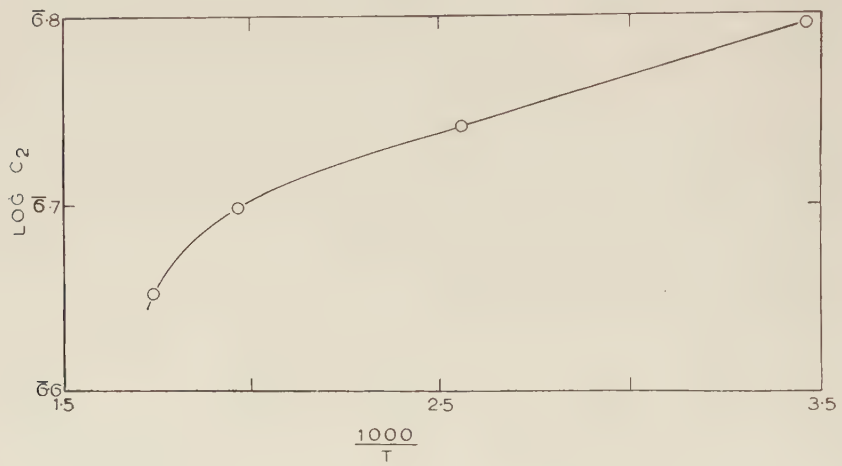

Variation of log C_2 with temperature.

so that a plot of log critical shear strain against $1/T$ should give a straight line. The experimental points lie on quite good straight lines as may be seen in fig. 3. From the slopes of the lines one obtains $Q = 0{\cdot}004$ ev for silicon in iron and $Q = 0{\cdot}006$ for oxygen in iron.

Cottrell (1953) calculated that the maximum binding energy of a solute atom with a dislocation is $a^3\mu\theta/2$. The value of θ ($= (1/a)da/dc$) is approximately 10^{-2} for dilute solutions of silicon in iron (Farquhar *et al.* 1945), $\mu = 8{\cdot}24 \times 10^{11}$ (Schmidt and Boas 1950) and $a = 2{\cdot}83$Å (Farquhar *et al.* 1945). Using these values, Q is 0·0058 ev. No value of Q can be calculated for the case of oxygen in iron owing to lack of data on the lattice parameters.

From the experimental point of view the variation of the critical shear strain with temperature gives a more accurate result than the method based on Granato and Lücke's model. However, the latter, in principle

at any rate, can give further information. For instance, from eqn. (3), one may calculate L_C the distance between solute atoms along a dislocation line. Using Granato and Lücke's value of 0·02 for $1/K$ one obtains a value of about 10^{-6} cm for L_C. Unfortunately, no other values of L_C are available for comparison.

§ 5. Conclusions

The variation of internal friction with amplitude is in good agreement with that deduced by Granato and Lücke from a model of dislocations pinned by solute atoms.

The binding energy between a silicon atom and a dislocation line in iron silicon alloy has been found to be approximately 0·004 ev. That for oxygen in iron is approximately 0·006 ev.

References

Caswell, H. I., 1957, *Thesis*, Cornell University.
Cottrell, A. H., 1953, *Dislocations and Plastic Flow in Crystals* (Oxford: Clarendon Press).
Farquhar, M. C., Lipson, H., and Weill, A. R., 1945, *J. Iron St. Inst.*, **152,** 457.
Gibbons, D. F., 1953, *Trans. Amer. min. (metall.) Engrs*, **194,** 1245.
Granato, A., and Lücke, K., 1956, *J. appl. Phys.*, **27,** 583, 789.
Kamentsky, L. A., 1957, *Thesis*, Cornell University.
Koehler, J. S., 1952, *Imperfections in Nearly Perfect Crystals* (New York: Wiley & Sons, Inc.), p. 197.
Nowick, A. S., 1950, *Phys. Rev.*, **80,** 249; 1954 a *Progr. Metal Phys.*, **4,** 1; 1954 b, *J. appl. Phys.*, **25,** 1129.
Schmidt, E., and Boas, W., 1950, *Plasticity in Crystals* (London).
Weertman, J., and Salkovitz, E. I., 1955, *Acta Met.*, **3,** 1.
Weinig, S., and Machlin, E. S., 1956, *Acta Met.*, **4,** 262.

Nuclear Orientation and the Hyperfine Structure Coupling in Cobalt Metal†

By M. A. Grace, C. E. Johnson‡, N. Kurti, R. G. Scurlock and R. T. Taylor§
The Clarendon Laboratory, Oxford

[Received April 21, 1959]

Abstract

The hyperfine structure coupling for cobalt in hexagonal cobalt metal has been determined using a nuclear orientation technique. The hyperfine structure coupling, represented as an effective magnetic field H_{eff} at the nucleus, is given by $H_{\text{eff}}=193\pm 20$ kgauss.

§ 1. Introduction

Measurements of the hyperfine structure coupling in ferromagnetic metals could lead, in principle, to further knowledge about the electronic states of the electrons responsible for the ferromagnetism. Such measurements are not, at present, possible by radio-frequency methods. In searching for other methods for determining the hyperfine structure coupling, the use of a nuclear orientation technique appeared to be possible.

In a ferromagnetic material it is known that the ferromagnetic electron moments are orientated parallel to each other within a single domain, at temperatures low compared with the Curie point. In general, a small magnetic field is sufficient to produce saturation so that all the domains are aligned with their axes of magnetization parallel. If there is a magnetic hyperfine structure coupling, each nucleus will find itself in an effective magnetic field, H_{eff}, which is the same for all isotopes of each component element in a given ferromagnetic substance (Marshall 1958). For a nucleus with magnetic moment μ_n a nuclear polarization should be set up at sufficiently low temperatures, i.e. when $\mu_n H_{\text{eff}} \approx kT$ or $T \approx 0{\cdot}01^\circ\text{K}$–$0{\cdot}05^\circ\text{K}$.

The time taken to establish the polarization is governed by the relaxation time of the nuclear spins with their surroundings. Clearly, if this time is long compared with the usual time of observation (about 10 min) the method loses its attractiveness for determining H_{eff}. Fortunately,

† Communicated by the Authors.
‡ Now at University of California, Berkeley, California, U.S.A.
§ Now at University of Liverpool.

in ferromagnetic metals, the nuclear spin relaxation time is expected to be reasonably short as a result of the presence of conduction electrons.

The ordering of the nuclear spins may be observed by replacing some of the stable atoms by a suitable γ-ray emitting radio-isotope. The γ-rays will show an anisotropic intensity distribution depending on the degree of orientation of the nuclei. The quantity ϵ, equal to $1 - W(0)/W(\pi/2)$ where $W(0)$ and $W(\pi/2)$ are the γ-ray intensities parallel and perpendicular to the domain axes, is usually defined as the γ-ray anisotropy. For relatively small degrees of nuclear orientation and correspondingly small values of ϵ (i.e. not too low temperatures) it may be shown that

$$\epsilon = \text{constant} \left(\frac{\mu_n H_{\text{eff}}}{IkT}\right)^2$$

where I is the nuclear spin and the constant depends in a known fashion upon the mode of radioactive decay of the nucleus being 39/14 for ^{60}Co. Hence if μ_n and I are known, H_{eff} can be determined from the measurement of the γ-ray anisotropy at a particular temperature.

§ 2. Preliminary Experiments

The first experiments were carried out to determine H_{eff} in hexagonal cobalt, the anisotropic γ-emission from ^{60}Co being used to measure the nuclear orientation. A single crystal of dimensions $10 \times 2 \times 2$ mm (kindly given by Dr. J. Galt of the Bell Telephone Laboratories) was used. Although, as mentioned in the introduction, magnetic saturation of the specimen can be achieved by an external field, this is not necessary in the case of cobalt, if a single crystal is used. It is known that in cobalt, the domains are predominantly aligned parallel and antiparallel to the hexagonal axis with very few closure domains. Hence in a single crystal, macroscopic alignment (not polarization) of the nuclear spins will obtain at sufficiently low temperatures†.

The crystal was irradiated with thermal neutrons in the Harwell pile to give a final activity of 5 μc of ^{60}Co. After capturing a thermal neutron the ^{60}Co nucleus is in a highly excited state and emits one or more high energy capture γ-rays. As a result it recoils with an energy of up to 50 ev, leaving its lattice site and perhaps locally destroying the crystal lattice structure. Some annealing process is required so that the ^{60}Co atoms can diffuse back to correct lattice sites. Although it seems likely that this annealing takes place quite rapidly at room temperature (see, for instance, Cottrell (1958)) the crystal was nevertheless kept for four weeks at 350°c, just below the crystallographic transition point. After annealing, the cobalt crystal was immersed in a mixture of powdered potassium chrome alum and glycerol which was then cooled to 0·04°k by adiabatic demagnetization. The γ-ray intensities along and perpendicular to the

† We are very grateful to Dr. C. P. Bean, General Electric Research Laboratory, (Schenectady) for drawing our attention to this possibility, which considerably simplified the experimental arrangement.

axis of the cobalt crystal were measured in the usual way with two scintillation counters. A small but definite γ-ray anisotropy of $1{\cdot}5 \pm 0{\cdot}5\%$ was established (Grace *et al.* 1955). This result showed that some nuclear orientation of the ^{60}Co nuclei had been achieved, thus demonstrating the existence of a magnetic hyperfine structure coupling in cobalt metal. It also suggested that the magnitude of H_{eff} was about one third of that observed for the Co^{++} ion in paramagnetic salts. At about the same time, the nuclear orientation of ^{60}Co in a ferromagnetic material was reported by Khutsishvili (1955) who found larger anisotropies. A possible explanation of the small value of H_{eff} found by us was that the cobalt did not attain thermal equilibrium with the chrome alum. Since the γ-ray anisotropy was so small, the measurement was not sufficiently accurate to see whether the anisotropy was actually increasing with time. However, the following calculation shows the likelihood of the specimen not reaching temperature equilibrium during the measuring time of 10 min.

At temperatures well below 1°K the rate of transfer of heat across an area of contact A cm^2 between two solids is given by

$$\dot{Q} = \alpha A(T_1^3 - T_2^3) \text{ erg/sec}$$

when T_1 and T_2 are the temperatures of the two solids and the experimental value of α is about 10^3 erg sec^{-1} cm^{-2} deg^{-3} (Mendoza 1948, Robinson 1954). Suppose one solid is the cobalt with specific heat C given by $(CT_1^2/R)_{\text{hfs}} = b$; and the other solid is the heat sink with a temperature $T_2 \ll T_1$ and with sufficiently large heat capacity for this condition to remain valid during the cooling of the cobalt. If we neglect heat evolution in the cobalt due to radioactivity, the heat condition equation is

$$-C\,dT_1/dt = \alpha A T_1^3.$$

Replacing C by bR/T^2 and integrating, the time t to cool from 1° to T°K is given by

$$t = bR/4A \,.\, 1/T^4 \times 10^{-3} \text{ sec.} \quad . \quad . \quad . \quad . \quad . \quad . \quad (1)$$

The value of ϵ of 0·015 at 0·04°K leads to a value of b equal to $1{\cdot}3 \times 10^{-4}$, so that during the time of observation of 10 min, the cobalt specimen, mass 0·25 g, A equal to 0·8 cm^2, would only have cooled to 0·08°K. This made it likely that the hfs coupling was considerably larger. The correspondingly larger specific heat would then make the cooling problem greater. It was therefore necessary to increase the cooling efficiency by increasing the effective area of contact between cobalt and chrome alum heat sink.

Another consequence of the large nuclear specific heat is that a large heat reservoir would be required. If we assume for the nuclear specific heat, a value of b equal to 10^{-3}, which is about the smallest found in Co^{++} salts, we can calculate the amount of chrome alum required to cool the specimen of 0·25 g from 1°K to 0·03°K. Consider the following two ways of cooling assuming 25 kG at 1°K as the initial conditions.

First suppose the demagnetization is carried out so slowly that the cobalt is always in thermal equilibrium with the heat sink. In this case,

by equating the entropy of magnetization of the chrome alum with the entropy change from 1° to 0·03°K of both cobalt and chrome alum, we find 1·5 g of chrome alum is required, i.e. a weight ratio of 6 : 1.

If on the other hand, one carried out the cooling irreversibly i.e. demagnetizing the salt rapidly and allowing it to arrive at thermal equilibrium with the cobalt, ten times as much chrome alum would be needed. Experimentally, a compromise must be made to obtain a reasonably fast heat transfer bearing in mind that irreversible 'hysteresis' heating in the cobalt probably arises during the demagnetization.

Assuming irreversible cooling of the cobalt specimen and using eqn. (1), the time taken to cool from 1°K to 0·04°K and 0·03°K would be 156 sec and 480 sec respectively when the effective area of thermal contact A is 250 cm². Experimentally, these times are convenient.

§ 3. Measurement of H_{eff} in Cobalt Metal

For the measurement of H_{eff}, the experiments were carried out with a specimen in which the effective area of contact between cobalt and chrome alum was increased to 250 cm² by soft-soldering, with 60% Sn–40% Pb solder, the cobalt to the ends of a number of copper fins immersed in the heat sink pill. For the calculations outlined in the previous section, the thermal resistance due to the soldered junction was neglected: this is permissible down to 0·02°K provided the solder layer is of the order of 10^{-2} mm or less. The chrome alum heat sink was made up using a variation on the method developed by Robinson (1954) and Kurti *et al.* (1956). The chrome alum crystals were finely ground and a 50/50 mixture of glycerol and saturated aqueous solution of chrome alum added until the resulting mixture had the consistency of jam. About twenty copper fins, 0·15 mm thick and 13 mm wide, were painted with the 'jam', assembled together and sealed into a cylindrical Perspex case so that the lower ends of the fins projected out. These ends were tightly bound with cotton so as to make the assembled heat sink pill as rigid as possible at room temperature.

Spohr (1958) has found that such a specimen deteriorates if kept at room temperature for more than a few hours, presumably because the glycerol takes up water of crystallization from the chrome alum. For this reason, the pill was cooled in liquid oxygen after the assembly was completed, and was only allowed to warm up to room temperature for the two hours necessary for mounting in the low temperature cryostat. Since a long time constant to attain thermal equilibrium was expected, a separate thermometer was considered necessary to measure the temperature of the cobalt. This thermometer was made up in a similar way to that used for the heat sink pill, using finely ground cerium magnesium nitrate in place of the chrome alum. The ends of a number of copper fins were immersed in the 'jam' of cerium magnesium nitrate and glycerol so that the area of thermal contact within the thermometer pill was 200 cm².

Cerium magnesium nitrate was used since it has a small heat capacity in zero field over the temperature range above 0·01°K and therefore its temperature, measured from the magnetic susceptibility of the salt, should closely follow that of the cobalt specimen.

Finally, the assembly was completed by soft-soldering together the ends of the two sets of copper fins projecting from the heat sink and thermometer pills to the cobalt crystal, which had its axis horizontal (fig. 1, Pl. 110). The assembled specimen was then mounted rigidly in the helium cryostat by screwing it to the end of a thin-walled 1/8 in. stainless steel tube, 6 cm long, soldered to the top of the inner vacuum space.

§ 4. Experimental Procedure and Results

The adiabatic demagnetization of the chrome alum heat sink was carried out so that the cooling of the cobalt specimen was approximately isentropic. After isothermal magnetization at 1°K, the inner vacuum space was pumped for 5–10 min. The magnetizing field was then reduced from 25 kG at the rate of about 100 gauss/sec to one-tenth of its original value when the chrome alum heat sink cooled to about 0·1°K. After maintaining this field for 5 min, to allow the cobalt to cool to thermal equilibrium, the field was reduced to zero at the same rate of 100 gauss/sec. At this rate of reduction, the total eddy current heating in the copper and the cobalt is calculated to be less than 20 ergs, and is therefore negligible compared with the heat to be removed from the cobalt. During some demagnetizations from 25 kG the field was kept at a second steady value of 1 kG for 5 min before reducing it to zero, but no increased cooling of the cobalt was observed.

After demagnetizing to zero field, the γ-ray detectors were placed in position around the cryostat, and simultaneous measurements were made of the γ-ray anisotropy and of the d.c. magnetic susceptibility, hence the 'magnetic' temperature of the cerium magnesium nitrate thermometer. During magnetization this thermometer pill was exposed to a field of about one-half of that at the chrome alum cooling pill, and hence on demagnetization it cooled to about 0·003°K. Because of the rather large heat content of cerium magnesium nitrate at the lowest temperatures it took, according to the conditions, between 2 and 5 min for the thermometer to come into equilibrium with the cobalt specimen. After this initial period and at temperatures above about 0·03°K there was good thermal equilibrium between the cobalt and the thermometer. It was also found that the temperature of the cobalt, as indicated qualitatively by the γ-ray anisotropy, took several minutes after demagnetization to approach that of the chrome alum heat sink.

Because of the slow warming-up rate of the assembly a temperature interval of only about 10% was covered after each cooling. Demagnetizations from different initial conditions were used to cover the whole temperature range above 0·03°K.

The results are shown in fig. 2, giving the square root of the γ-ray anisotropy as a function of $1/T$. Each point represents the mean of 6–8 individual γ-ray anisotropy determinations spread over temperature intervals of about 10%. As expected the points lie on a straight line, given by

$$\sqrt{\epsilon} = (8{\cdot}9 \pm 0{\cdot}9) \times 10^{-3}\ 1/T. \quad . \quad . \quad . \quad . \quad . \quad . \quad (2)$$

Taking the best value (Dobrowolski 1957) for the nuclear moment of ^{60}Co to be $\mu_{60} = 3{\cdot}8$ n.m. and $I_{60} = 5$, the value of the effective field is

$$H_{\text{eff}} = 193 \pm 20 \text{ kG (Grace } et\ al. \text{ 1957)}\dagger.$$

Assuming a Hamiltonian $\mathscr{H} = AI_z S_z$, the hyperfine structure constant A for ^{59}Co ($\mu_{59} = 4{\cdot}64$ n.m., $I_{59} = 7/2$) in the metal is $0{\cdot}0128 \pm 0{\cdot}001$ cm^{-1}.

Fig. 2

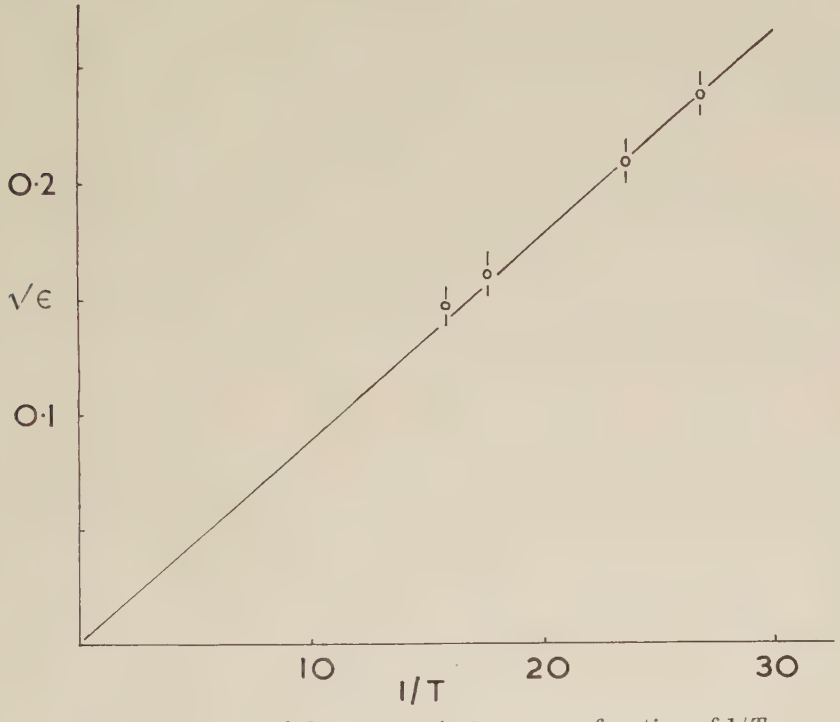

The square root of the γ-ray anisotropy as a function of $1/T$.

The relatively large γ-ray anisotropies provide a very convenient method for measuring the temperature of the nuclear spin system and hence of the cobalt metal. We have used this method to examine heat

† This is smaller than the value quoted in this reference. The difference is due to the fact that in that publication no correction was made for the effect of the chrome alum heat-sink on the susceptibility measurement of the cerium magnesium nitrate thermometer.

transfer at these low temperatures. For this purpose, the area of thermal contact within a heat sink pill was increased to 560 cm^2 when indeed considerably further cooling of the cobalt crystal was obtained. This was shown by the maximum γ-ray anisotropy of 0·143 attained 15 min after demagnetizing the heat sink to zero field. The results are shown in fig. 3, which gives as a function of time both the γ-ray anisotropy ϵ and the absolute temperature T, the latter being calculated from eqn. (3). From this cooling curve a value of $\alpha = 1{\cdot}6 \times 10^3$ erg sec^{-1} cm^{-2} deg^{-3} was deduced for the heat transfer coefficient of eqn. (1) in reasonable agreement with the value given by Mendoza (1951) and Robinson (1954).

Fig. 3

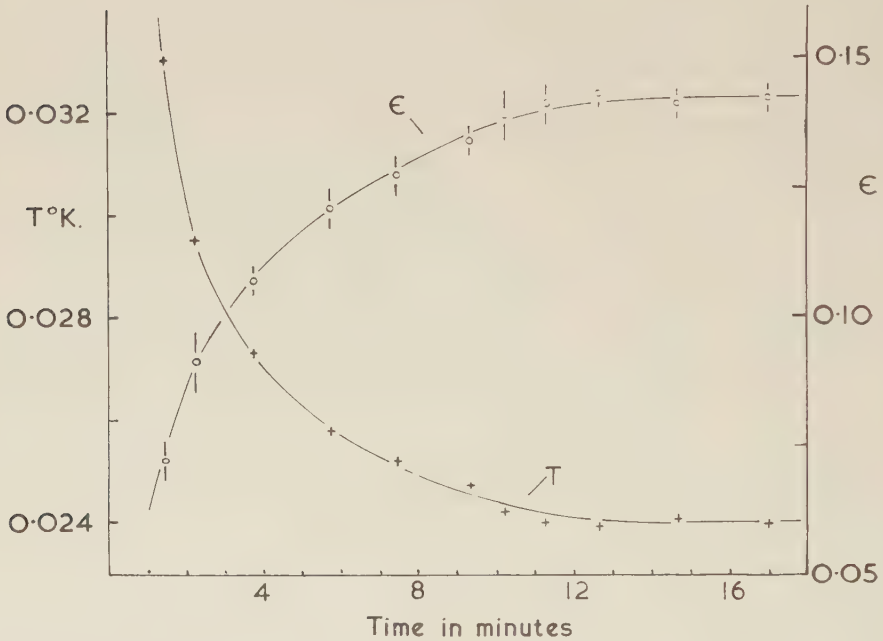

Plot of γ-ray anisotropy and absolute temperature of cobalt as function of time after demagnetization.

§ 5. Conclusion

Once these nuclear orientation experiments had demonstrated that the hyperfine coupling in cobalt metal was considerable, it became clear that specific heat measurements would provide an alternative method of measurement (see, for example, Heer and Erickson 1956). Such measurements were carried out by Heer and Erickson (1957) and Arp *et al.* (1957). Below 1°K, both lattice and spin-wave contributions are negligible, so that the specific heat C/R between 0·3°K and 1°K can be represented by

the sum of an electronic term (γT) and a hyperfine coupling term (b/T^2). Heer and Erickson find $b = CT^2/R = 4{\cdot}0 \times 10^{-4}$ while Arp, Kurti and Peterson give $CT^2/R = 4{\cdot}7 \times 10^{-4}$. The values of H_{eff} calculated from these results are 183 and 200 kG respectively, in good agreement with the value of 193 kG found in the nuclear orientation experiments.

It is clear that both nuclear orientation and specific heat experiments have their merits for extending the measurement of H_{eff} to ferromagnetic alloys. Unfortunately, ^{59}Co is the only suitable naturally occurring isotope with non-zero nuclear spin in the iron group of ferromagnetics so that specific heat experiments are limited to the measurement of H_{eff} for cobalt in alloys containing a relatively high percentage of cobalt. These measurements can be made with reasonable accuracy. On the other hand, the accuracy of nuclear orientation measurements is not so good; but since the measurements require only a minute concentration of the γ-emitting isotope (20 μC for the specimen) they can be made on very dilute alloys. In addition, nuclear orientation measurements are not limited to cobalt and could be used to determine H_{eff} for other elements by using a suitable γ-emitting istope. It should be emphasized that one complication to the nuclear orientation experiment on cubic alloys is that an external field is required to saturate the specimen.

A quantitative comparison of the results on cobalt metal, with those obtained in Co^{++} salts is difficult, since in the salts the hyperfine structure coupling cannot be strictly represented by an effective magnetic field at the nucleus. A qualitative comparison with the specific heats of magnetically diluted Co^{++} salts which vary from $CT^2/R = 10 \times 10^{-4}$ to 25×10^{-4} (Bleaney and Ingram 1951) indicates that in cobalt metal there is no appreciable conduction electron polarization as suggested by Zener (1951) since this would tend to increase the effective field and hence the specific heat as compared with the salt.

A theoretical discussion of the various contributions to the effective magnetic field at the nuclei in ferromagnets has been made by Marshall (1958) using the Van Vleck (1945, 1953) model of ferromagnetism. He considered the three main contributions to H_{eff}, namely that from s-electrons, from d-electron spins and d-electron orbits, and calculated a total field for hexagonal cobalt in reasonable agreement with the experimental results.

Marshall pointed out, that the validity of the Van Vleck model he used could be tested more completely by extending the measurements of H_{eff} to alloys of cobalt with iron or nickel and observing the effect of change in crystal symmetry and of the electronic structure of the other alloying constituents on the various contributions to H_{eff}. A series of experiments on cobalt–iron and cobalt–nickel alloys have been carried out recently by Baldock *et al.* (1959) and a preliminary report given by Kurti (1959).

It seems, in conclusion, that the measurement of the hyperfine structure coupling in ferromagnetic metals and alloys by nuclear orientation and specific heat techniques forms a useful tool for the study of ferromagnetism.

Acknowledgments

We wish to express our grateful thanks to Dr. W. Marshall for many helpful and illuminating discussions. This work was carried out during the tenure of a maintenance grant from the Department of Scientific and Industrial Research by R.G.S. and R.T.T.

References

Arp, V., Kurti, N., and Peterson, R., 1957, *Bull. Amer. phys. Soc.*, **2,** 388.
Baldock, D. N., Exell, R., Kurti, N., Marshall, W., Scurlock, R. G., and Sowter, C. V., 1959 (to be published).
Bleaney, B., and Ingram, D. J. E., 1951, *Proc. roy. Soc.* A, **208,** 143.
Cottrell, A. H., 1958, Symposium on Vacancies and other Point Defects in Metals and Alloys, Inst. of Metals.
Dobrowolski, W., Jones, R. V., and Jeffries, C. D., 1956, *Phys. Rev.*, **101,** 1001.
Grace, M. A., Johnson, C. E., Kurti, N., Scurlock, R. G., and Taylor, R. T., 1955, *Comm. Conf. Basses Temperatures* (Paris), p. 263.
Grace, M. A., Johnson, C. E., Kurti, N., Scurlock, R. G., and Taylor, R. T., 1957, *Bull. Amer. phys. Soc.*, **2,** 136.
Heer, C. V., and Erickson, R. A., 1956, *Bull. Amer. phys. Soc.*, **1,** 217; 1957, *Phys. Rev.*, **108,** 896.
Khutsishvili, G. R., 1955, *J. exp. theor. Phys.*, **29,** 894.
Kurti, N., 1959, *J. appl. Phys.*, **30,** 215S.
Kurti, N., Robinson, F. N. H., Simon, F. E., and Spohr, D. A., 1956, *Nature, Lond*, **178,** 450.
Marshall, W., 1958, *Phys. Rev.*, **110,** 1281.
Mendoza, E., 1948, *Ceremonies Langevin-Perrin College de France*, p. 53.
Robinson, F. N. H., 1954, Thesis, Oxford.
Spohr, D. A., 1958, Thesis, Oxford.
Van Vleck, J. H., 1945, *Rev. mod. Phys.*, **17,** 42; 1953, *Ibid.*, **25,** 220.
Zener, C., 1951, *Phys. Rev.*, **83,** 298.

The Solubility of Krypton in Liquid Lead, Tin and Silver†

By G. W. Johnson and R. Shuttleworth
Metallurgy Department, The University of Leeds

[Received May 4, 1959]

Abstract

By means of radioactive ^{85}Kr the solubility of krypton in liquid lead and liquid tin has been measured. In the temperature range 800°C to 1300°C for lead and 1100°C to 1300°C for tin the Ostwald coefficient r (volume of gas dissolved in unit volume of metal) varies with temperature according to the empirical relation

$$r = \frac{r_\infty}{\text{antilog} T_S/T},$$

and the thermodynamic equation

$$r = \frac{h^3}{(2\pi mkT)^{3/2}} \frac{1}{a^3} \exp\left(\frac{S}{R}\right) \exp\left(-\frac{H}{RT}\right),$$

where $1/a^3$ is the number of metal atoms in unit volume, m the mass of a krypton atom, H is the energy needed to transfer an atom at rest in the gas into solution in the metal, and S the vibrational entropy of a krypton atom dissolved in the liquid metal. Experimental results are given in the table.

Metal	r_∞	T_S (°K)	$2{\cdot}3RT_S$† (kcal/mole)	S (cal/°K/mole)	H (kcal/mole)
Lead	0·18	7180	32·8	24·1	37
Tin	1·3	10000	46	30	50

† The heat of solution.

The values of H are approximately equal to the surface area of a krypton atom multiplied by the surface energy of the liquid metal, and the vibrational entropies of the gas atoms are less than those of the metal atoms corresponding to a greater vibrational frequency.

No solubility was detected in liquid silver showing that $r < 10^{-7}$, i.e. when krypton pressure is one atmosphere the atomic fraction dissolved is less than 10^{-11}.

§ 1. Introduction

In a theoretical treatment Rimmer and Cottrell (1957) stated that the solubility of the inert gases in solid metals should be very small because the large inert gas atoms would have a large strain energy. However, they suggested that appreciable solubility might be expected in liquid metals. To investigate these large strain energies it was decided to measure the solubility of krypton in solid and liquid metals, and this paper reports the results for liquid lead, tin and silver.

† Communicated by the Authors.

Since the number of atoms of a monatomic gas which dissolve in a volume of metal is proportional to the pressure it is convenient to specify the solubility by Ostwald's coefficient r (Hildebrand and Scott 1950).

$$r = \frac{\text{Number of gas atoms in unit volume of metal}}{\text{Number of gas atoms in unit volume of gas}}$$
$$= \text{Volume of gas dissolved in unit volume of metal.}$$

Lannung (1930) has measured the solubilities of helium, neon and argon, in water and various organic liquids and found $r \sim 10^{-1}$. These organic molecules are larger than the inert-gas atoms; the heat of solution tends to zero as the size of the gas atoms increase because the van der Waals binding energies between two organic molecules and between a gas atom and an organic molecule are about the same. An attempt to measure the solubility of argon in uranium was made by Johns (1946) who concluded that at 600°C, r was less than 10^{-2}. Preliminary measurements by Mitra (1956) of the solubility of xenon in liquid bismuth gave $r \sim 10^{-2}$, but owing to neglect of adsorption it is likely that the solubility is much overestimated. Van Wieringen and Warmoltz (1956), using a mass spectograph, found that the solubility of helium in silicon at 1208°C was $r = 3 \times 10^{-6}$, and the solubility in germanium at 863°C was $r = 7 \times 10^{-7}$.

Diffusion coefficients of argon, krypton and xenon in silver have been measured by LeClaire and Rowe (1955) and Tobin (1957, 1958). They obtained a supersaturated solution by using an electric discharge to cause the inert-gas atoms to adhere to the metal surface.

In the present work krypton was used because of the high sensitivity with which radioactive ^{85}Kr can be estimated. ^{85}Kr is produced by fission of uranium and decays by emission of beta particles of maximum energy 0·7 MeV. After purification (Arrol *et al.* 1954) the gas is supplied as pure krypton in which 3% of the atoms are ^{85}Kr, and it is possible to detect about 10^{-8} cm^3 of the gas.

§ 2. Experimental Technique and Results

There were three stages in the experimental work: (*a*) the gas and liquid metal were thoroughly mixed to obtain equilibrium, (*b*) the gas was diluted and its beta-activity measured, and (*c*) the metal was rolled into thin foils and its activity measured.

At Harwell a metal sample 4 cm long and ^{85}Kr gas were sealed in an 8 cm length of 6 mm diameter silica tube. To ensure thorough stirring of the gas and liquid metal a silica rod was fixed perpendicular to the tube and rotated at two revolutions a minute by an electric motor. The tube was rotated in a furnace for two days for equilibrium to be reached and then stopped and the tube left vertical for one day for any gas bubbles in the metal to rise to the surface. On removing the tube from the furnace the metal solidified retaining the dissolved krypton.

To measure the high activity of the gas with a Geiger counter it was necessary to take a 10^7th part. This was done by breaking the silica

tube in a 50 l. glass carboy containing air and 1% inactive krypton, after mixing by convection currents the mixture was passed through a small spiral 1 in. in diameter machined in the face of a brass block and covered with *Scotch Tape*. The spiral section was 0·01 in. wide by 0·01 in. deep with a separation of 0·02 in. between adjacent turns. The gas activity was

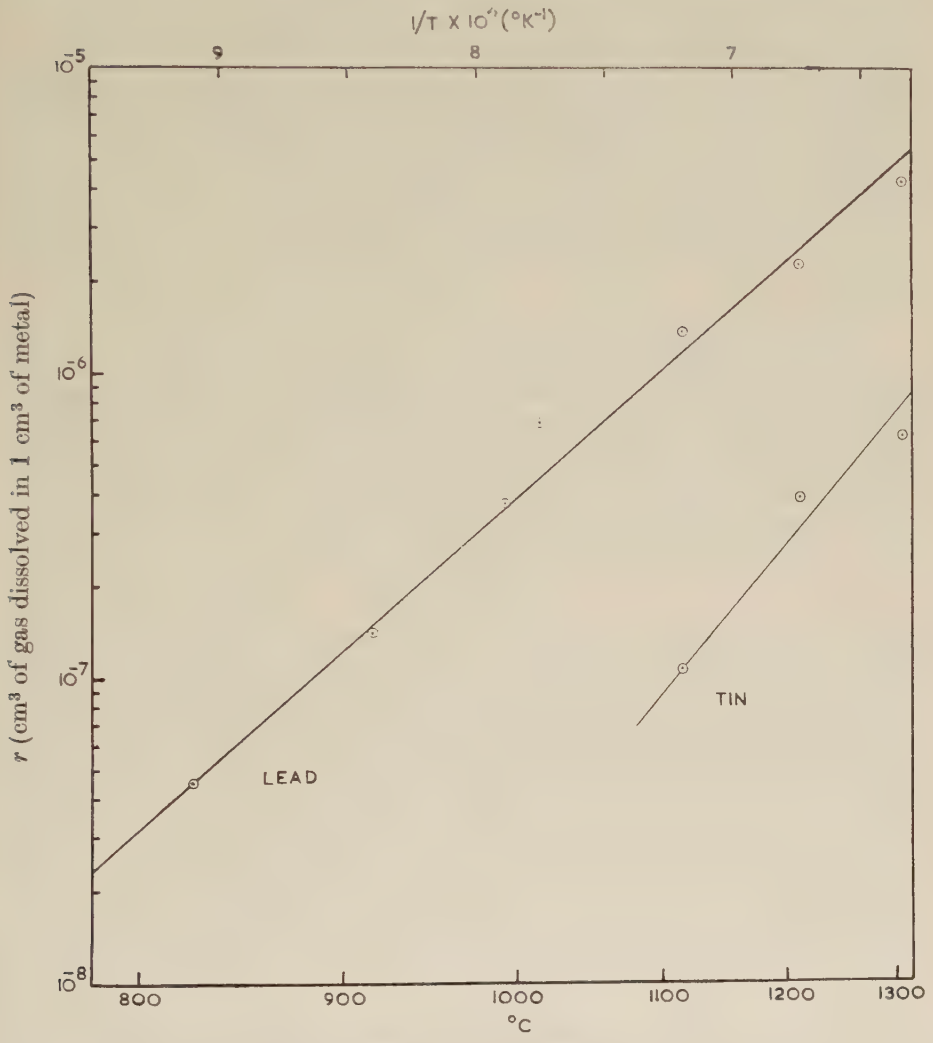

The variation with temperature of the Ostwald solubility coefficient r.

measured by a 1 in. diameter end-window Geiger-Müller counter placed close to the spiral and a small correction for absorption by the *Scotch Tape* was made using the absorption coefficient given by Gleason *et al.* (1951). Gas activities measured with spirals cut in brass and lead blocks were not appreciably different.

The surface of the sample had a high activity of about 10 000 counts a minute and this was ascribed to an adsorbed layer of krypton (about 1/100 of a monolayer) since a light machining of the surface removed the activity. This adsorption phenomenon will be discussed in a later paper. After the surface had been machined-off transverse discs 3 mm thick were cut from the specimen and rolled into thin foils about 0·005 cm thick, and their activities measured with the Geiger-Müller counter.

To check that the observed activity was due to the dissolved krypton, and not to some impurity, the beta absorption coefficient was measured by placing lead foils of different thicknesses above the specimen; and the absorption coefficient was found to be the same as for ^{85}Kr.

Corrections for self-absorption were made by using an experimentally determined absorption coefficient which agreed closely with the value given by Gleason *et al.* (1951). The corrected activity N_t is given by the equation

$$N_t = \frac{\mu t}{[1-\exp(-\mu t)]} . N_0, \quad (\mu_{\mathrm{Pb}} = 375\ \mathrm{cm}^{-1},\ \mu_{\mathrm{Sn}} = 234\ \mathrm{cm}^{-1})$$

where μ is the absorption coefficient, t the foil thickness, and N_0 the observed activity; this gives a correction factor of $N_t/N_0 \sim 2$ for a lead foil 0·005 cm thick, and enables the activity in unit volume of the metal to be calculated.

Results are shown in the figure and the solubility increases with temperature according to the equation

$$r = \frac{r_\infty}{\mathrm{antilog}\, T_S/T}.$$

The smallest solubility which can be measured is $r \sim 10^{-7}$ (atomic fraction when krypton pressure is 1 atm of $\sim 10^{-11}$). This limits the lowest temperature at which measurements can be made to 800°C for lead and 1100°C for tin, and the small temperature range for tin means that T_S can only be found approximately.

Table 1

Metal	r_∞	T_S (°K)	$2{\cdot}3RT_S$† (kcal/mole)
Lead	0·18	7180	32·8
Tin	1·3	10000	46

† The heat of solution.

§ 3. Discussion

From the variation of solubility with temperature it is possible to find the energy H needed to transfer an atom at rest in the gas into solution in the metal, and the vibrational entropy S of a krypton atom dissolved in the liquid metal.

The chemical potentials of a monatomic gas μ_g and the gas dissolved in a liquid μ_l are

$$\mu_g = kT \ln[h^3/(2\pi mkT)^{3/2}] + kT \ln C_g,$$
$$\mu_l = \mu^+ + kT \ln(a^3 C_l),$$

where $\mu^+ = H - TS.$

C_g is the number of gas atoms in unit volume of the gas, C_l the number of gas atoms in unit volume of the metal, and $1/a^3$ the number of metal atoms in unit volume of the metal (Fowler and Guggenheim 1949). For equilibrium the chemical potentials are equal giving

$$r = C_l/C_g = X \exp(-\mu^+/RT) \quad \ldots\ldots (1)$$

where $$X = \frac{h^3}{(2\pi mkT)^{3/2}} \frac{1}{a^3} = 4{\cdot}053 \frac{\rho}{MT^{3/2}}$$

and ρ is the density of the liquid metal and M its molecular weight.

In general H and S vary with temperature but they can be found from the instantaneous slopes of the graphs $\log(r/X)v1/T$, and $T\log(r/X)vT$, because of equation (1) and the thermodynamic relations

$$\partial(\mu^+/T)/\partial(1/T) = H \quad \text{and} \quad \partial\mu^+/\partial T = -S.$$

Values of H and S are given in table 2. The heat of solution $2{\cdot}3RT_S$ is given in table 1 and is less than H by $\frac{5}{2}RT$ because this is the enthalpy of the atoms in the gas.

3.1. *Theoretical Estimates of H and S*

A theoretical estimate of the heat of solution of krypton in a liquid metal can be made by considering that the energy H is made up of three terms: the energy H_h to make a hole in the liquid of the size of a krypton atom, the vibrational energy of a krypton atom when placed in that hole, and the negative van der Waals interaction energy between the krypton atom and the surrounding metal atoms.

The energy to make a hole in the liquid can be estimated by multiplying the surface area of a sphere of the same radius as a krypton atom (1·98 A) by the surface energy of the liquid metal extrapolated to 0°K

$$(\gamma_{Pb} = 488\,\text{erg/cm}^2,\ \gamma_{Sn} = 717\,\text{erg/cm}^2,\ \gamma_{Ag} \sim 900\,\text{erg/cm}^2).$$

The vibrational energy of a krypton atom will be approximately the same as $H_{vib.}$ the vibrational energy of a metal atom which is known from specific heat data (International Critical Tables 1926, Smithells 1955). An approximate estimate can be made of the van der Waals interaction energy by comparing it with the adsorption potentials of the inert gases on metals. Wilkins (1938) obtained a value of 5 kcals/mole for the adsorption potential of argon on platinum, and the van der Waals

interaction energy of a krypton atom dissolved in a liquid metal would be expected to be somewhat greater than this. Values of H_h and H_{vib} are given in table 2.

The vibrational entropy S of a krypton atom in the liquid metal depends on the frequency of vibration ν at high temperatures according to the relation,

$$S = 3R + 3R\ln(kT/h\nu)$$

(Mayer and Mayer 1940), where ν is proportional to the curvature of the potential field in which the vibration takes place. In table 2 values of S are compared with S_m the vibrational entropy of the metal derived from specific heat data (International Critical Tables 1926, Smithells 1955).

Equation (1) can be used to find values of S from the data of Van Wieringen and Warmoltz (1956), and gives the vibrational entropy of helium in solid germanium as 0·3 cals/°K/mole and of helium in silicon as a small negative value. The helium is dissolved interstitially and these surprisingly low entropies suggest a systematic error in the experiment.

Table 2

Metal	H (kcal/mole)	S (cal/°K/mole)	S_m (cal/°K/mole)	H_{vib} (kcal/mole)	H_h (kcal/mole)
Lead	37	24·1	28·1	10·2	34·6
Tin	50	30	27·2	11·7	50·8

3.1.1. *Lead*

The probable error in H is about $\pm 0{\cdot}5$ kcal/mole, and the calculated and experimental values of H would be the same if the van der Waals interaction energy were 7·8 kcals/mole. S has a probable error of about $\pm 0{\cdot}5$ kcals/mole, and taking any systematic errors into account it seems that the vibrational entropy of a krypton atom is definitely less than that of a lead atom and corresponds to a greater vibrational frequency.

3.1.2. *Tin*

The results for tin are less accurate because of the small temperature range in which measurements can be made, but they confirm the method of estimating the solubility. When considering the vibrational entropies it is only possible to say that within the limits of experimental error the vibrational entropies of the krypton and tin atoms are about the same.

3.1.3. *Silver*

No solubility was detected, and this would be expected since $H_h \sim 64$ kcal/mole, $H_{vib} = 10{\cdot}6$ kcal/mole, and $S_m = 23$ cal/°K/mole, giving an estimated solubility of $r = 5 \times 10^{-11}$ which is below the limits of detection.

§ 4. Conclusions

The results suggest that the factor determining the solubility of krypton in liquid metals is the surface energy per unit area of the liquid metal even though the radii of krypton and the metal atoms are appreciably different (Kr = 1·98 A, Pb = 1·75 A, Sn = 1·58 A). These conclusions are confirmed by preliminary measurements on liquid indium which will be published later.

Acknowledgment

The authors are grateful to the U.K.A.E.R.E. for sponsoring this work and providing a maintenance grant for one of the authors (G. W. J.).

References

Arrol, W. J., Wilson, E. J., Evans, C., Chadwick, J., and Eakins, J., 1954, 2nd Radioisotope Conference, Oxford, BB83, ed. J. E. Johnston.

Fowler, R., and Guggenheim, E. A., 1949, *Statistical Thermodynamics* (Cambridge : University Press), p. 81, 374.

Gleason, G. I., Taylor, J. D., and Tabern, D. L., 1951, *Nucleonics*, **8**, 12.

Hildebrand, J. H., and Scott, R. L., 1950, *The Solubility of Nonelectrolytes* (New York: Reinhold), p. 4.

International Critical Tables, 1926, ed. E. W. Washburn, **5** (New York: McGraw-Hill), p. 89.

Johns, I. B., 1946, *U.S. Atom. Ener. Comm. Publ.* (MDDC-290), 1.

Lannung, A., 1930, *J. Amer. chem. Soc.*, 52.1, 68.

Le Claire, A. D., and Rowe, A. H., 1955, *Rev. Metallurgie*, 52, 94.

Mayer, J. E., and Mayer, M. G., 1940, *Statistical Mechanics* (New York: J. Wiley), p. 242.

Mitra, C. R., and Bonilla, C. F., 1956, *U.N.O. Conference on Peaceful Uses of Atomic Energy*, **9**, 331.

Rimmer, D. E., and Cottrell, A. H., 1957, *Phil. Mag.*, **2**, 1345.

Smithells, C. J., 1955, *Metals Reference Book* 2 (London: Butterworths), pp. 604, 639.

Tobin, J. M., 1957, *Acta Met.*, **5**, 398; 1958, A.E.C., R. and D. Report, HW-53639.

Van Wieringen, A., and Warmoltz, N., 1956, *Physica*, **22**, 849.

Wilkins, F. J., 1938, *Proc. roy. Soc.* A, 164, 510.

Ductile Fracture in Metals†

By K. E. Puttick
Department of Metallurgy, Cambridge‡

[Received March 6, 1959]

Abstract

Cup-and-cone fracture in single-phase ductile metals appears to originate at holes formed by drawing away of material from non-metallic inclusions, as suggested by Tipper. In copper, the holes expand under the triaxial stresses in the neck and coalesce in a macroscopic fissure; in α iron fine cracks are formed by the stress concentrated at the holes. In coarse-grained material shear cracks are formed on the surface of the neck.

Pure polycrystalline aluminium separates at the neck of a tensile specimen by slipping-off along a plane of shear. This is thought to be the usual mode of failure in materials in which work-hardening has been exhausted.

There has been some speculation recently on the mechanism of plastic fracture in metals (e.g. Petch 1956) but more metallographic observations of the initial stages of the process are needed. Since the fracture usually begins in the interior of a tensile specimen, the difficulty in such studies is to stop the crack before complete separation; in attempting to do this it is useful to remember the following argument put forward by Orowan (1955). The neck of a test piece is a small plastic element attached to a large spring consisting of the rest of the specimen and the testing machine, the elasticity of which is mainly determined by the characteristics of the machine. As the neck deforms it contracts, which (ignoring work-hardening) lowers the load required for further flow, and extends, which relaxes the spring-applied load. As long as the drop in applied load is greater than the decrease in flow load the test is stable, but when this condition no longer obtains the machine 'runs away'. Generally this point is probably related to the initiation of a crack, but not necessarily—a sufficiently 'soft' machine would run away as soon as a neck began to form, since a large extension results in a small drop in applied load. (This condition could be realized in practice by dead loading a non-work-hardening material.) A perfectly hard machine, on the other hand, should be capable of controlling the test throughout the spread of a fracture.

A manually operated testing device can be made to simulate a hard machine if, during the formation of a neck, the load is 'pulsed' by dropping it below the yield load, raising it until flow just takes place, and lowering it quickly. The experiments to be described were made using this method on a Hounsfield tensometer, which is well adapted for it.

† Communicated by the Author.

‡ Now at The Royal Institution, Albemarle Street, London, W.1.

Copper test pieces were machined from B.S. 1433 rod, which is manufactured from Tough Pitch High Conductivity copper of total purity 99·9%. The chief impurities in this material are bismuth (0·001–0·0025%) and lead (0·005%); metallographic examination revealed the presence of small non-metallic inclusions, possibly particles of refractory, aligned during rolling. Tests were made on the as-rolled metal and on specimens of various grain sizes produced by annealing.

The as-rolled material (which showed almost no uniform reduction of area) and annealed fine-grained metal, both of which had a grain size of about 0·05 mm. developed standard cup-and-cone fractures. A section through the neck of a specimen which had been strained so as to induce slow growth of the fracture is shown in fig. 1 (Pl. 111): there is a large central cavity surrounded by numerous smaller holes. These are found on closer examination to originate at inclusions (fig. 2, Pl. 111) either by drawing away of the metal or by fracture across the inclusion itself. The cavities are opened out by the triaxial stresses and strains accompanying formation of the neck, and eventually link up as in fig. 3 (Pl. 112) to form the large fissure which determines final rupture (fig. 4, Pl. 112). There seems to be no genuine cracking in the sense of parting of metal–metal interfaces.

The fracture surface of ductile metals tends to become more jagged and irregular with increase of grain size, though regions of inner and shear fracture can usually be distinguished. The reason for this behaviour was apparent on examining specimens of coarse-grained copper on which the test was stopped before separation; cracks could be seen on the surface of the neck. Sectioning of one such specimen proved that these can form before a large internal cavity, which therefore grows under the influence of the stress system of the external crack. Figure 5 (Pl. 112), for instance, is a photograph of a specimen (grain size 1 mm) having a large surface crack which has initiated at the minimum section and propagated along the surface at an angle of roughly 45°, which is typical of such cracks. The surface fracture grows into the metal, however, in the same way as the internal cavity grows outward, by the opening and linking up of inclusion holes. Figure 6 (Pl. 113) shows the internal and external fractures growing toward each other.

To examine more closely the formation and propagation of the surface cracks, a specimen with a grain size of about 1 mm was strained until a small crack appeared, after which the surface of the neck was ground and polished as smooth as possible without altering the natural contour. This test piece was again carefully strained in tension, when another crack appeared at the minimum section as soon as flow began (fig. 7, Pl. 113). Ahead of the cracks could be seen narrow zones of deformed metal along directions of shear on the surface, which the crack was clearly beginning to follow. The appearance is sketched in fig. 8 (Pl. 113), since the deformed zones, though easily recognized under suitable illumination, are difficult to photograph convincingly.

Similar tests were also made on specimens of ingot (Armco) iron (B.I.S.R.A. catalogue AD/AL) which contains these major impurities:

C	S	Ni	Cr
0·026%	0·035%	0·038	0·01

with traces of a number of others. Specimens were annealed in vacuo at 850°C and air cooled.

Control of the internal fracture in ferrous metals is considerably more difficult than in copper, but with care it is possible to arrest it before final separation. A section of a test piece containing a central fissure shows that fracture is initiated by the opening of cavities associated with inclusions as in copper, but ahead of these runs a system of fine non-crystallographic cracks through the metal itself. Figure 9 (Pl. 114) is a centre section of the neck illustrating the large cavities where the fracture presumably originated, and fig. 10 (Pl. 114) a section slightly off centre revealing the cracks. Closer examination shows that the cracks run from one inclusion site to another (fig. 11, Pl. 115) even though the inclusion cavities themselves have not grown appreciably.

The mechanisms of fracture in copper and iron containing non-metallic inclusions are, therefore, somewhat different. In fine-grained copper the internal rupture is a fairly simple process, that of expansion and coalescence of inclusion holes, as suggested by Tipper (1949) on the basis of some experiments on notched bars. Failure no doubt occurs when the holes attain a critical size which is related to the dispersion of the inclusions, and the growth of the holes depends on the transverse stresses in the neck. It may be possible to analyse an adequate model of such a process by the methods of macroscopic plasticity.

An abstract of the work of H. C. Rogers, in the U.S.A., has recently appeared (1958); he reports that in his coarse-grained copper specimens holes formed at grain boundaries. If these were inherently rigid enough to provide sites for microcracks (as envisaged by Petch) similar cavities should have been seen in the present study, but there were none. Perhaps in Rogers' material non-metallic inclusions were segregated at grain boundaries.

In iron it appears that inclusion cavities form and grow as in copper, but that at a critical size genuine cracks are nucleated, which then link up other inclusion sites. It seems reasonable to suppose that the cracks are initiated at points of high tensile stress, and that since they do not require additional strain they must propagate much more rapidly than holes can expand plastically†. Such fast cracks must surely influence the onset of cleavage fracture in low-temperature deformation of iron.

How does failure occur in a metal without inclusions? It was found that test pieces of high purity aluminium (> 99·9%) with a grain size of

† It was observed that there were not many large holes visible away from the main fracture, no doubt because only one or two holes of critical size are needed to initiate cracks.

about 2 mm separated by slipping-off on a plane at approximately 45° to the axis, as in fig. 12 (Pl. 116). At the beginning of this process it was noticeable that the contour of the neck, though very irregular, developed a marked discontinuity in slope where this plane intersected the surface, and some surface grains along this line subsequently tore apart.

This behaviour resembles that predicted by Onat and Prager (1954) and Prager (1956) for necking of an ideal plastic material in *plane* deformation. They show that if the stresses do not depart widely from a state of simple tension, a linear yield condition can be used to simplify the equations of flow, which lead to the discontinuous velocity field illustrated in fig. 13. Deformation occurs only in the shaded regions, while the other parts of the specimen move as rigid bodies. Instantaneous flow is confined to the planes of discontinuity AD, EF.

No doubt in the present experiments this theoretical flow pattern is modified by a number of factors:

(*a*) The departure from two-dimensional flow.

(*b*) Inhomogeneity of strain from grain to grain.

(*c*) Appreciable transverse stresses may have been present in the neck before the onset of the localized shear.

(*d*) The grips allowed relative lateral motion of the two parts of the specimen, so that deformation on a single plane (i.e. slipping-off) was possible. The neck might draw down to a chisel fracture in rigid grips.

Nevertheless, the essential condition for this kind of instability is probably the exhaustion of strain-hardening, so that the material is almost ideally plastic (though possibly some initial asymmetry in the neck is necessary). To be precise, it is initiated when the slope of the true stress–strain curve falls below a critical value; although this curve is difficult to determine in the later stages of necking, especially in coarse-grained specimens, it is known that hardening does decrease to zero during extensive deformation in torsion and compression tests. It is consistent with this criterion that fine-grained material (about 0·25 mm) drew down to a much narrower neck before slipping-off occurred, since the slope of the stress–strain curve at a given strain is a decreasing function of grain size.

It may be concluded that the usual mode of neck formation in which flow takes place thoughout the central region, the surface contour is smooth, and progressively greater hydrostatic tensions are developed in the interior, can only be maintained as long as the material strain hardens†. Cup-and-cone fracture must generally be initiated under these conditions

† Bridgman (1952) has described how, when the ductility of metals is increased by hydrostatic pressure, the shear component of cup-and-cone fracture increasingly predominates, until at very large deformations " only a single shearing plane survives, and the final failure is by slip on this single plane entirely across the section, rotational symmetry having entirely disappeared in the final act of fracture ".

because it begins in the centre of the neck where the transverse stresses are greatest; but holes can also grow by a localized shear like that depicted in fig. 13, as Orowan (1948) has pointed out. A specimen containing a hole, as in fig. 14 (*a*), will deform by slip along the planes AB, CD, since this requires the smallest tensile force. The hole will then enlarge parallel to the slip planes, as in fig. 14 (*b*) (or, if planes EB, CF, also operate, may

Fig. 13

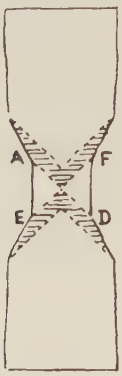

Flow pattern in neck of ideal plastic material in plane strain according to Onat and Prager. AD, EF are slip planes.

Fig. 14

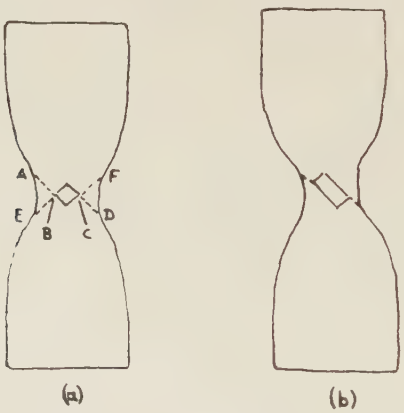

Growth of hole by shear (Orowan).

remain geometrically similar). Although the deformation envisaged by Orowan was also two-dimensional, the similarity between the process illustrated in fig. 14 and the observed behaviour of surface cracks in copper sketched in fig. 8 strongly suggests that the external fractures do propagate from existing holes in this way. Again, the process is only to be expected

when the material does not harden, which explains why these shear cracks are not observed except in coarse-grained metal; in fine-grained metal the cavities in the neck lead to cup-and-cone fracture during the period of strain-hardening.

Swift (1939) and Backofen *et al.* (1954) observed that rods of steel and copper subjected to plastic twisting greater than a certain critical value fractured in a subsequent tensile test on helical surfaces without necking. In this case the torsion presumably exhausted strain hardening so that in the tensile test localized zones of shear formed as soon as the yield stress was reached, leading to the growth of surface fractures as in figs. 8 and 14.

To sum up: there are two stages in the formation of a neck in a tensile test. During the first stage the material strain hardens; any holes present are enlarged by the hydrostatic tensions developed in the interior of the specimen and may lead to tensile fracture. When strain hardening is exhausted localized slip begins on planes of maximum shear stress, and holes may grow into shear fractures on these planes. If fracture does not supervene during either stage complete slipping-off finally ensues.

Acknowledgments

I wish to thank Professor A. H. Cottrell, Professor R. King, and Mrs. C. F. Tipper for discussions on this subject; Professor G. Wesley Austin and Dr. J. Nutting for allowing me to use the facilities of the Metallurgy Department, Cambridge; and the D.S.I.R. for financial support.

Note added in proof.—I have not considered here the formation of the shear cone in cup-and-cone fracture. Geometrically, this cannot be accomplished by slip on a single surface; it is also probably complicated by adiabatic heating of the material at the high strain rate prevailing during the final stages of separation.

References

Backofen, W. A., Shaler, A. J., and Hundy, B. B., 1954, *Trans. Amer. Soc. Metals*, **46**, 655.
Bridgman, P. W., 1952, *Large Plastic Flow and Fracture* (McGraw-Hill).
Onat, E., and Prager, W., 1954, *J. appl. Phys.*, **25**, 491.
Orowan, E., 1948–49, *Rep. Progr. Phys.*, **12**, 185; 1955, *J. appl. Phys.*, **26**, 900.
Petch, N. J., 1956, *Phil. Mag.*, **1**, 186.
Prager, W., 1956, *Rheology*, Vol. 1, ed. Eirich (New York: Academic Press).
Rogers, H. C., 1958, *J. Met.*, Sept. 1958, p. 589.
Swift, H. W., 1939, *J. Iron St. Inst.*, **140**, 181.
Tipper, C. F., 1948–49, *Metallurgia*, **39**, 133.

Examination of Fission Fragment Tracks with an Electron Microscope†

By E. C. H. Silk and R. S. Barnes
A.E.R.E., Harwell

[Received August 19, 1959]

Abstract

Thin sheets, removed by cleavage from the surface layers of mica exposed to fission fragments from uranium, have been examined in transmission in the electron microscope. Fission fragment tracks which are less than 300 Å in diameter and greater than four microns in length have been seen, superimposed upon a general background introduced by associated neutron bombardment. The nature of the tracks is discussed. The technique can be used to study radiation induced atomic displacements, and the nature and behaviour of the particles themselves, with higher resolution than has previously been possible.

Examination of thin sheets of crystals in transmission in an electron microscope can reveal the location of lattice defects. Defects produced by the passage of fission particles have been observed in mica in this way, and these observations will be described. Although fission fragment tracks have already been observed both in cloud chambers and in nuclear emulsions, neither of these methods is capable of the high resolution attainable with the electron microscope (~ 50 Å). Crystal defects in mica, such as dislocation lines, have also been studied but these will be discussed in a later publication.

Sheets of muscovite mica were alternated with sheets of aluminium upon which a layer of uranium, less than one micron thick, had been vacuum evaporated. These sandwiches were irradiated in BEPO for a few minutes. Then after removal of the coated aluminium sheets, the surface layers of the mica which had been in contact with the uranium were removed by cleavage. These were placed between two strips of adhesive tape, which were subsequently pulled apart to cleave the mica. The surface layers were repeatedly cleaved in this way until sufficiently thin to transmit electrons in the electron microscope. By this method thin sheets of mica from the surface, or various depths beneath the surface, could be selected. These sheets of mica, up to 0·01 cm in size, were recovered by placing the tape in trichloroethylene, which dissolved the adhesive, and filtering the solution through an electron microscope grid.

The thin mica sheets were examined in a Siemens microscope operating at 100 kv. Tracks of the fission fragments which escaped from the uranium during the neutron bombardment could be seen in those pieces

† Communicated by the Authors.

sufficiently thin for good electron transmission (probably less than 1000 Å thick). Figures 1, 2 and 3† are photographs showing these dark tracks which are randomly arrayed and oriented about the sheet. The tracks are generally straight, less than 300 Å diameter, and range from those which pass normally through the sheet and appear as dark dots, to those travelling almost in the plane of the thin sheet and are greater than four microns long. The number of long tracks is greatest in the surface layers, but even here the number of full range tracks would only represent about 1/100 of the total, due to the extreme thinness of the mica sheet.

The numbers of tracks shown in figs. 1, 2 and 3 are roughly proportional to the exposure times in BEPO and the numbers of tracks estimated from each are respectively 2 ($1{\cdot}5\times10^6$), $1{\cdot}1\times10^6$ and $0{\cdot}8\times10^6\,\mathrm{cm^{-2}\,sec^{-1}}$. Since there was $1{\cdot}7\times10^{-4}\,\mathrm{g\,cm^{-2}}$ of natural uranium deposited upon the aluminium foil in each case except the first, where twice this amount was deposited, and the thermal neutron flux in BEPO was $1{\cdot}2\times10^{12}\,\mathrm{cm^{-2}\,sec^{-1}}$, the number of fission events in the uranium is calculated to be $2{\cdot}1\times10^6\,\mathrm{cm^{-2}\,sec^{-1}}$, but twice this in the first. As the uranium thickness is less than one micron and the range of the fission fragments in uranium is about five microns, less than 1/5 of them will come to rest in the uranium. Because usually two fragments result from each fission event and these are ejected from both sides of the uranium layer, the number of fragments crossing the mica surface should be about $1{\cdot}7\times10^6\,\mathrm{cm^{-2}\,sec^{-1}}$; in sufficiently good agreement with the measured values that it can be assumed that each fission particle produces an observable track along most of its length.

Sheets of mica placed in BEPO without the layer of uranium have shown no similar effects even when irradiated for a dose of $7\times10^{17}\,\mathrm{cm^{-2}}$ (i.e. about 1000 times the neutron dose given in the above experiments). The neutron irradiation does, however, produce a change in the background appearance of the mica (the photographs appear mottled) suggesting the existence of a large number of small unresolved dark spots. The photographs containing fission fragment tracks also show this effect to a lesser degree, whereas it is quite absent from photographs of mica which has not been irradiated. This background is probably caused by the displacements produced by the neutrons themselves, which should consist of small locally damaged regions well spaced along the path of a fast neutron.

Some tracks show a waviness on a fine scale, as seen in fig. 2. In fig. 4 in particular some tracks show ends which are more intensely darkened than the rest of the tracks. Both figs. 2 and 4 show tracks which are dashed along their length.

The initial energy of a fission fragment, which may be any element in the range of atomic weight from 72 to 161 with a charge of about +20e, is about 100 MeV. Thus its initial velocity will be about $10^9\,\mathrm{cm\,sec^{-1}}$, and it should lose most of its energy by exciting the electrons of the atoms in mica until near the end of its range (Kinchin and Pease 1955).

† All figures are as plates.

The fission fragment will also make a Rutherford collision with a nucleus about every hundredth atom along its path, and the energy transferred to the struck atom will range from ~ 100 ev to about half the energy of the fragment itself (Kinchin and Pease 1955). In the more energetic collisions the struck nucleus should itself produce a track. Collisions ejecting an atom of the mica a distance greater than a few hundred Ångströms are rare. Such an event is shown in fig. 4. Here, before the collision at B the fission fragment track (AB) consisted of a series of short rather irregular dashes, spaced about 500 Å apart. These dashes may well represent low energy atoms ejected by Rutherford collisions. After the collision the track (BC) is deflected through a few degrees and appears continuous, possibly because the energy of the fission fragment became too low for further Rutherford collisions, the collisions becoming of the hard-sphere type.

The intermittent nature of some of the tracks suggests that the darkening is produced by groups of displaced atoms which would occur only at intervals along the track and not by ionization which would result in continuous damage.

During observation in the microscope the sheets became a little heated and extinction contours swept the field of view. The tracks gave best contrast when they were near to extinction contours, as did dislocation lines. The contrast effects were not similar to those at dislocations, being symmetrical and consistent with a path of cylindrical damage. After a few seconds with increased beam intensity the tracks began to disappear due to the heating of the sheets. Figure 5 shows a sequence of photographs (*a*), (*b*) and (*c*), taken from the same area, where the tracks broke up and eventually annealed away. The background appearance of the mica after annealing became even less clear than before.

This electron microscope technique of observing fission tracks should help our understanding of the atomic displacements produced in solids by fast moving atomic particles, as well as give information on the rate of energy loss, nature and behaviour of the particles themselves.

Acknowledgments

We should like to thank Mr. B. J. Sheldon who performed most of the experimental work, Mr. C. J. Jackson and Mrs. B. C. Jenkins who operated the electron microscope and Mr. M. W. Thompson for useful discussions.

Reference

Kinchin, G. H., and Pease, R. S. 1955, *Rep. Progr. Phys.*, **18**, 1.

The Apparent Sidereal Daily Variation of Cosmic Ray Intensity During the Recent Sunspot Minimum†

By S. P. Baliga and T. Thambyahpillai‡
Physical Laboratories, University of Ceylon, Colombo

[Received April 24, 1959]

Abstract

The unusually large changes of phase which occurred in the cosmic ray solar daily variation during the year 1954 have been found by Conforto and Simpson (1957) to simulate strong sidereal daily variations. These authors have suggested that their results represent a genuine sidereal effect which is observable only during periods of extremely low solar activity, as in 1954. A systematic search for sidereal effects during this year has been made using the results from the Carnegie Institution stations as well as Colombo, Hobart and Tokyo. Although no significant sidereal effects were seen at Colombo, the other data show substantial sidereal daily variations with a remarkable consistency in phase. The time of maximum at the equator was 19 hr L.Sid.T. while at higher latitudes it was about 22 hr L.Sid.T. The character of the solar diurnal variations and the relations between their seasonal changes and sidereal daily variations are discussed and it is concluded that at least a part of the observed sidereal effects were spurious.

§ 1. Introduction

It is well known that the solar daily variation of cosmic ray intensity (primary energies below about 5×10^{10} ev) exhibits rather small changes of amplitude and phase during the course of the year, with the result that the data show substantial diurnal variations following solar time even when averaged over annual groups, the purpose of the averaging procedure being to smooth out the seasonal changes and to eliminate the effects of superposed sidereal daily variations. The detection of a true sidereal effect, on the other hand, proved to be a difficult problem, because of the small sidereal amplitudes observed and the uncertainties introduced by the seasonal variations of the solar effect which could simulate sidereal daily variations.

The period of a few years near the sunspot minimum of 1954, however, was exceptional in that large changes in the phase of the solar daily variation occurred during the year. Steinmaurer and Gheri (1955), Miyazaki (1955), Possener and van Heerden (1956) and Sekido have observed these changes in ionization chamber and counter telescope data. Conforto and Simpson (1957) have examined the results from a number of widely separated stations operating neutron monitors, ion chambers or counter arrays and they point out that during 1954 the monthly means of the solar diurnal

† Communicated by the Authors.
‡ Now at the Imperial College of Science and Technology, London.

variations advance progressively in phase in such a manner as to maintain the time of maximum roughly constant, when reckoned in sidereal hours. Thus, the sidereal daily variations during this year, whether real or apparent, were substantially larger than during other years and should have reflected changes in the primary cosmic ray intensity because they were also observed in the neutron flux which is not influenced by atmospheric temperature variations. They have also drawn attention to the extremely low level of solar activity during 1954, which would make conditions in the solar system favourable for the observation of stellar time variations in the low energy band of the primary spectrum. At other times, the scattering and modulating actions of magnetic and electric fields carried by plasma clouds thrown out from the sun would obscure any anisotropic distributions in the radiation arriving from outside the solar system. However, the question as to whether the observed sidereal effects were genuine or spurious has not been settled with any degree of certainty and additional results, which are of relevance, are presented in this paper.

§ 2. The Experimental Arrangement used at Colombo

Two counter arrays pointing in the vertical direction were used to make continuous measurements of the cosmic ray intensity at Colombo (Ceylon: geog. lat. 07° N; sea-level). One telescope consisted of three trays of G.M. counters, each of sensitive area 60×20 cm^2 placed one above the other, the separation between extreme trays being 13 cm. The only absorber in this case was the roof with an effective absorption of 2 g per cm^2. The other recorder had a sensitive area of 40×30 cm^2 with a separation between extreme trays of 45 cm and carried a lead absorber of thickness 15 cm between the trays. These recorders will be referred to as measuring the total and hard components respectively of the charged particle radiation. The telescopes were arranged with the longer edge of the former and the shorter edge of the latter along the east/west line in order to examine the smoothing effects of increasing the angles of acceptance in the east/west plane. The three-fold coincidence rates of the total and hard component recorders were about 25 000 and 8500 per hour respectively. The data have been corrected for the barometer effect using total barometer coefficients of $-3{\cdot}2$ and $-2{\cdot}4\%$ per cm Hg for the total and hard components respectively, as determined by the correlation of day to day changes of cosmic ray intensity and station pressure.

§ 3. The Apparent Sidereal Daily Variation of 1954

The observations used in the present analysis were made with counter telescopes and ionization chambers and have been corrected only for the effects of atmospheric pressure changes. The measured intensities will therefore include solar daily variations reflecting the systematic alterations in the temperature structure of the atmosphere during the course of the day. According to recent investigations (Dorman 1957) this solar time variation of atmospheric origin has an amplitude of over $0{\cdot}1\%$

when averaged over a year, the maximum of the intensity occurring in the early hours of the morning. Moreover, in temperate latitudes, substantial changes of amplitude appear to take place in this part of the daily variation from one season to another, while small changes of phase too can occur. Consequently, arranging the data for a year according to sidereal time cannot effectively eliminate the solar time changes and the resulting sidereal daily variation will be contaminated by spurious contributions from the solar component.

Of the methods developed to analyse ion-chamber data for sidereal daily variations, the one adopted by Elliot and Dolbear (1951) appears to have led to consistent results. This method of approach is designed to effect an unambiguous separation of the sidereal and solar components of the daily variation by making the solar part maintain a constant amplitude and phase throughout the year.

Now the seasonal changes in amplitude and phase of the daily variations, caused by meteorological factors should be six months out of phase at two stations located at the same latitude in the northern and southern hemispheres respectively. Averaging the data from two stations such as Cheltenham (39° N; s.l.) and Christchurch (43° S; s.l.) should therefore markedly reduce the annual variation, which would be completely eliminated if the local meteorological conditions at the two places were identical. Again, at equatorial stations like Colombo and Huancayo (12° S; 3350 m alt.), the variation, over the months, of the atmospheric part of the solar daily variation is likely to be small. It appears, then, that the seasonal variability and therefore the spurious sidereal daily variations due to atmospheric influences can, to a large extent, be eliminated.

The question now arises as to whether the atmospheric component was the only solar daily variation observable during 1954. Whereas, radiosonde measurements of atmospheric temperature distributions assign a phase around 02 hr to the atmospheric diurnal variation, the annual means of the solar diurnal variations observed during the year 1954 are later in phase by about 3 to 6 hours. Barring the possibility of serious errors in the atmospheric soundings, this phase discrepancy can be explained only if the primary radiation entering the atmosphere exhibited a solar daily variation, and it is, at present, an open question as to whether this extra-atmospheric component remained substantially constant throughout 1954. It is worthy of note that variations of amplitude and phase occurring in this part of solar daily variation can simulate sidereal daily variations which will not, in general, be eliminated by the above procedure.

At Colombo, the annual means of the solar diurnal variations in both total and hard components had nearly the same amplitude of 0·20% and phase 07 hr local time. The seasonal departures of the 24 hr components of the daily variation from the annual mean can be seen from fig. 1, which is a harmonic dial indicating solar time. The data were divided into three-monthly groups called Spring≡February, March and April; Summer≡ May, June and July; and so on, and the solar first harmonics computed

for each group. The annual mean solar vector was then subtracted from the seasonal ones, and the end-points of the difference vectors so obtained are plotted in the diagram.

Fig. 1

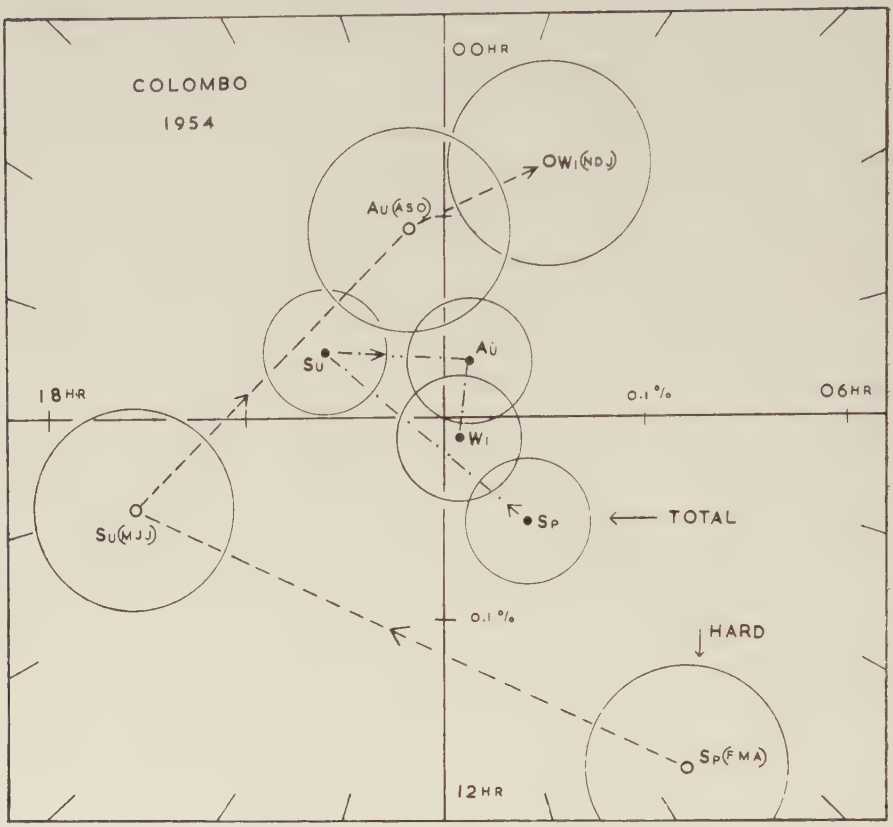

Solar time dial showing the tips of the seasonal (difference) vectors at Colombo, with standard deviation circles. The results for 1954 of the wide-angle total intensity recorder and the narrow-angle hard component recorder are plotted.

Now, a constant sidereal diurnal variation superposed on a solar diurnal variation of fixed amplitude and phase should cause the end-points to be arranged in a regular anti-clockwise progression on the circumference of a circle, the spacing of the points being uniform. It is evident from the diagram that, on the contrary, the hard component shows a clockwise arrangement while a similar but much less marked trend is seen in the total intensity. Thus, a direct setting of the data to sidereal time leads to insignificant daily variations.

The results of a similar treatment of the ion-chamber data from Huancayo and Cheltenham/Christchurch (Lange and Forbush 1957) are plotted in fig. 2. The distribution of the difference vectors found by subtracting the respective annual mean solar vectors from the bi monthly solar

vectors can be seen from the solar time dials on the left. Although a sidereal daily variation should cause the amplitudes to be equal and the phases to advance in 4 hr steps in a regular anti-clockwise progression, the vectors in the diagram do not show any such regularity. However, it is possible that small residual changes of the solar component of atmospheric origin can produce distortions; correcting the data, assuming that these residual variations are represented by the seasonal changes of 1953 and 1955, appears to produce some improvement, as will be seen from the harmonic dials on the right. The sidereal diurnal variations calculated from the Carnegie Institution data are given in the table.

Fig. 2

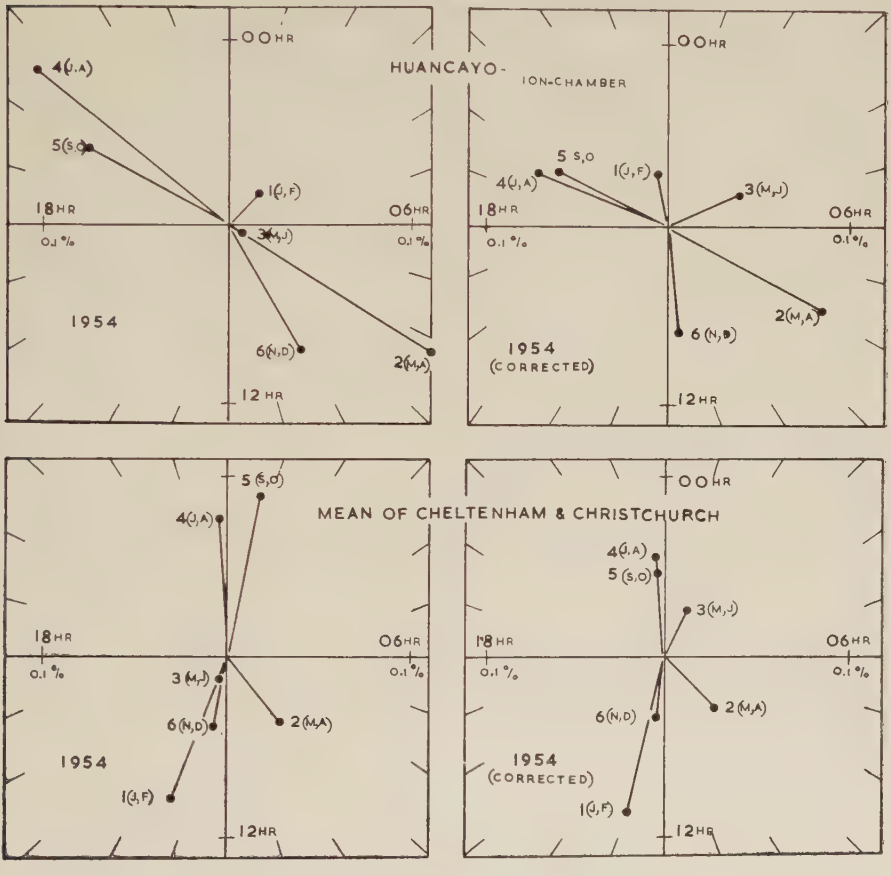

The harmonic dials on the left give the bi-monthly (difference) vectors for 1954 at Huancayo and Cheltenham/Christchurch. The dials on the right show the same vectors after correction (vide text).

Observations with an ionization chamber at Tokyo (36° N; s.l.) by Miyazaki (1955) and with a cubical meson telescope at Hobart (43° S; s.l.) were also available for analysis, but, owing to the differences in the directional sensitivities of the detecting equipment, there is some doubt

as to the effectiveness with which the seasonal variability can be eliminated by averaging these data. Also the Thompson method of sidereal analysis is not applicable here, as it allows only for amplitude changes in the solar component. The presence of a solar variation of primary origin, however, should cause changes in both amplitude and phase of the total solar daily variation, even if the meteorologically induced part retained a constant phase while changing its amplitude.

We have, therefore, fitted the experimental results to the following equation:

$$100(\Delta I/I) = A_{\text{prim}} \cos(2\pi Nt - \phi_{\text{prim}}) + A_{\text{sid}} \cos\{2\pi(N+t)1 - \phi_{\text{sid}}\} + \{\bar{A}_{\text{atm}} + A_{\text{seas}} \cos(2\pi t - \phi_{\text{seas}})\}\cos(2\pi Nt - \phi_{\text{atm}}).$$

The annual means of the solar and sidereal daily variations observed during 1954 at a number of stations. The counter telescope and ionization chamber data have been corrected only for barometric changes, with the exception of the Freiburg data which have been corrected, in addition, for atmospheric temperature effects

Station	Instrument	Solar diurnal variation		Sidereal diurnal variation		Ratio of sidereal to solar amplitudes
		Amplitude (%)	Phase in hours local solar time	Amplitude (%)	Phase in hours local sidereal time	
Cheltenham/ Christchurch	I.C.	0·06	07·30	0·05	22·30	0·8
Climax	N.M.	—	16·00	—	21·30	2·0
Colombo	C.T.	0·20	07·00	Not significant	—	0·1
Freiburg	I.C.	—	08·50	—	22·20	1·0
Hobart	C.T.	0·17	06·50	0·06	23·20	0·3
Huancayo	N.M.	—	—	—	19·20	9·0
Huancayo	I.C.	0·10	05·30	0·06	19·00	0·6
Rome	C.T.	—	05·00	—	20·50	1·6
Tokyo	I.C.	0·10	05·30	0·06	21·00	0·6

In the equation, the unit of measurement of the time t is one year and N is the number of solar days per year. The first two terms A_{prim}, ϕ_{prim} and A_{sid}, ϕ_{sid} denote the solar and sidereal diurnal variations respectively of the radiation entering the atmosphere, whilst the last term represents the solar component of fixed phase ϕ_{atm} and varying amplitude, due to atmospheric temperature changes. It is reasonable to assume that A_{sid}, ϕ_{sid} remain constant throughout the year, while radio-sonde measurements indicate that ϕ_{atm} can, as a first approximation, be taken to have a fixed value.

The amplitude modulated atmospheric term with a period of one solar day (frequency N) can be expressed in terms of an unmodulated carrier of the same period and two side-bands with respective periods of one sidereal day (frequency $N+1$) and one† anti-sidereal day (frequency $N-1$) (Farley and Storey 1954). Proceeding on the assumption that the extra-atmospheric solar daily variation A_{prim}, ϕ_{prim} remains constant, the following total daily variations can be separated out.

(i) The Solar Component $\equiv A_{\text{prim}} \cos(2\pi Nt - \phi_{\text{prim}}) + A_{\text{atm}} \cos(2\pi Nt - \phi_{\text{atm}})$;

(ii) The Sidereal Component $\equiv A_{\text{sid}} \cos\{2\pi(N+1)t - \phi_{\text{sid}}\} + \frac{1}{2}A_{\text{seas}} \cos\{2\pi(N+1)t - (\phi_{\text{atm}} + \phi_{\text{seas}})\}$;

(iii) The Anti-sidereal Component $\equiv \frac{1}{2}A_{\text{seas}} \cos\{2\pi(N-1)t - (\phi_{\text{atm}} - \phi_{\text{seas}})\}$.

Using the data for one complete year, these three component daily variations can be determined and the anti-sidereal component be used to eliminate the spurious sidereal daily variation introduced by atmospheric variations. If, however, A_{prim}, ϕ_{prim} are not constant throughout the year, the varying solar daily variation will, in general, contribute additional terms to the sidereal and anti-sidereal daily variations.

The solar and sidereal components of the daily variation deduced from the experimental data are given in the table. The anti-sidereal component at Tokyo had an amplitude of 0·02% and phase 01–30 hr, while the corresponding values for Hobart were 0·08% and 01–40 hr.

Now, consider the first harmonic vectors of the solar daily variation of bi-monthly groups of data, plotted on a solar time dial. Because of the presence of variations of periodicity differing slightly from 24 solar hours, each bi-monthly vector can be imagined to be composed of three vectors, of which the solar part is fixed in magnitude and direction while the sidereal one rotates in the anti-clockwise sense and the anti-sidereal one in a clockwise sense at the rate of two hours per month. As a result, the tips of the six bi-monthly vectors should be arranged on an ellipse.

The ellipses of best fit to the Tokyo and Hobart results are shown in fig. 3, the expected positions of the tips of the bi-monthly vectors being indicated by open circles. The tips of the solar first harmonics for the corresponding two month periods are shown for comparison as full circles on the same diagram. The rather poor fit of the Hobart points to the ellipse indicates irregular changes of the primary solar daily variation.

Now we consider the anti-sidereal components in the fitted equation. It is known that aerological measurements used with the Dorman scheme of atmospheric corrections yield a value of 02 hr for the phase ϕ_{atm}. Moreover, the largest amplitudes of the atmospheric daily variations should

† Anti-sidereal time is shown by a clock which is in step with a solar time clock at the autumnal equinox but loses on the solar clock at the rate of two hours per month.

occur around June in the northern hemisphere and near December in the southern hemisphere. Hence the phases ($\phi_{atm} - \phi_{seas}$) of the anti-sidereal components should be 08 hr at Tokyo and 20 hr at Hobart. The large discrepancies between observation and the expected results give clear indication that these anti-sidereal components are not of purely atmospheric origin.

Even if we concede that the above value for the phase ϕ_{atm} is in serious error owing to insolation effects on the temperature elements, anti-sidereal components of entirely atmospheric origin should have about the same amplitudes at Tokyo and Hobart, but the phases should be exactly opposite to each other. The absence of these characteristics shows that the solar daily variations belonging to the primary radiation were not constant throughout 1954.

Fig. 3

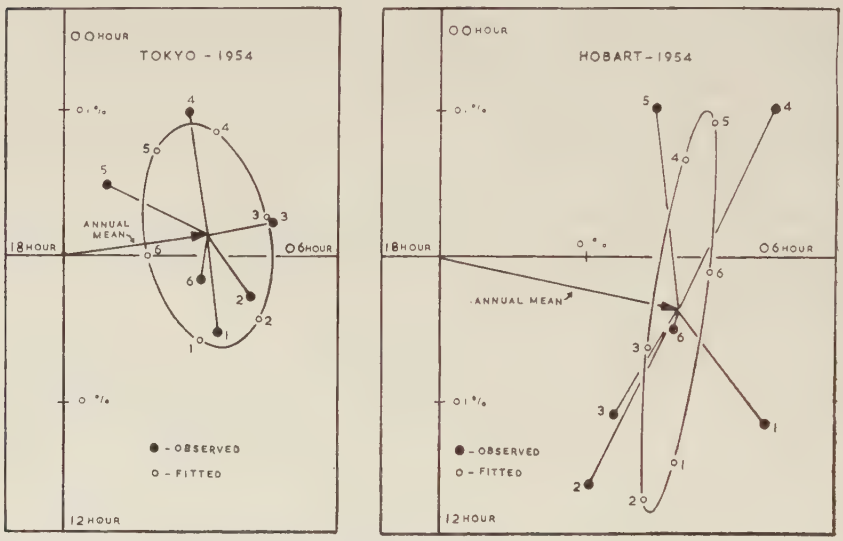

Solar time dials showing the mean solar vectors for 1954 at Tokyo and Hobart, together with the ellipses of *best* fit to the end-points (full circles) of the bi-monthly vectors. The expected positions of the end-points, are plotted as open circles.

Under the circumstances, therefore, there is no justification for the use of the observed anti-sidereal components to apply corrections for the spurious sidereal daily variations produced by seasonal changes in atmospheric conditions.

§ 4. Discussion

We have summarized the available data on the annual averages of the solar and sidereal diurnal variations of 1954 in the table. Whereas percentage amplitudes of the 24 hr sine waves have been found by Fourier methods here, Conforto and Simpson (loc. cit.) have adopted a different

definition for the amplitudes of their 24 hr vectors. In order to effect an inter-comparison between the two sets of results, we have included ratios of sidereal to solar diurnal amplitudes in the table. The phases given by the two methods, however, appear to show good agreement. The sidereal phases given by Conforto and Simpson have been changed by 12 hr so as to make them conform to the conventional definition of sidereal time.

It will be seen from the table that, in spite of the rather small sidereal amplitudes of 0·06% in the ionizing radiation and the presence of spurious atmospheric contributions of magnitudes unknown at present in some of the data, there is remarkably good agreement between the phases at middle latitude stations, these being grouped around 22 hr L.Sid.T. The maximum intensity at Huancayo, which is close to the geomagnetic equator, occurred at about 19 hr, while no significant variations were observed at Colombo.

The question naturally arises as to whether the absence of significant stellar time changes at Colombo was a characteristic of the primary radiation or was due to atmospheric masking of genuine sidereal effects. If the former is true, this absence and the small value of less than 0·1 for the ratio of sidereal to solar diurnal amplitudes should play an important role in the interpretation of the observed sidereal daily variations. Now, one can envisage a situation where the seasonal changes of the atmospheric daily variation generate a spurious sidereal variation of phase opposite to that in the primary radiation, thereby causing a marked reduction in the observed sidereal amplitude. However, as the necessary aerological information for Colomob is not available, we have to rely, for purposes of resolving this question, on the observed recurrence from year to year of the general pattern of behaviour of meteorological variables. The neutron data from Huancayo show that the sidereal variation of the more energetic primaries was much smaller in 1955 than in 1954, and therefore, any recurring spurious effects neutralizing the primary variation during 1954 should be evident in the Colombo data for 1955. The data for 1955–1956, however, again do not show significant sidereal changes and, as was implied in the method of analysis, atmospheric obscuration appears to be ruled out.

Moreover, reasoning of this kind indicates that the major part of the seasonal changes at Colombo (fig. 1) which simulated a strong anti-sidereal variation in the hard component was caused by extra-atmospheric factors.

The solar diurnal variations observed during this year should find an adequate explanation in any theory designed to account for the sidereal variations and these will be considered next. It will be seen from the table that, with the exception of the temperature corrected Freiburg data, the solar phases of the ionizing radiation fall within a narrow band between 05–00 hr and 07–30 hr. We have already noted the implication of the substantial differences between these values and the phase of the atmospheric daily variation, as estimated from aerological data. It may

be suggested that, alternatively, this discrepancy can be explained in terms of instrumental errors in the temperature measurements, resulting from the heating of the thermometric elements by solar radiation during day-light hours; that is to imply that the effective maximum of atmospheric temperature taken over the entire atmosphere occurs actually near sunset rather than at the indicated 14 hr. In that case, it would be impossible to explain amplitudes as large as 0·20% at Colombo and 0·17% at Hobart as atmospheric effects, since, for the same reasons, the true diurnal amplitudes of atmospheric temperature should be much smaller than the observed ones. Besides, the east/west directional measurements made at London by Elliot and Rothwell (1956) show conclusively that during a period of one year which includes eight months of 1954, solar diurnal variations of origin, other than atmospheric, were present in the observations.

Thus, there can be little doubt that significant solar diurnal variations existed in the primary cosmic radiation incident at Colombo, Hobart and London, and, if the accuracy of Dorman's temperature corrections is assumed, at other stations as well. Also, there is evidence to show that these solar diurnal variations of primary origin underwent seasonal changes during 1954. As seen earlier, such a conclusion is unavoidable while considering the anti-sidereal components at Tokyo and Hobart, and it is confirmed by the seasonal changes of the hard component at Colombo. This reasoning is independent of the existence or otherwise of genuine sidereal effects.

Now, if as indicated above, seasonal fluctuations occurred in the solar daily variations of the primaries, it is hardly conceivable that spurious sidereal variations were not generated in the process. Thus, irrespective of the type of mechanism responsible for the solar effects, it should be conceded that at least a part of the observed sidereal variations were spurious. In fact, the seasonal variations of 1954 could have arisen from the same mechanism as is responsible for the world-wide secular changes of phase reported by Thambyahpillai and Elliot (1953) in which case the entirety of the sidereal effects may have been spurious.

It is worthy of note that, contrary to the suggestion made by Conforto and Simpson, the solar time of maximum given by the ion-chamber at Huancayo is several hours earlier during the sunspot minimum of 1954 than that of 1944, and consequently, there is no evidence of a break-down of the 22 year cycle of phase changes at equatorial stations.

An extremely interesting feature of the equatorial data will now be discussed briefly. It was seen that the intensity variations at Colombo were almost entirely solar diurnal in character, with no appreciable sidereal component but the neutron flux at Huancayo showed just the reverse characteristics. The ionization chamber at Huancayo, however, registered significant amplitudes of both types of diurnal variation. The earlier discussion showed that these remarkable characteristics reflected the properties of the primary radiation and were not caused by atmospheric influences. As both stations are close to the geomagnetic equator, it

follows that the diurnal variation characteristics of the primary radiation with energies exceeding about 15×10^9 ev were radically different for the three recorders.

In explaining these differences, the following factors have to be borne in mind: (i) While Colombo is situated near sea-level, Huancayo is at an altitude of 3350 m and an extrapolation for the multiplicity function from the latitude effect (Dorman 1957) indicates that the mean energy of the primaries to which the instruments responded should have been the highest for those at Colombo and the lowest for the neutron monitor at Huancayo, with an intermediate value for the ion-chamber. (ii) The directional sensitivities of the three recorders were widely different, and (iii) Colombo is 7° due north and Huancayo 12° due south of the geographical equator, and thus, the recorders at the two stations would have scanned two different strips on the celestial sphere.

The fundamental differences in the properties of the diurnal variations noted above are of exceptional importance in deciding whether the solar diurnal variations represent anisotropic distributions existing outside the earth's magnetic field or, as suggested by Elliot and Rothwell (1956), are produced by modulation within the region occupied by the earth's magnetic field. But consider this difficulty. As pointed out by Elliot (1952), it is certainly true that, during an earlier epoch, a systematic diminution of the solar diurnal amplitude occurred from the equator to the poles. During 1954, however, the solar diurnal variations at the equator do not show well-defined characteristics. In view of this, it is extremely difficult to estimate the contribution of the daily variation measured by the east recorder at London, made by particles which enter the earth's magnetic field along trajectories making small angles with the equatorial plane and which are so deflected as to arrive from easterly directions at London. Yet, this contribution played a vital role in the discussion given by Elliot and Rothwell on the origin of the solar daily variations, because their measurements were made during 1954 to 1955. Moreover, the solar diurnal amplitudes at Godhavn showed substantial increases during the period 1948–1950, and were about the same magnitude as at lower latitudes. Thus, the same pattern of latitude variation is not maintained throughout different cycles of solar activity. It appears, then, that a further examination of this question in the light of these results is necessary.

In conclusion, it appears that at least a part, if not the entirety of the sidereal effects of 1954 were spurious. There is little doubt, however, that the complex phenomena described here cannot find adequate explanation in a simplified picture suggesting the cessation of solar modulation processes during periods of very low solar activity which, in turn, permits the observation of anisotropies existing outside the solar system.

Acknowledgments

The authors wish to thank Professor A. W. Mailvaganam for the facilities provided for making measurements at Colombo. The whole-hearted

cooperation of Mr. S. D. Samuel in the construction and maintenance of the recording equipment is gratefully acknowledged. The staff of the Faculty of Engineering have assisted us by loaning computing machines. The kind courtesy of Miss I. Lange and Dr. S. E. Forbush in sending us a copy of their recent publication is deeply appreciated.

References

Conforto, A. M., and Simpson, J. A., 1957, *Nuovo Cim.*, **5,** 1052.
Dorman, L. I., 1957, *Cosmic Ray Variations* (Moscow: State Publishing House).
Elliot, H., 1952, *Progress in Cosmic Ray Physics,* Vol. I (Amsterdam); 1957, CSAGI guide.
Elliot, H., and Dolbear, D. W. N., 1951, *J. atmos. terr. Phys.*, **1,** 205.
Elliot, H., and Rothwell, P., 1956, *Phil. Mag.*, **1,** 669.
Farley, F. J. M., and Storey, J. R., 1954, *Proc. phys. Soc. Lond.* A, **67,** 996.
Lange, I., and Forbush, S. E., 1957, Carnegie Inst. of Washington Publ. 175, Vol. XX.
Miyazaki, Y., 1955, *J. sci. Res. Inst., Tokyo,* **49,** 267.
Possener, M., and van Heerden, I. J., 1956, *Phil. Mag.*, **1,** 253.
Steinmaurer, R., and Gheri, H., 1955, *Naturwissenschaften,* **42,** 10, 204.
Thambyahpillai, T., and Elliot, H., 1953, *Nature, Lond.*, **171,** 918.

CORRESPONDENCE

The Generation of Point Defects by Deformation and Fatigue in Alkali Halides

By R. W. Davidge, C. E. Silverstone and P. L. Pratt
Department of Physical Metallurgy, University of Birmingham

[Received April 29, 1959]

In a recent note Taylor and Pratt (1958) have shown how point defects generated by the intersection of arrays of dislocations in ionic crystals can account for transient increases in the ionic conductivity. This experimental evidence supported the earlier interpretation by Seitz (1952) of conductivity enhancements, rather than the alternative interpretation by Fischbach and Nowick (1958) in terms of the dispersion of finely precipitated impurities. Further evidence in support of the dislocation generation of point defects comes from the density changes measured by Vaughan *et al.* (1958) in deformed KCl crystals. From a consideration of the mechanisms by which individual dislocation intersections can give point defects, Cottrell (1957) has suggested that jogs on screw dislocations are forced to create vacancies particularly during the unloading stage of deformation, and thus he suggests that cyclic loading may well produce more vacancies than unidirectional loading. The purpose of this note is to show that density changes comparable to those in KCl are found in NaCl crystals deformed normally in compression, and that strikingly larger density changes are produced by fatigue in compression.

Specimens typically $0{\cdot}8\,\text{cm} \times 0{\cdot}4\,\text{cm} \times 0{\cdot}4\,\text{cm}$ were cleaved from a melt grown single crystal, annealed at 650°C, and furnace cooled. The crystals were fatigued in compression using an Amsler Vibrophore direct stress machine, operated at 100 c/s, very kindly put at our disposal by Dr. T. Broom. The required mean stress was applied to the specimens and the stress was continually adjusted to compensate for the small amount of creep which occurred. After two minutes, when the creep rate became negligible, cycling was commenced and continued for 2×10^5 cycles. Small adjustments were required to keep the stress at a constant level during the initial stages of the fatigue, but the final compressive strains were not significantly greater than those found in single loadings to the mean stress. Density measurements were obtained by suspending crystals, cleaved out of the centres of the test specimens, in a linear thermal gradient established in ethylene dibromide. The method is accurate to a density change of $\pm 2 \times 10^{-6}\,\text{g/cm}^3$. The results in fig. 1 show that compressive fatigue is more effective by about an order of magnitude in producing vacancies than is simple compression. A linear decrease in

density starts at about 4·5% compression in the simply deformed crystals, with a slope equivalent to $2{\cdot}6 \times 10^{17}$ vacancies per cm^3 per % strain (assuming that all density changes are due to vacancies). This result may be compared with the density changes in KCl, investigated by Vaughan *et al.* (1958), who found that density decreases started above 11% strain with vacancies being produced at the rate of 3×10^{17} per cm^3 per % strain. In the fatigued crystals, density changes commence after only 2% strain, with a rate of vacancy production similar to that in normal compression. Above about 7% strain in fatigue the density change begins to approach a saturation value.

Fig. 1

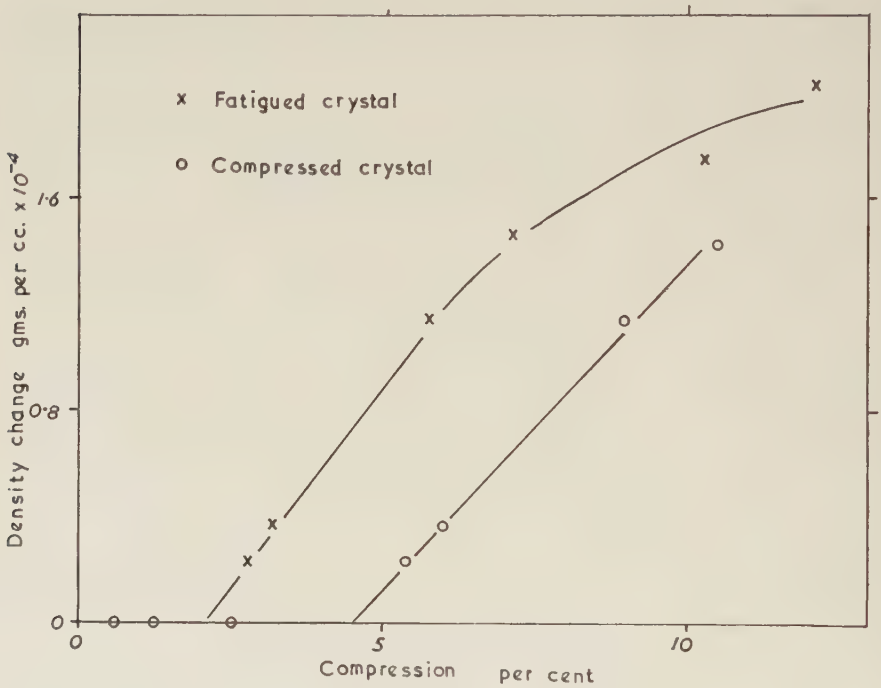

The change in density of fatigued and simply deformed NaCl as a function of compressive strain.

To confirm that the changes in density were due to the production of vacancies and to see the distribution of these vacancies, crystals were irradiated with filtered 50 kv x-rays to produce colour centres. After optical bleaching, crystals deformed in simple compression showed a very faint unresolved blue coloration, whereas fatigued crystals showed a series of distinct blue striations parallel to certain of the active slip planes (fig. 2, Pl. 120). By comparing the distribution of these striations with the stress-birefringence pattern it was clear that only a small proportion of the active slip planes were strongly coloured. The coloration is similar to

that observed by other workers in highly stressed rock-salt (for a review see Przibram 1956).

These measurements help to confirm our belief that plastic deformation leads to the production of vacancies by the intersection of dislocations, and it is of interest to note that this is not in fact in contradiction with the γ-ray coloration results of Nowick (1958). He admits the possibility of the concept of the generation of vacancies for a crystal deformed by 8·5%, but not for one deformed by 4%, whereas our measurements show that vacancies begin to be generated in NaCl only after about 4·5% strain. The enhanced generation of vacancies in fatigue agrees well with Cottrell's suggestion of the importance of the unloading part of the cycle, and offers strong support for the ideas put forward by Broom *et al.* (1955), Broom and Ham (1957, 1959) to explain fatigue-hardening in pure metals, and the over ageing of age-hardened alloys during fatigue. In metals these vacancies should cluster and then collapse to form dislocation loops, as shown by Segall and Partridge (1959), whereas in ionic crystals the vacancies appear to be stable in the form of small clusters, which can be made visible by x-irradiation and optical bleaching.

References

Broom, T., Molineax, J. H., and Whittaker, V. N., 1955, *J. Inst. Met.*, **84,** 357.

Broom, T., and Ham, R. K., 1957, *Proc. roy. Soc.*, **242,** 166; 1959, *Ibid.* (to be published).

Cottrell, A. H., 1957, *Inst. Met. Monograph and Report Series*, **23,** 1.

Fischbach, D. B., and Nowick, A. S., 1958, *J. Phys. Chem. Solids*, **5,** 302.

Nowick, A. S., 1958, *Phys. Rev.*, **111,** 16.

Przibram, K., 1956, *Irradiation Colours and Luminescence* (London: Pergamon Press).

Segall, R. L., and Partridge, P. G., 1959, *Phil. Mag.*, **4,** 912.

Seitz, F., 1952, *Advanc. Phys.*, **1,** 43.

Taylor, A., and Pratt, P. L., 1958, *Phil. Mag.*, **3,** 1051.

Vaughan, W. H., Leivo, W. J., and Smoluchowski, R., 1958, *Phys. Rev.*, **110,** 652.

REVIEWS OF BOOKS

Group Theory and its Application to the Quantum Mechanics of Atomic Spectra. By Eugene P. Wigner. Translated from the German by J. J. Griffin; expanded and improved edition. [Pp. 372.] (Academic Press: New York and London). Price $8.80.

This is a very welcome translation from the German of Professor Wigner's book which has stood as a classic in its field since 1931. About half the book is devoted to building up rigorously the theory of group representations with particular reference to the full rotation group and the symmetric group, the remainder dealing in detail with the applications to atomic energy levels, eigenfunctions and selection rules. Today the theory finds an even greater application in nuclear physics.

Three new chapters have been added in translation: one on Racah coefficients, a short one on the physical interpretation and classical limits of Wigner and Racah coefficients, and one on time reversal symmetry. Some minor improvements have also been made.

The treatment is introductory throughout in the sense that it starts from the beginning, but it must be mentioned that the book is not really very suitable as a first introduction to group theory for most physicists, because the treatment is so complete in its mathematical detail that the wood is often lost for the trees.

V. H.

The Physical Theory of Neutron Chain Reactors. By A. M. Weinberg and E. P. Wigner. (The University of Chicago Press.) [Pp. 800.] $15.

There has long been a need for a text-book on the theory of nuclear reactors that placed more emphasis on the basic physics in the theory and less on the semi-empirical methods that have great vogue in this field. The present work does much to fulfil this need. Its authors combine physical insight with expert knowledge of many branches of reactor theory and they have produced a masterly treatise on the subject.

The work is divided into four main sections. The first gives the elements of the nuclear physics involved, the second deals with the theory of neutron transport, the third, general reactor theory and the last, heterogeneous reactors.

The writing is lucid, the diagrams simple and clear, and, in addition to the theoretical treatment, there is a wealth of experimental information both in the text and in the many tables. An index to the latter at the end of the volume is a very convenient feature. Overall, the book can be recommended unhesitatingly to those working in the reactor field and also to those outside it who would like a deeper understanding of the physical processes involved.

G. L. S.

Information Theory and Statistics. By Solomon Kullback. (New York: John Wiley; London: Chapman and Hall, 1959.) [Pp. xviii+395.] 100*s*.

The author of this book presents an account of a large part of standard statistical theory based on the underlying concept of information as a logarithmic measure, such as developed by Shannon. It is very much a book for the statistical specialist and workers in control engineering or psychology, for example, should not be misled by the use of 'Information Theory' in the title. The most they might get out of the book is a mathematical account of some properties of Shannon's measure of information contained in the first five chapters. The remainder of the book deals with sampling from Poisson and binomial populations, contingency tables, multivariate analysis and linear hypotheses. The treatment throughout is at a fairly sophisticated mathematical level with many examples.

D. W. L.

Basic Physics of Atoms and Molecules. By U. Fano and L. Fano. (New York: Wiley & Sons, 1959.) [Pp. 414.] 80*s*.

Mécanique Quantique. By A. Messiah. (Paris: Dunod, 1959.) [Pp. 430.] 3900 fr.

A valuable by-product of the courses in quantum theory which now grace most undergraduate curricula in physics and applied mathematics is a crop of useful textbooks. There is now a broad spectrum to choose from, ranging from the naive, specially simplified, introduction to the sophisticated, specially complicated, treatise. These two new books are welcome, for each presents new aspects of this formidable, fascinating discipline.

Dr. and Mrs. Fano write with the advantages and disadvantages of a doctrine that quantum theory can be understood by a direct study of various experimental phenomena. The physical significance and role of eigenestates, probability, superposition, interference, exclusion, etc. are demonstrated through chosen experiments in atomic physics, and from these the modern theory of the structure of atoms and molecules is built up. A beginner may well find this account very illuminating, and may be astonished to learn how much can be made plausible by elementary verbal argument without recourse to heavy algebra. The pictures of wave functions and the discussion of the theory of chemical bonds are particularly valuable. But the doctrine makes the book needlessly difficult, for the desire to establish the logical necessity of wave mechanics directly out of the phenomena involves the setting up of a mathematical formalism which is not particularly clear, nor at all familiar to the average student of the subject. The Schrödinger equation, however unsatisfactory as a basis, is unavoidable, and there is quite enough mathematical analysis that must be learnt anyway, without trying to do the whole calculation from back to front. If one objects to ψ, then one should use the Dirac brackets, which offer full scope for abstract argument. A student would get most out of the book by translating the mathematics into the conventional notation as he went along.

A widely accepted standard notation is important for the next stage of the subject, the passage to the abstract operator formalism, which is the central topic of the first volume of Dr. Messiah's treatise. There is no attempt here to discuss all the physical problems which demand quantum mechanical solutions but the standard systems of free particles, central forces and scattering are dealt with. The treatment and notation follow the best current conventions, the theory being expounded rather than justified. But the value of the book is its lucidity, the complete and explicit development of the mathematical analysis the continual re-emphasis of physical concepts, and the great care that has been taken to clarify the basic difficulties of the subject, especially in relation to the statistical interpretation of microphysics. It is sober, and elegant, in the great tradition of French mathematical physics; it is also perhaps the best place to find the answers to those tricky questions raised by tiresomely clever students after an insufficiently plausible lecture. J. M. Z.

Theory of Relativity. By W. Pauli. Translated by G. Field. (London: Pergamon Press, 1959.) [Pp. 241.] 35*s*.

This translation, with supplementary notes, of Pauli's article, written in 1921 when he was a very young man, will be welcomed by students and experts alike.

Astronomy. By Theodore G. Mehlin. (New York: John Wiley and Sons, Inc.) [Pp. viii+392.] 64*s*.

It is difficult for an English reviewer to assess fairly the merits of this book, for it is written to meet a requirement of the American educational system that has no exact counterpart here: the ' College Course '.

A distinguished American scientist, the story goes, was asked by a young student at a College reunion dinner what subject he studied. To the reply ' astronomy ', the student responded " Oh, I finished astronomy last year ". And with this book the student may also finish astronomy in a year, from atomic structure through stellar atmospheres to metagalaxy; without tears and indeed without any particular mental pains at all. (English units of measurement are used freely throughout " on the grounds that very few American students can think in terms of the metric system ".)

Of its kind the book is admirable—the paper is glossy, the illustrations good, and the material of the text up-to-date and on the whole accurately presented. The book differs a little from others of its genre: putting the stars first is a suitable reflection of current astrophysical interests, and the author claims some originality for a more logical presentation of material, based on his teaching experience.

The book is almost innocent of any formal mathematical presentation. It is explained on p. 22 that 10^{-24} is " scientific shorthand meaning divided by a million, million, million, million "; but on p. 34 the brightness of the sun is still expressed as " about 400,000 million million thousand watt electric light bulbs ". (" This number is so large that if every man, woman and child in the United States were to break a bulb a second for the next 700 years, that would only account for one-thousandth of one per cent of the total number.")

The only serious criticism one can make of books such as this is that at best they give a readable description of what astronomers are about: at worst they might leave a College student with the idea that he has understood the way they go about it. Occasionally in the text a sharp, painful shock should be jabbed into the student, to awaken him to the realization that nature does not yield her secrets as easily and comfortably as his three-semester easy science option might suggest.

D. W. D.

The Physics of Electricity and Magnetism. By William Taussig Scott. (New York : John Wiley & Sons, Inc., 1959.) [Pp. 635+xvi.]

The logical basis of electromagnetism is a controversial subject and it is rare to find two teachers who agree completely about the best method of teaching it. In particular there are two ways of presenting magnetism. The older way invokes the accurate experiments which can be made with bar magnets and magnetometers, and uses the concept of magnetic pole as analogous to electric charge. It treats the electric and magnetic intensities **E** and **H** as similar field vectors. The more modern way is based on forces between moving charges and treats **E** and **B** (magnetic induction) as the fundamental field vectors. The idea of magnetic pole is introduced much later as a useful fiction when studying magnetic materials. Professor Scott's book must be one of the best expositions of the more modern view and his arguments should be appreciated by even the strongest supporters of the older system. Teachers of Physics students taking a final honours course will need to consider this book seriously when recommending a text-book on Electricity and Magnetism. The writing is clear and there are many good diagrams. Concepts which students find difficult, for example vector potential and displacement current, are carefully explained.

The symbols ϵ_0 μ_0 are used and can make the equations valid in any self-consistent units. Many equations in this book are labelled " M.K.S.", an unnecessary restriction since they are equally valid in other systems, depending on the choice of values of ϵ_0 and μ_0. Some equations are given twice, the second version being in Gaussian units. The treatment of units is perhaps a weak feature of this book. Although μ_0 has different numerical values in different systems of units, we find the view that μ_0 is dimensionless and that the units ' gauss ' and ' oersted ' are interchangeable.

K. G. B.

Fluctuation Phenomena in Semi-conductors. By A. Van der Ziel. (Butterworths, 1959.) [Pp. 168+viii.] 35*s*.

In recent years, considerable progress has been made in the theory of noise in semiconductors, to which Professor Van der Ziel and his colleagues at Minnesota have made many important contributions. The present review is therefore both timely and authoritative. After two short chapters on measurement and mathematical techniques the author discusses the theories of generation noise and '$1/f$' noise in bulk crystals, leading up to a description of noise in devices such as transistors, diodes and photoconductors. Very little knowledge of semiconductors is assumed so that even the rectification characteristic of a PN junction is briefly explained.

It is, perhaps, not unnatural that the author stresses the theory of noise as opposed to experimental results. However, experimental work is frequently dismissed with two lines and a reference while the development of the appropriate expression for, say, generation noise in N-type material with traps is given fully. Of the 18 figures, not one illustrates an experimental result. McWhorter's theory is presented as *the*, rather than *a* theory of $1/f$ noise. While no one will deny the importance, perhaps dominance, of the crystal surface, I feel the subject is not as clear cut as the author's treatment would suggest.

With these provisos I would strongly recommend this book to all interested in noise in conductors, whether they have any experience in semiconductors or not. It joins monographs by Dr. T. S. Moss and by Messrs. W. D. Lawson and S. Nielsen edited by Dr. C. A. Hogarth. So why is the paper used of poorer quality ?

A. F. G.

Elements of Materials Science. By L. H. Van Vlack. (Addison Wesley Publishing Company Inc., 1959.) [Pp. 528.] 66*s*.

This is a very elementary book designed to explain to engineering students the structure and uses of all solid materials. With such a large task the author has succeeded well and covers this vast subject in a logical order and with an interesting presentation.

The book starts with an introduction to the ideas of binding in solids and an account of common crystal structures. The properties of metal are then described, followed by those of ceramics, organic materials and polymers. The properties of solid material containing more than one phase are then dealt with both in thermodynamic equilibrium and in metastable states. Finally the behaviour of materials subjected to mechanical forces, chemical attack, electric and magnetic fields, and irradiation with nuclear particles is described.

In short the book covers in a descriptive fashion most of the essentials of the separate disciplines of metallurgy, ceramic and polymer science, rheology and parts of solid state physics and inorganic chemistry. The author has achieved a notable success in the way in which he has organised the presentation of the material. A large number of easy numerical examples included at the end of each chapter should give the student a good idea of the magnitudes of quantities involved.

The excessive simplification of theoretical ideas leads to the choice of a number of unfortunate examples, but this could hardly be avoided. One criticism is, however, the occasional reliance on undocumented pictorial argument.

The subject matter covered should be familiar to anyone concerned with the nature of solids and in these days of intense scientific specialization the book is rather refreshing.

A. K.

BOOK NOTICES

Photographie Corpusculaire. By Centre National de la Recherche Scientifique. (Strasbourg.) [Pp. 451.]

Statistical Estimates and Transformed Beta-Variables. By G. Blom. (New York: John Wiley & Sons). [Pp. 176.] 40*s.*

The Potential Theory of Unsteady Supersonic Flow. By J. W. Miles. (Cambridge: University Press.) [Pp. 220.] 45*s.*

Properties of Matter. By Champion and Davy. (London: Blackie & Son Ltd.) [Pp. xvi+334.] 40*s.*

Integral Equations. By F. Smithies. (Cambridge: University Press.) [Pp. vii+172.] 27*s.* 6*d.*

Dynamics of Flight. By B. Etkin. (New York: John Wiley & Sons, Inc.) [Pp. xiv+519.] 120*s.*

Three Dimensional Dynamics. By C. E. Easthope. (London: Butterworths Scientific Publications.) [Pp. viii+277.] 42*s.*

The Calculation of Atomic Structures. By Douglas R. Hartree. (New York: John Wiley & Sons, Inc.)

Nuclear Masses and their Determination. Edited by Professor H. Hintenberger. (London: Pergamon Press.) [Pp. ix+267.] 84*s.*

Progress in Biophysics and Biophysical Chemistry. By J. A. V. Butler and B. Katz. (London: Pergamon Press.) [Pp. 409.] 105*s.*

The Physics of Rubber Elasticity. By L. R. G. Treloar. (Oxford: University Press.) [Pp. 343.] 40*s.*

The Structure of the Nucleus. Edited by W. O. Milligan. Proceedings of the Robert A. Welch Foundation. Conference on Chemical Research. (Houston, Texas.) [Pp. 168.]

La Structure et l'évolution de l'univers. Edited by R. Stoops. Institut International de Physique Solvay, Onzième Conseil de Physique. Bruxelles 9–13 June 1958. [Pp. 309.]

Growth of Crystals. Reports at the First Conference on Crystal Growth March 5–10, 1956. Edited by A. Shubnikov and N. N. Sheftal. Publishers: Consultants Bureau Inc. English translation (Chapman & Hall), 1958. Original Russian text published by Academy of Sciences, USSR Press, Moscow, 1957. 120*s.*

Propriétés Optiques et Acoustiques des Fluides Comprimés et Actions Intermoleculaires. Colloques Internationaux du Centre National de la Recherche Scientifique. No. LXXVII. Bellevue, Juillet 1–6, 1957. Publishers: Centre National de la Recherche Scientifique, Paris, 1959.

The Structure of Electrolytic Solutions. Edited by Walter J. Hamer. Publishers: Wiley (Chapman & Hall). Based on a Symposium held in Washington, D.C. in May 1957, sponsored by The Electrochemical Society, Inc., New York, and The National Science Foundation, Washington, D.C. [Pp. 441.] 148*s.*

Lectures in Theoretical Physics, Volume I. Lectures delivered at the Summer Institute for Theoretical Physics, University of Colorado, Boulder, 1958. Edited by W. E. Brittin and L. G. Dunham. Publishers: Interscience Publishers. [Pp. 414.] 45*s.*

Fig. 3

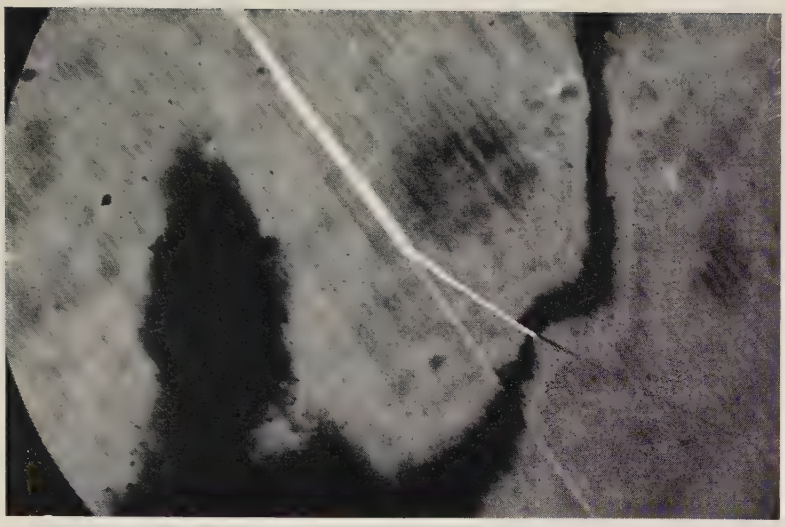

Single crystal 50 Å gold film after deformation on a silver substrate.
×50 000.

Fig. 4

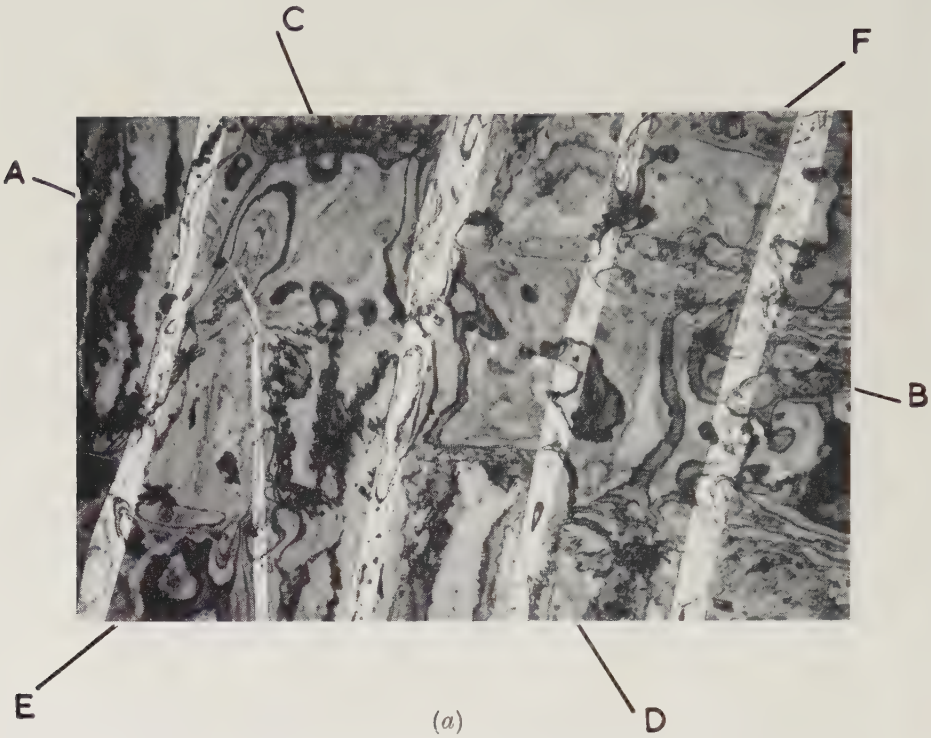

(*a*)

Gold single crystal/carbon polycrystal double-layer after deformation on a silver substrate. ×10 000.

(*b*)

Same as fig. 4 (*a*) at higher magnification. ×35 000.

Fig. 5

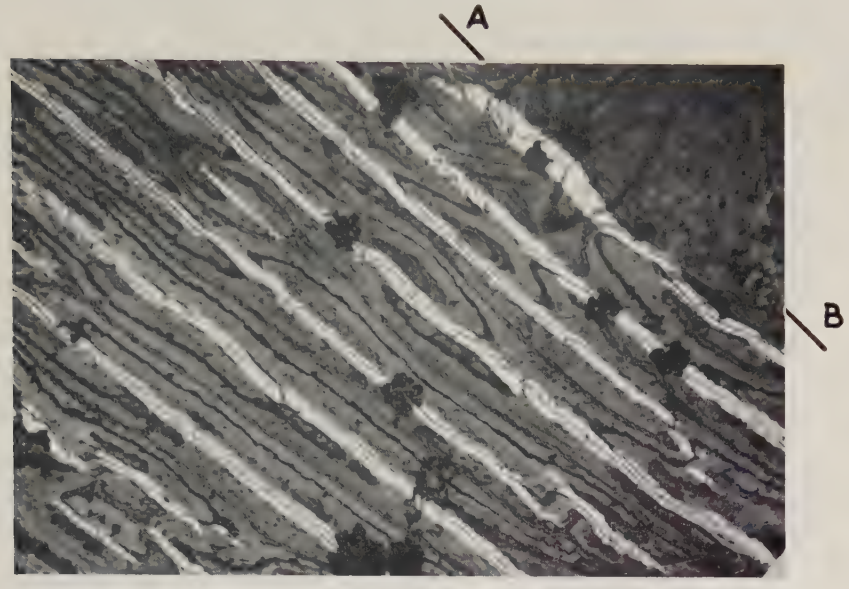

Gold single crystal platinum polycrystal double-layer after deformation on a silver substrate. ×10 000.

Fig. 6

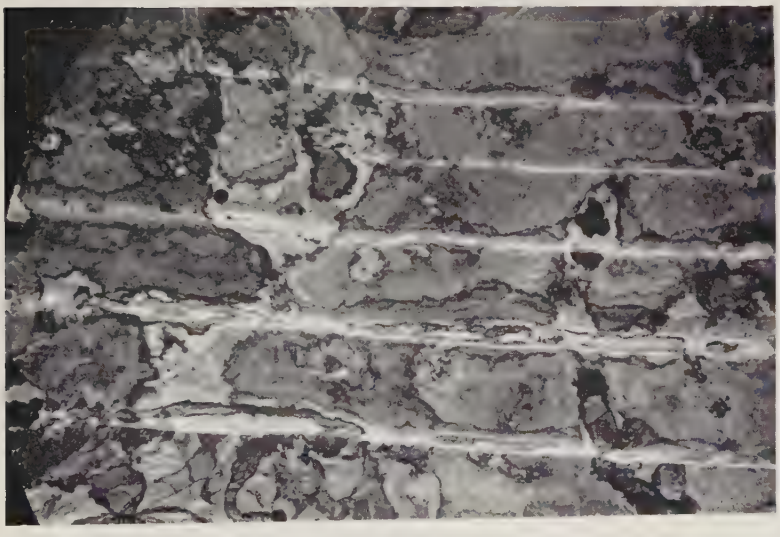

Gold single crystal film after deformation on a silver substrate. Overlying iron polycrystalline film has been removed. ×10 000.

Fig. 7

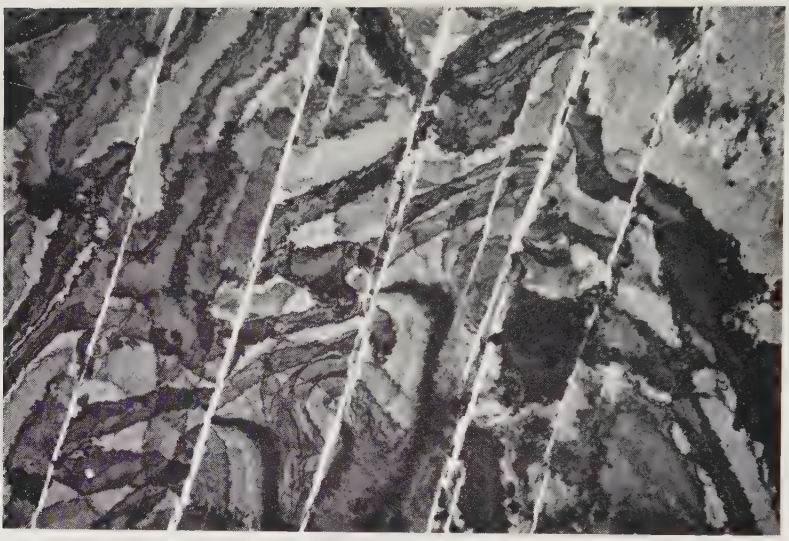

Gold single crystal film after deformation on a silver substrate. Overlying iron polycrystalline film, laid down at 100°C, has been removed. ×10 000.

Fig. 8

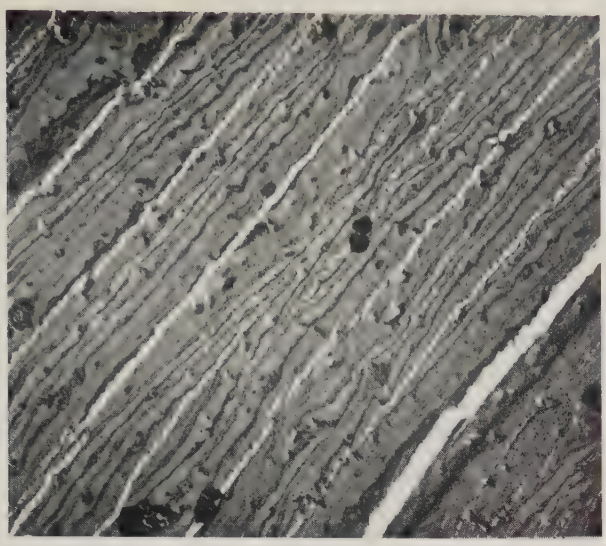

Gold single crystal, chromium polycrystal double-layer after deformation on a silver substrate. ×10 000.

Fig. 9

Gold single crystal film after deformation on a silver substrate. Overlying chromium polycrystalline film has been removed. ×50 000.

Fig. 10

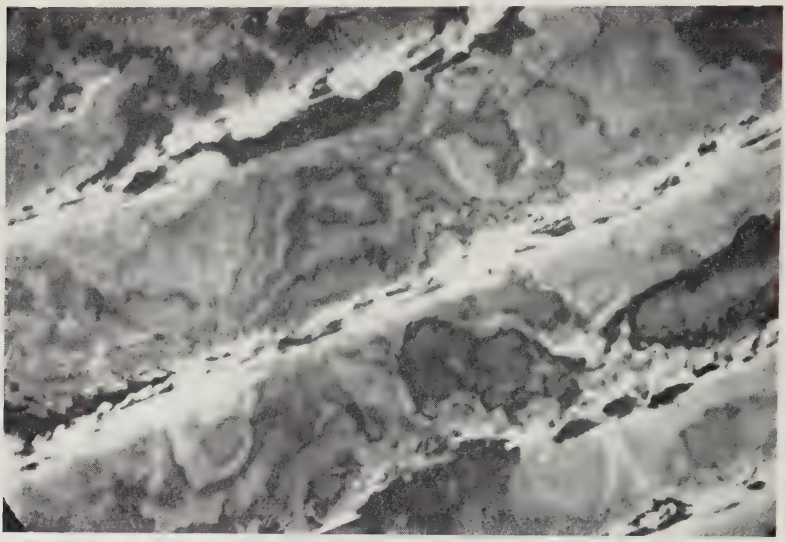

Gold single crystal film after deformation on a silver substrate. Overlying iron polycrystalline film, laid down at 120°c has been removed. ×50 000.

Fig. 11

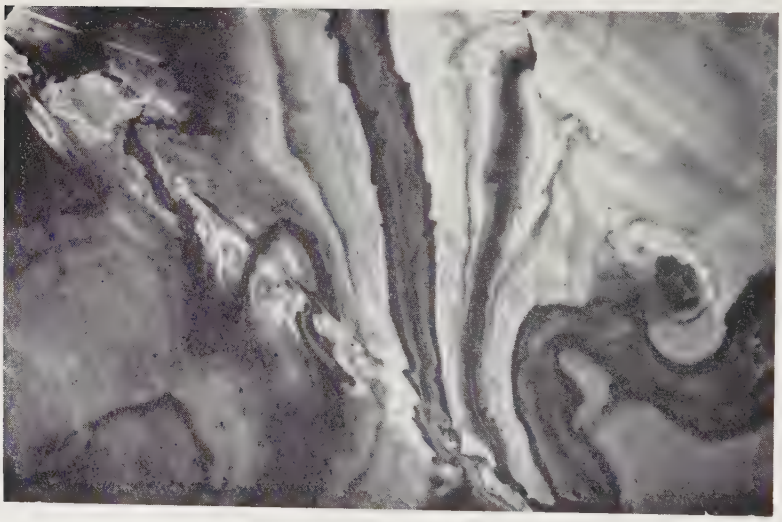

Gold single crystal film after two deformations on a silver substrate. The first deformation is in the presence of an overlying iron polycrystalline film and the second is in its absence. ×50 000.

Fig. 1

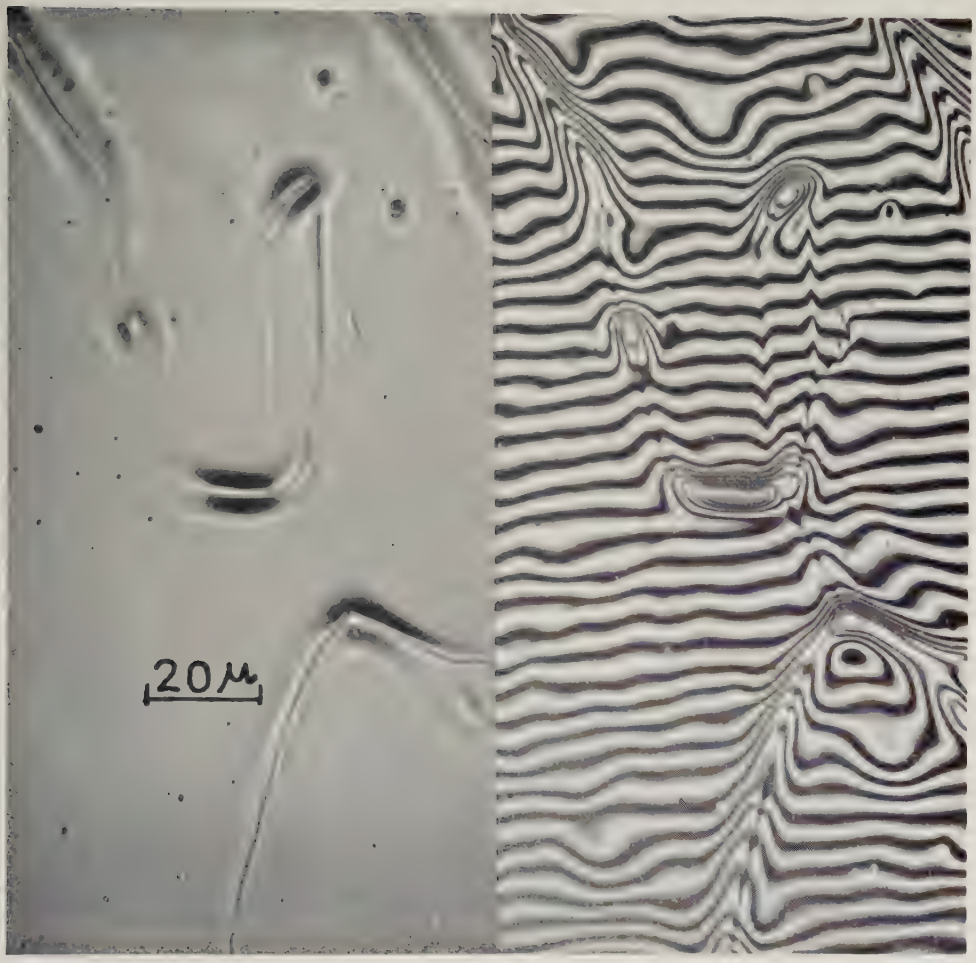

Ordinary and interferometric photographs of grain boundary ridges in impure Ni. Specimen heated 8 hours at 1200°c. One fringe corresponds to a change in height of 3×10^{-5} cm.

Fig. 2

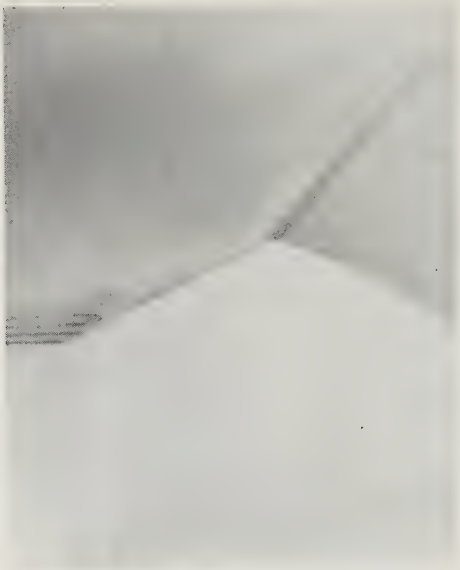

1 μ

Large angle grain boundaries in a typical area in an annealed specimen. $\times 20\,000$.

Fig. 3

1 μ

Long dislocations in a region of high dislocation density in a specimen stressed to 1 kg mm^{-2} in tension. $\times 20\,000$.

Fig. 4

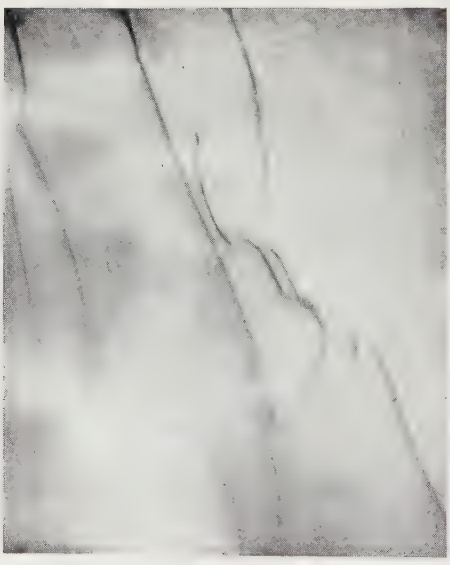

1 μ

Long dislocations in a region of high dislocation density in a specimen stressed to 2 kg mm^{-2} in tension. $\times 25\,000$.

Fig. 5

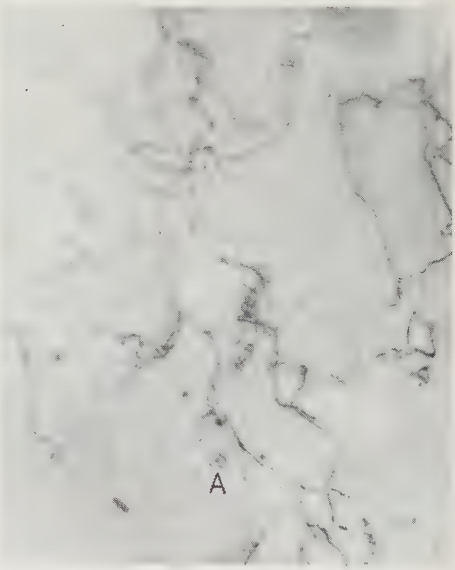

1 μ

A group of dislocations in a specimen stressed to 3 kg mm^{-2}. Note the dislocation loops at A. $\times 20\,000$.

Fig. 6

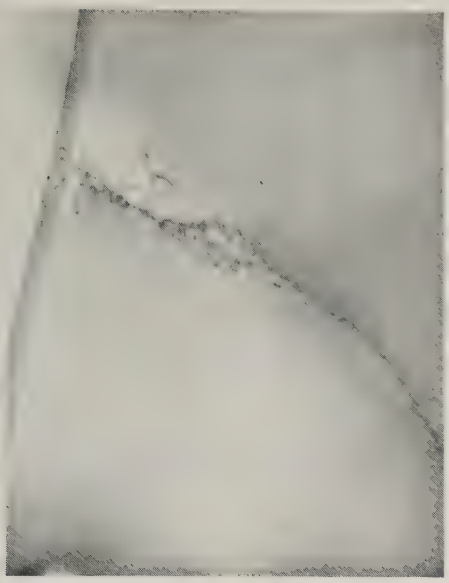

1 μ

A well-developed sub-boundary and a large angle boundary in a specimen stressed to 4 kg mm^{-2} in tension. $\times$25 000.

Fig. 7

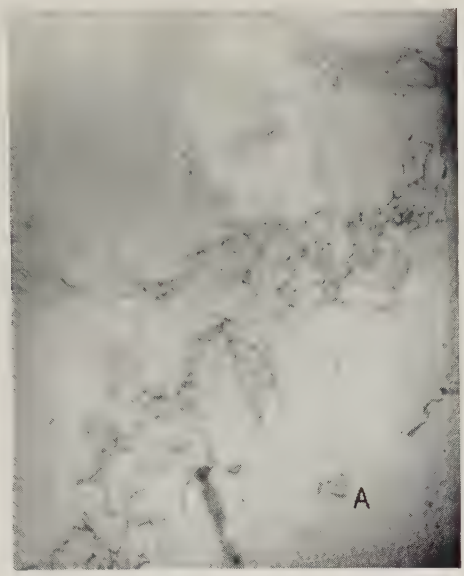

1 μ

A typical area in a specimen stressed to 4 kg mm^{-2} in tension. Note the dislocation loops at A. $\times$20 000.

Fig. 8

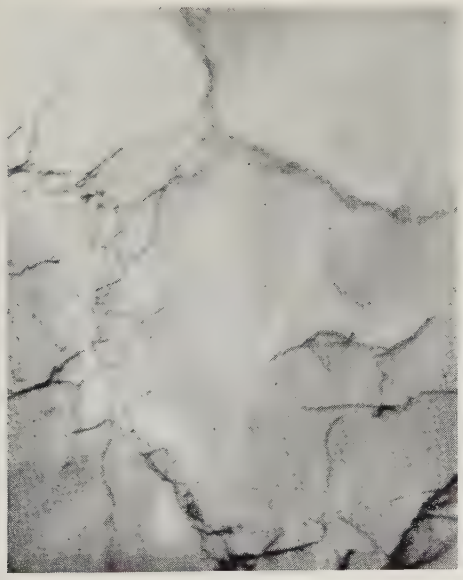

1 μ

Specimen stressed to 4 kg mm^{-2} in tension showing development of subgrains. $\times$20 000.

Fig. 9

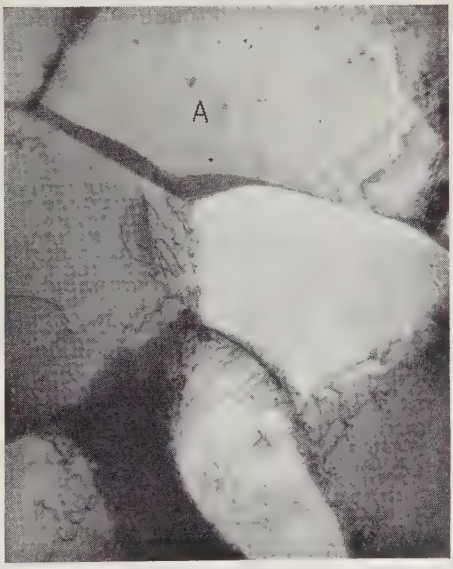

1 μ

Well-developed subgrains in a specimen stressed to 7 kg mm^{-2} in tension. Note dislocation loops at A. $\times$20 000.

Fig. 10

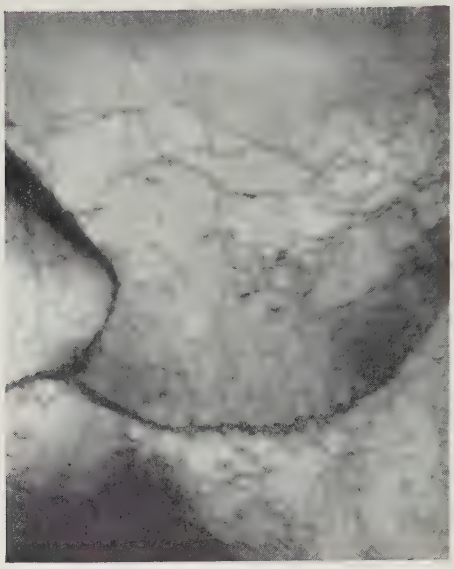

Specimen failed by fatigue after 10^5 cycles showing subgrain boundaries in high stress fatigue. ×20 000.

Fig. 13

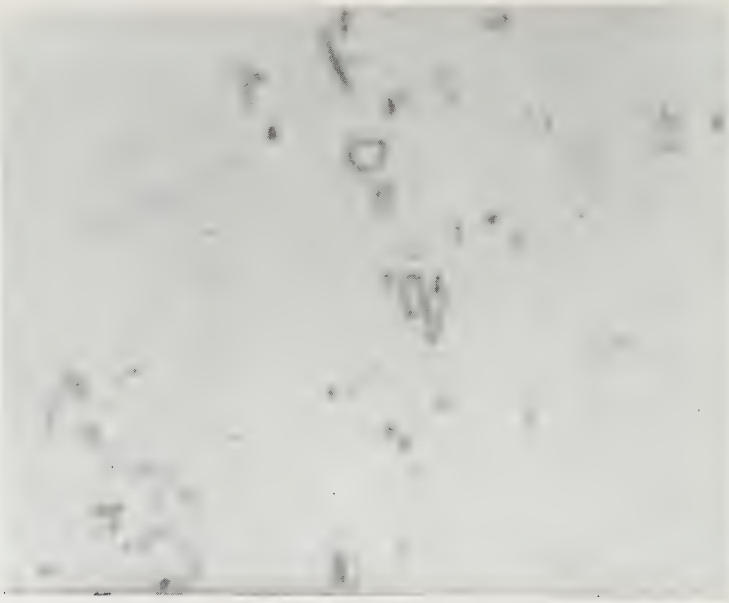

Fatigue specimen after $2{\cdot}5 \times 10^6$ cycles showing dislocation loops at higher magnification. ×95 000.

Fig. 11

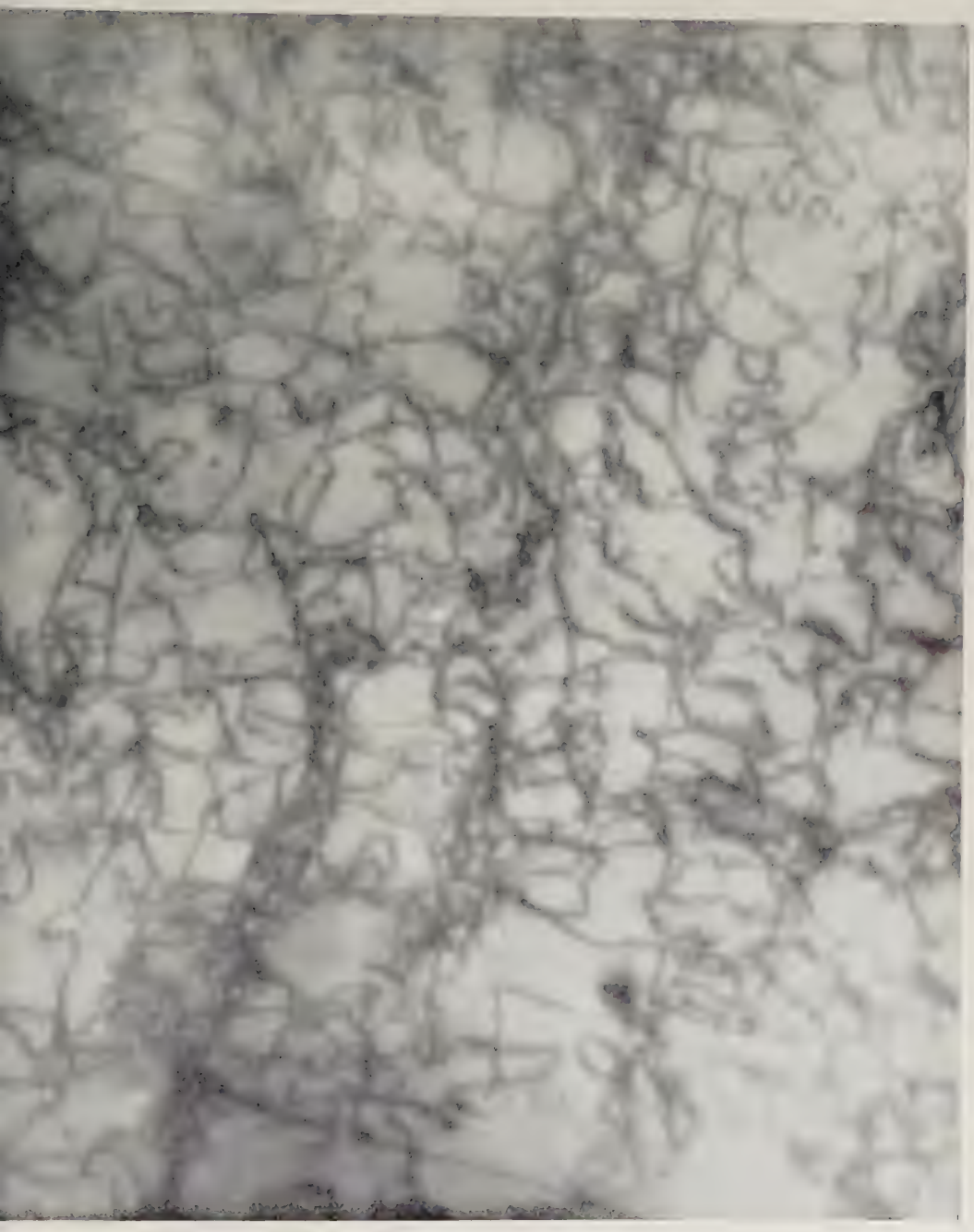

Specimen failed by fatigue after $1{\cdot}8 \times 10^6$ cycles. Note the high dislocation density and the absence of polygonization. ×50 000.

Fig. 12

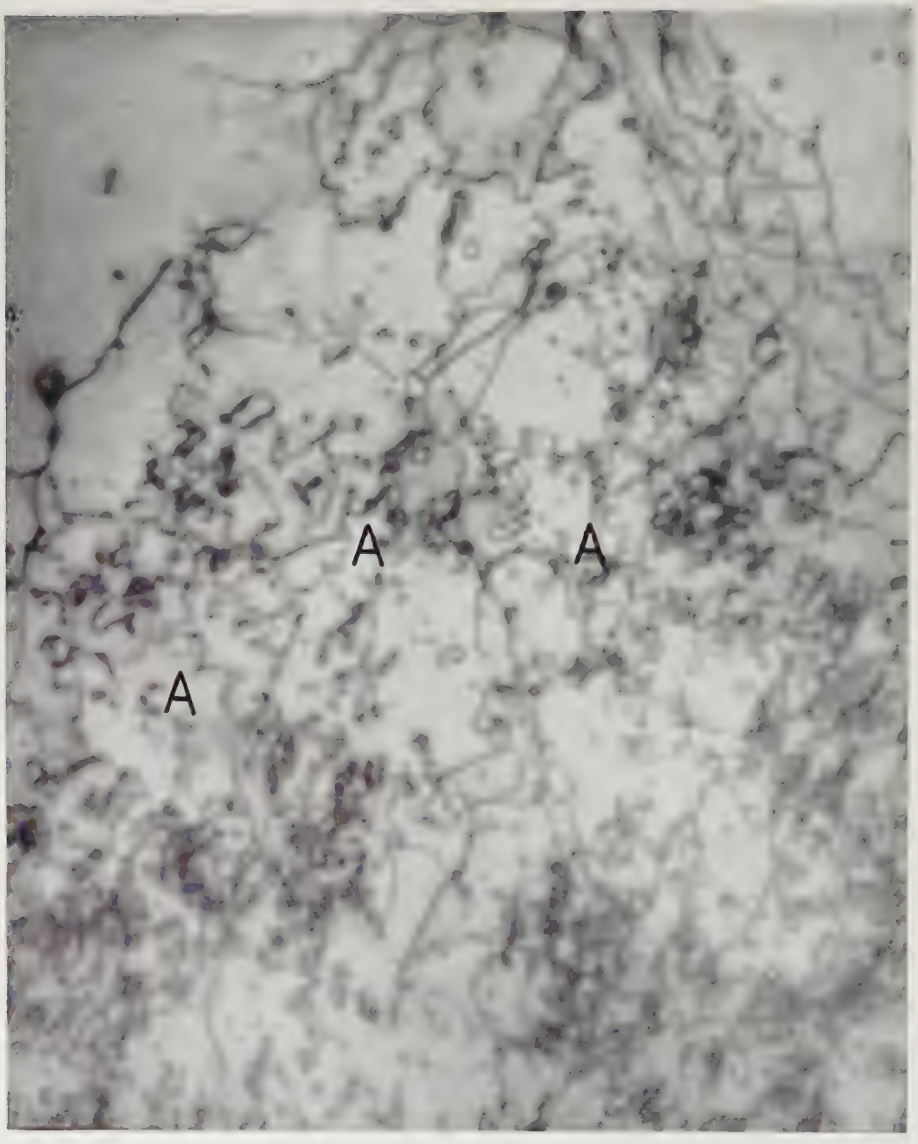

Fatigue specimen after $1{\cdot}4 \times 10^6$ cycles. Note the high density of dislocation loops and the irregular helical dislocations, e.g. at A. ×45 000.

Fig. 2

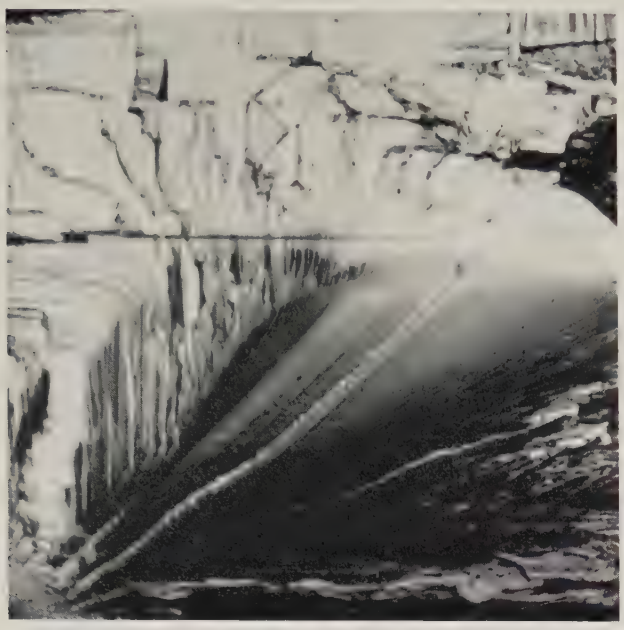

(*a*)

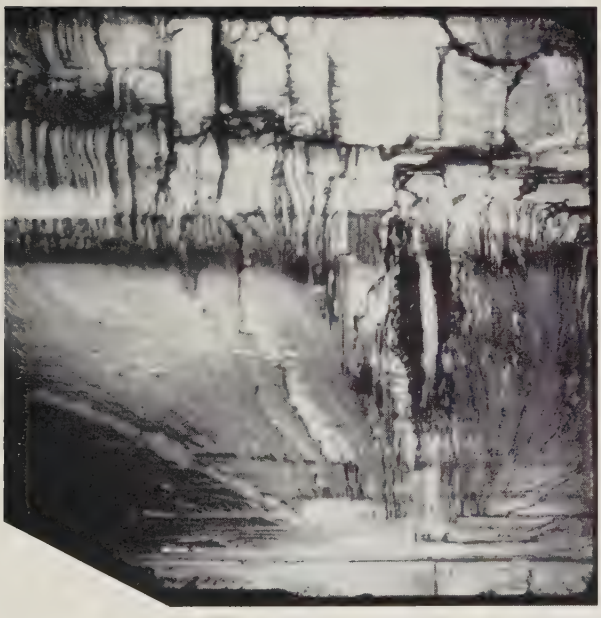

(*b*)

Characteristic fracture surfaces. ×25.

(*a*) Brittle specimen. Cleavage lines originate at the specimen corner. (*b*) Ductile specimen. Cleavage lines originate along the line inside the tension surface.

Fig. 4

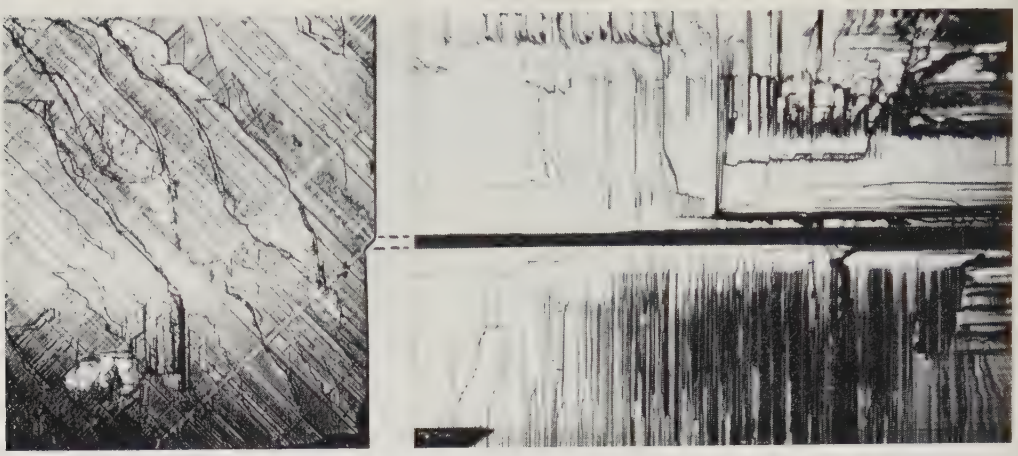

(*a*) (*b*)

Orientation of the step along which fracture starts. ×150.
(*a*) Profile of step, showing component parallel to slip direction. Crystal cleaved parallel to edge surface (I) and etched. (*b*) Photomicrograph of same step in fracture surface (II).

Fig. 5

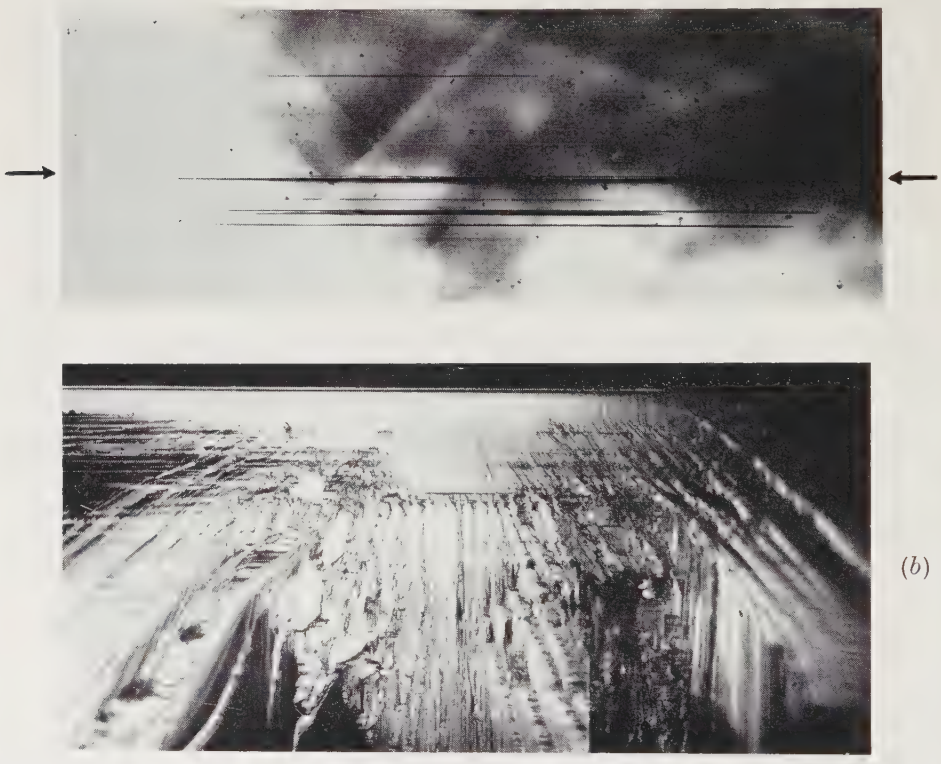

(*a*)

(*b*)

Fracture originating from a surface slit. ×50.
(*a*) Stable slit (defined by arrows) in the tension surface (III) before fracture. The other slits in this photomicrograph are beneath the crystal surface. (*b*) Fracture surface (II) photographed at the position corresponding to (*a*). The thin dark line just within the tension surface corresponds to the slip plane component of the stable slit.

Fig. 6

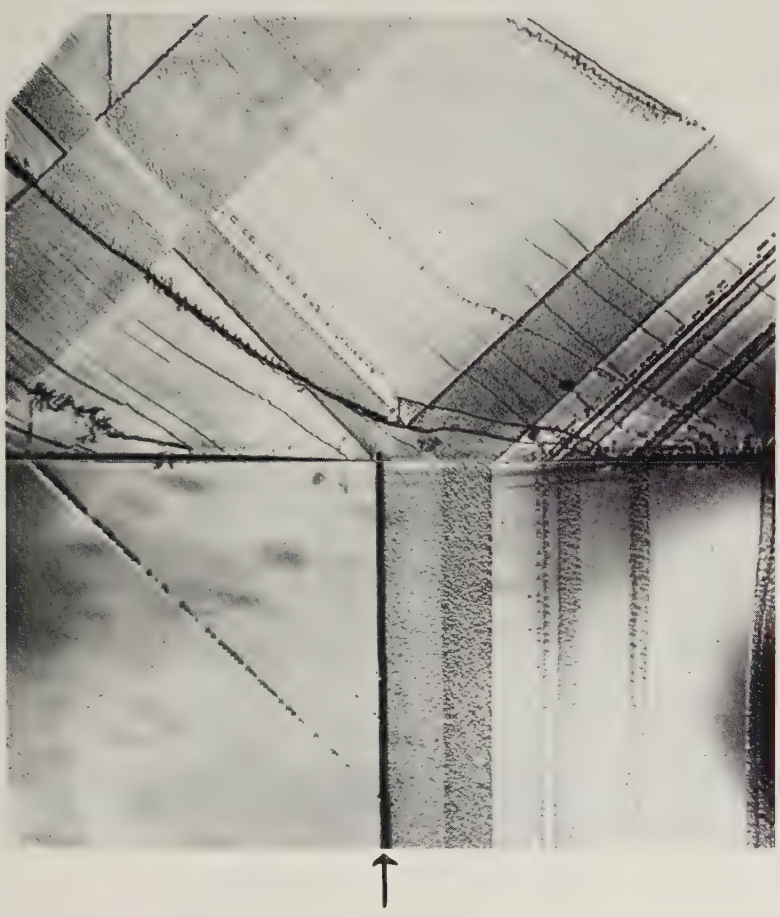

Composite photomicrograph of a stable surface slit showing its situation with respect to the slip bands. ×250.

(*a*) Edge surface (I). (*b*) Tension surface (III).

Note shear of intersecting slip bands in upper left-hand corner and growth of narrow slip band on right by expansion and multiplication of dislocation loops at the edge of the band.

Fig 7

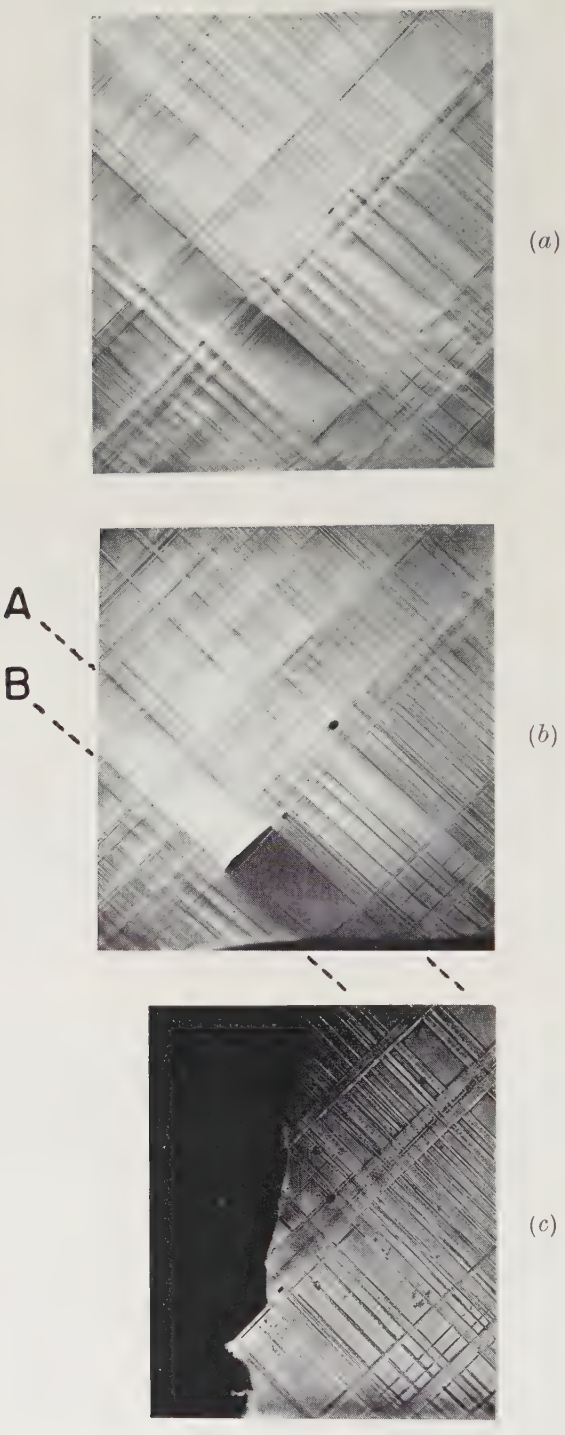

Sequence taken on edge surface (I) showing location of slit profiles with respect to slip bands. Slit in (*b*) spans the gap between ' narrower ' slip bands A and B, and in (*c*) provides the source of fracture. ×150.

Fig. 8

The location of slits with respect to bands of slip. ×150.

Fig. 10

The lengthwise growth of an internal slit. ×50.

Fig. 11

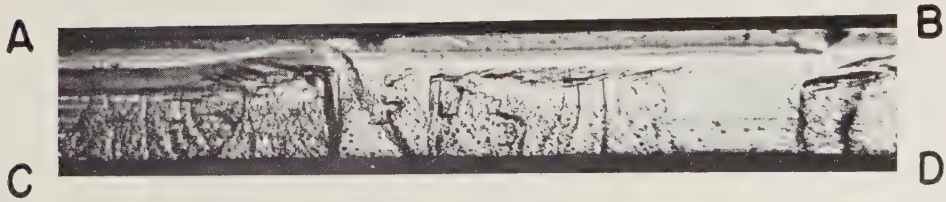

Surface of the secondary crack responsible for fracture in fig. 7 (*c*). Crack nucleated along line AB and propagated by cleavage in a direction perpendicular to AB (see fig. 12). ×320.

Fig. 1

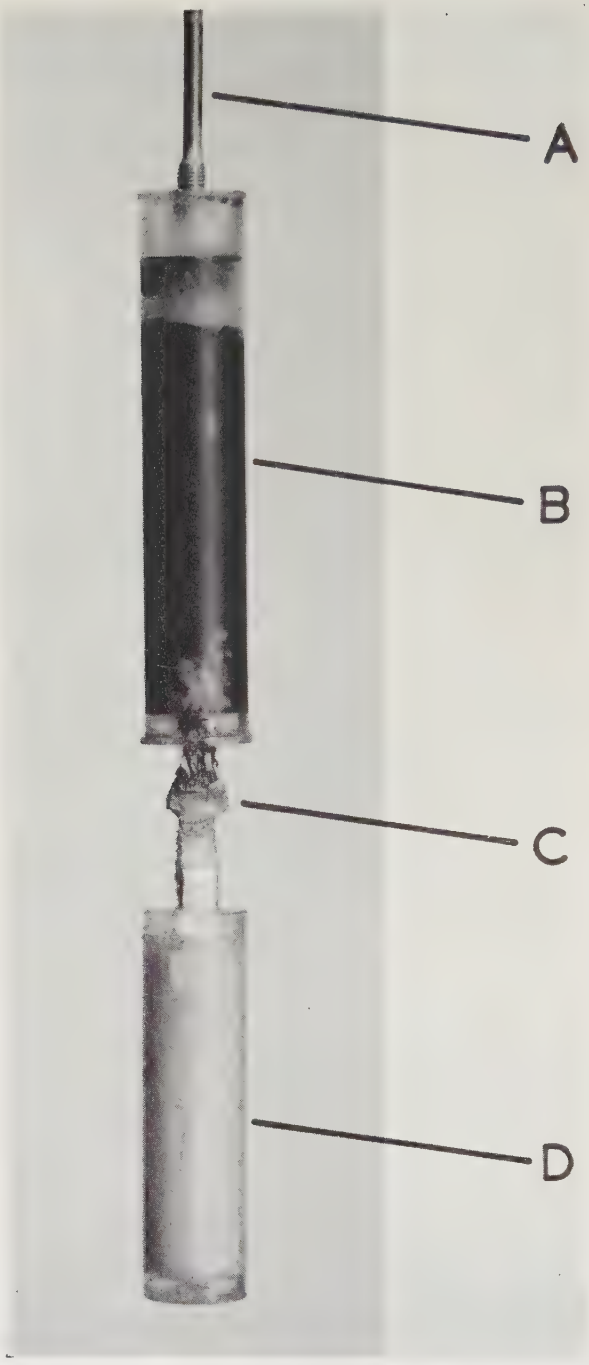

Final assembly of heat sink, thermometer and cobalt specimen.

A: supporting tube;
B: chrome potassium alum heat sink in Perspex container;
C: cobalt specimen;
D: cerium magnesium nitrate thermometer pill in Perspex container.

Fig. 1

Section through neck of tensile specimen (as-rolled copper: grain size 0·05 mm). ×9.

Fig. 2

(*a*) ×850. (*b*) ×1300.

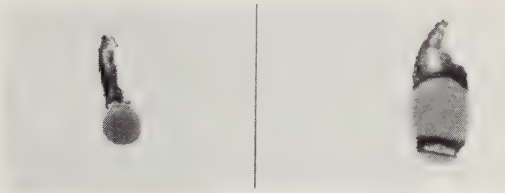

(*c*) ×850. (*d*) ×850.

Cavities forming at inclusions. Tensile axis vertical.

Fig. 3

Cavities coalescing in central region of fig. 1. × 300.

Fig. 4

Central fissure in fig. 1. ×90.

Fig. 5

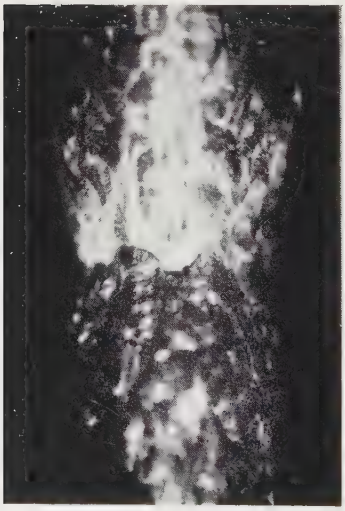

Surface crack in coarse-grained copper. ×6.

Fig. 6

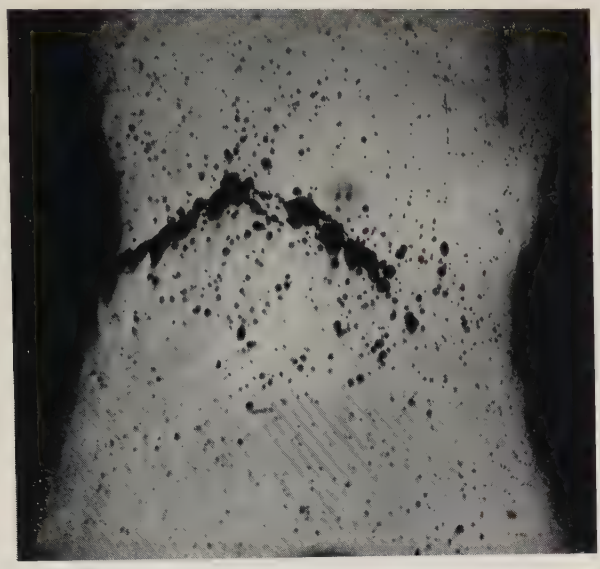

Section through specimen shown in fig. 5. ×12.

Fig. 7

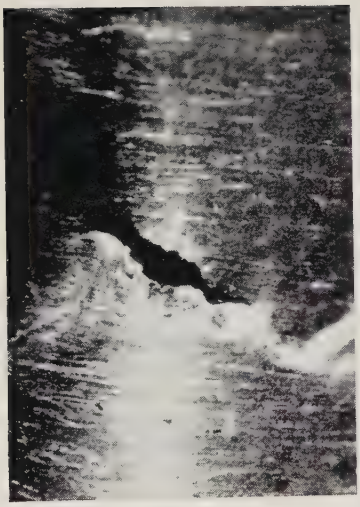

Surface crack in coarse-grained copper formed after polishing away surface layer. ×20.

Fig. 8

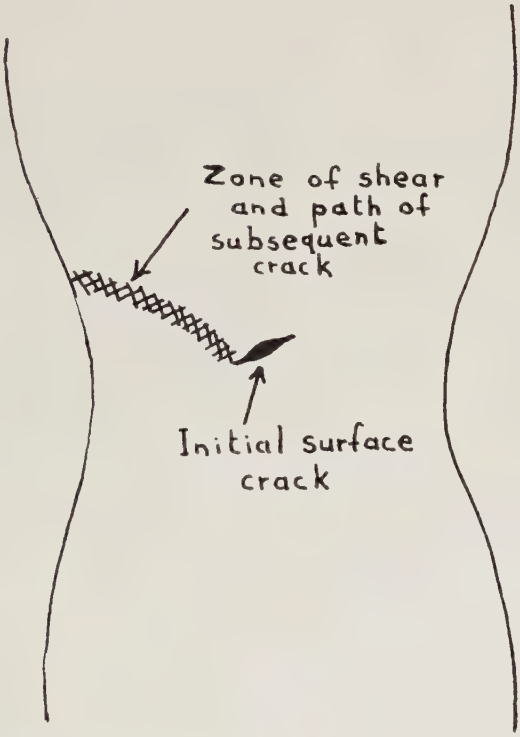

Initiation and propagation of surface crack in coarse-grained material.

Fig. 9

Holes in central section of neck of iron tensile test piece. ×90.

Fig. 10

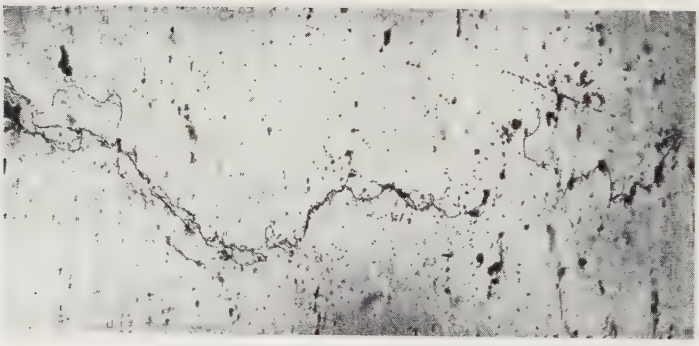

System of cracks originating at holes in fig. 9. ×90.

Fig. 11

(*a*)

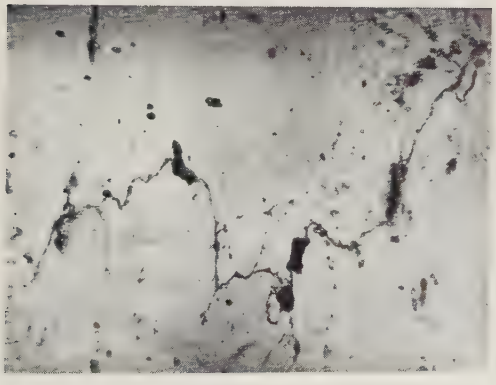

(*b*)

Details of fig. 10. Cracks in iron linking inclusion sites. ×350.

Fig. 12

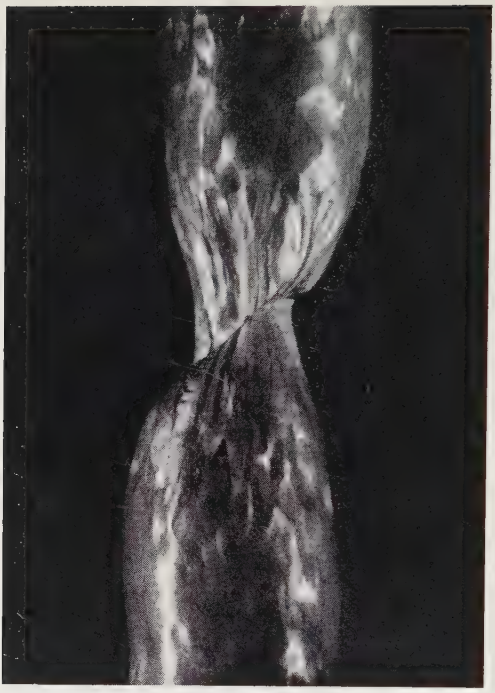

Slipping-off in pure polycrystalline aluminium. ×3.

Fig. 1

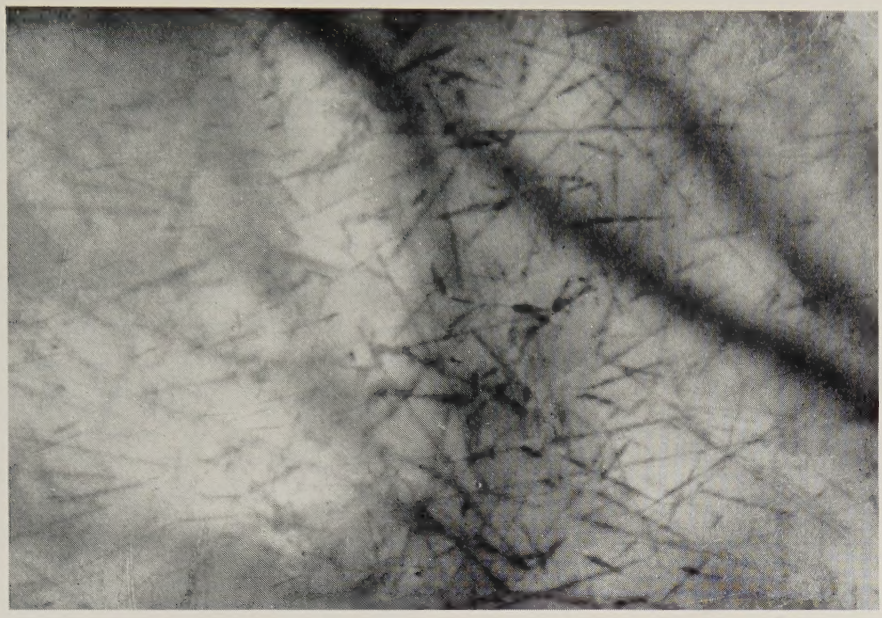

Tracks of fission fragments near the surface of mica irradiated next to a layer of uranium (0·34 mg cm^{-2}) for 20 min in BEPO. The tracks vary in width and length, the length being determined mainly by the thickness of the mica sheet. ×30 000.

Fig. 2

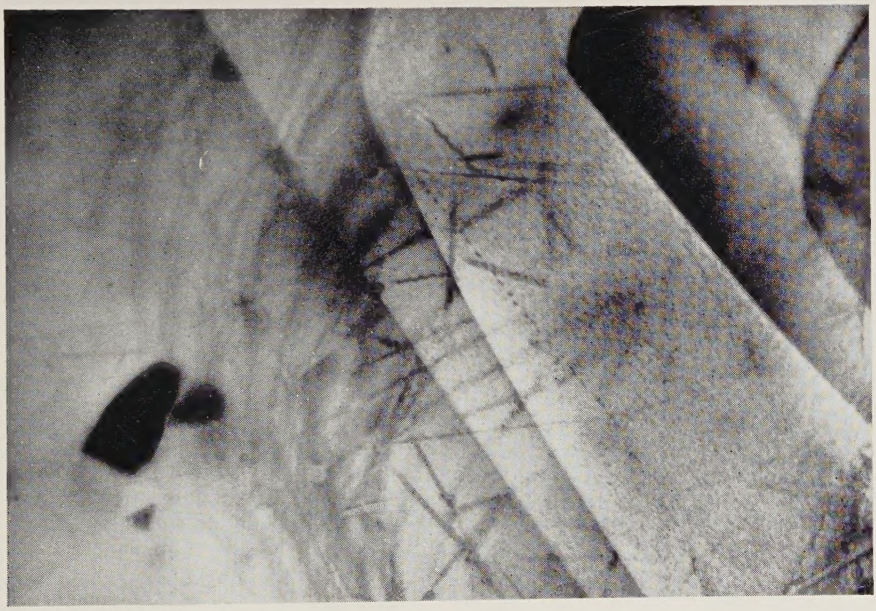

Tracks of fission fragments in the surface layer of mica irradiated for 15 min next to a layer of uranium (0·17 mg cm^{-2}) in BEPO. The thickness of the mica changes at the cleavage steps. ×30 000.

Fig. 3

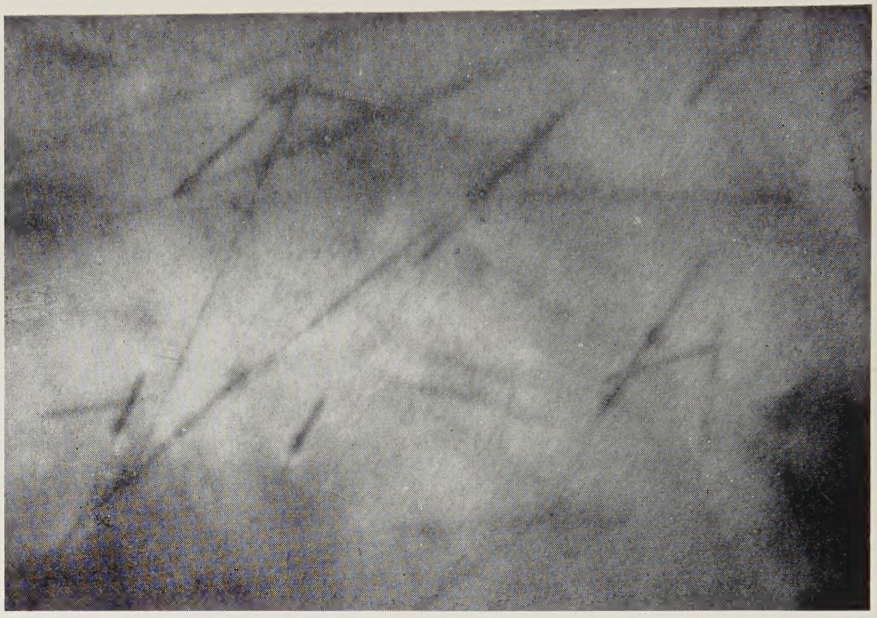

As for fig. 2 but irradiated for 5 min in BEPO. ×30 000.

Fig. 4

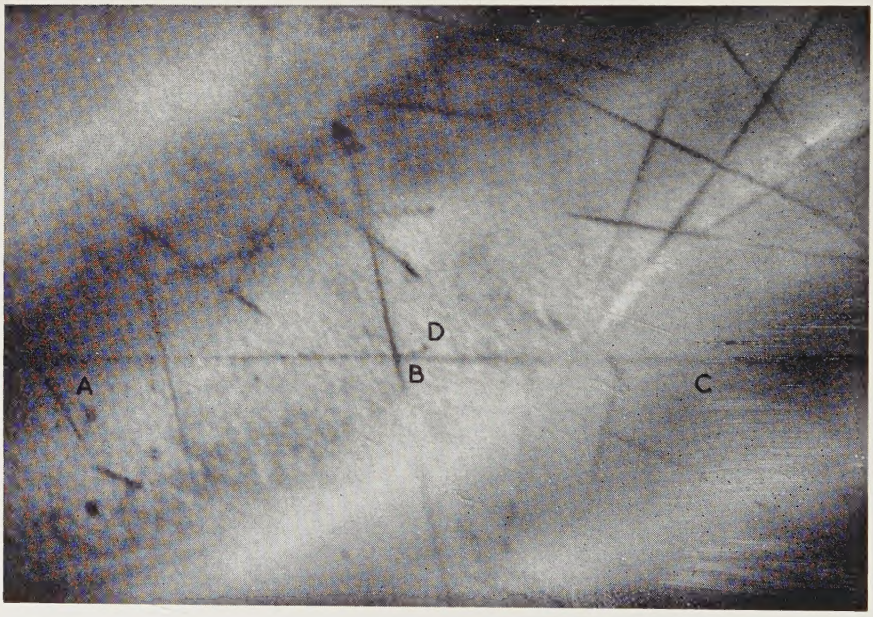

Fission fragment tracks in mica. Some tracks have darkened ends. The track ABC has a deflection at B and changes its nature where the extra track, BD appears. ×30 000.

Fig. 5

(*a*)

(*b*)

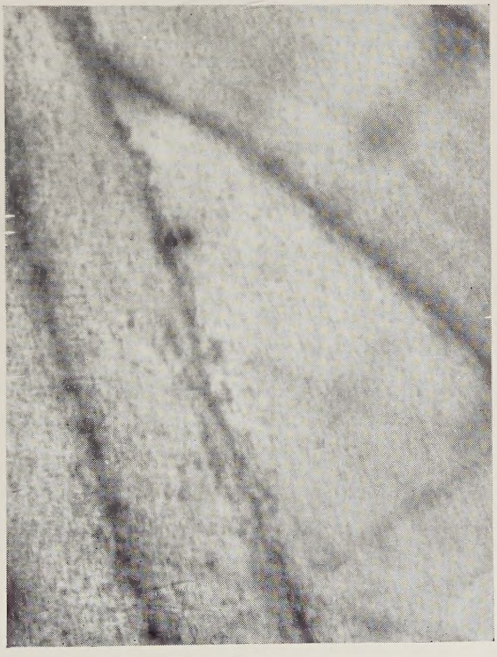

(*c*)

A series of photographs from the same area showing break up of fission fragment tracks in mica on annealing (*a*) after partial annealing, (*b*) after further annealing and (*c*) after prolonged annealing. The broad dark bands are extinction contours. $\times 30\,000$.

Fig. 2

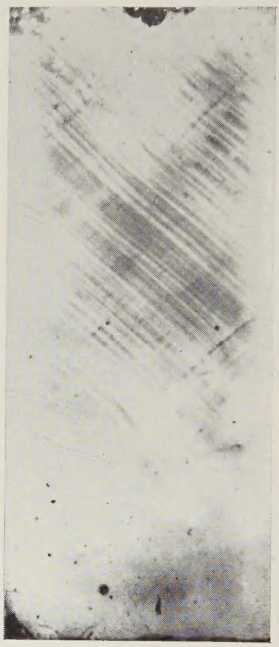

Striations in a crystal fatigued for 2×10^5 cycles to a compressive strain of 4·0%. ×7.